8-2022

Hybrid Smart Transformer for Enhanced Power System Protection Against DC With Advanced Grid Support

Moazzam Nazir
mnazir@clemson.edu

HYBRID SMART TRANSFORMER FOR ENHANCED POWER SYSTEM PROTECTION AGAINST DC WITH ADVANCED GRID SUPPORT

A Dissertation
Presented to
the Graduate School of
Clemson University

In Partial Fulfillment
of the Requirements for the Degree
Doctor of Philosophy
Electrical and Computer Engineering

---

by
Moazzam Nazir
August 2022

Accepted by:
Dr. Johan H. Enslin, Committee Chair
Dr. Ramtin Hadidi
Dr. Shuangshuang Jin
Dr. Zheyu Zhang

ABSTRACT

The traditional grid is rapidly transforming into smart substations and grid assets incorporating advanced control equipment with enhanced functionalities and rapid self-healing features. The most important and strategic equipment in the substation is the transformer and is expected to perform a variety of functions beyond mere voltage conversion and isolation. While the concept of smart solid-state transformers (SSTs) is being widely recognized, their respective lifetime and reliability raise concerns, thus hampering the complete replacement of traditional transformers with SSTs. Under this scenario, introducing smart features in conventional transformers utilizing simple, cost-effective, and easy to install modules is a highly desired and logical solution. This dissertation is focused on the design and evaluation of a power electronics-based module integrated between the neutral of power transformers and substation ground. The proposed module transforms conventional transformers into hybrid smart transformers (HST). The HST enhances power system protection against DC flow in grid that could result from solar storms, high-elevation nuclear explosions, monopolar or ground return mode (GRM) operation of high-voltage direct current (HVDC) transmission and non-ideal switching in inverter-based resources (IBRs). The module also introduces a variety of advanced grid-support features in conventional transformers. These include voltage regulation, voltage and impedance balancing, harmonics isolation, power flow control and voltage ride through (VRT) capability for distributed energy resources (DERs) or grid connected IBRs. The dissertation also proposes and evaluates a hybrid bypass switch for HST module and associated transformer protection during high-voltage events at the module output, such as,

ground faults, inrush currents, lightning and switching transients. The proposed strategy is evaluated on a scaled hardware prototype utilizing controller hardware-in-the-loop (C-HIL) and power hardware-in-the-loop (P-HIL) techniques. The dissertation also provides guidelines for field implementation and deployment of the proposed HST scheme. The device is proposed as an all-inclusive solution to multiple grid problems as it performs a variety of functions that are currently being performed through separate devices increasing efficiency and justifying its installation.

DEDICATION

This dissertation work is dedicated to my beloved father, who has always been a source of inspiration for me. I dedicate this thesis to my beloved mother who is longer in this world, but who had always motivated me to utilize education for making this world a better place.

I would like to thank my wife and sisters who always prayed for my success and always stood with me during my PhD journey.

Lastly, I dedicate this thesis to Almighty God, who gave me the strength, health, and guidance to achieve this important goal of my life.

ACKNOWLEDGMENTS

I would like to express the deepest appreciation to my PhD supervisor, Dr. Johan H. Enslin for his continued support and guidance throughout the course of my PhD. This dissertation would not have been possible without his help and utmost care.

I would also like to thank Klaehn Burkes from the Savannah River National Laboratory, Aiken, South Carolina for his continuous engagement and support during different tasks completed during this PhD.

I would also like to thank my PhD committee members, Dr. Ramtin Hadidi, Dr. Zheyu Zhang and Dr. Shuangshaung Jin for their guidance that played a pivotal role in enhancing the quality of my research work.

TABLE OF CONTENTS

LIST OF TABLES

LIST OF FIGURES

List of Figures (Continued)

Figure Page

List of Figures (Continued)

Figure Page

List of Figures (Continued)

Figure Page

CHAPTER ONE

INTRODUCTION

The direct current (DC) might flow in a power system due to geomagnetic disturbances (GMDs) that are the result of coronal mass ejection (CME) or a high-altitude nuclear detonation. The CME involves the discharge of a large mass of charged solar energetic particles from the sun's halo. Once the CME happens with proper trajectory, these particles travel toward the earth, shown in Figure 1.1, and this phenomenon is referred to as a solar storm. As the charged particles enter the magnetosphere, they collide with earth's magnetic field and the resultant disturbance leads to large amount of electric currents around the E-region of the ionosphere known as electrojets [2]. These currents induce electric fields of 6V/km or more on the earth's surface. The resulting potential acts between the neutrals of wye-grounded transformers that are connected at the ends of long transmission lines. This leads to the flow of quasi-DC currents, in the frequency range of 0.1mHz to 0.1Hz, into the transmission lines and back into the ground and commonly referred as geomagnetically induced currents (GICs). This induction process and the resultant flow of GICs is shown in Figure 1.2. During a strong GMD event, GIC values of 80 to 100A per phase for the three-phase power systems with a time duration of 100-1000s are probable for areas near the earth's poles [3]. The NERC TPL-007 defines a GIC threshold of 75A per phase for transformer thermal impact assessment following a GMD event [4].

Figure 1.1: Geomagnetic storm [1].

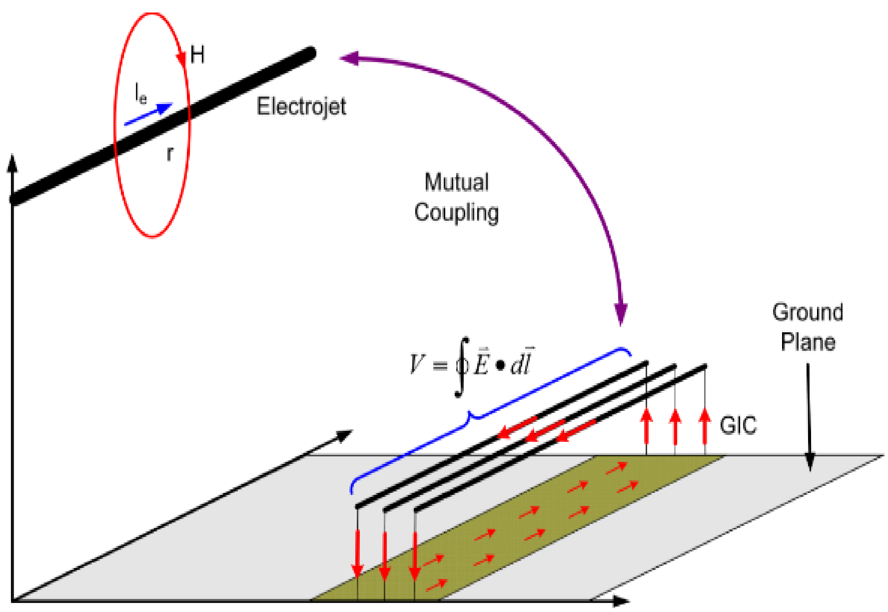

Figure 1.2: Mutual coupling between an electrojet and transmission lines [2].

Apart from CME, a nuclear detonation that occurs at a height of 30km or more above the earth's surface, commonly referred as a high-altitude nuclear electro-magnetic pulse (HEMP), may also lead to the flow of GICs in a power system. This event ejects gamma particles around the detonation area that ionize the air molecules on collision. The resulting electromagnetic signal interacts with the transmission lines similar to an electrojet. According to International Electrotechnical Commission (IEC) standard IEC-61000-2-9, the HEMP can be categorized into three regions based on its time response: E1, E2 and E3 as shown in Figure 1.3.

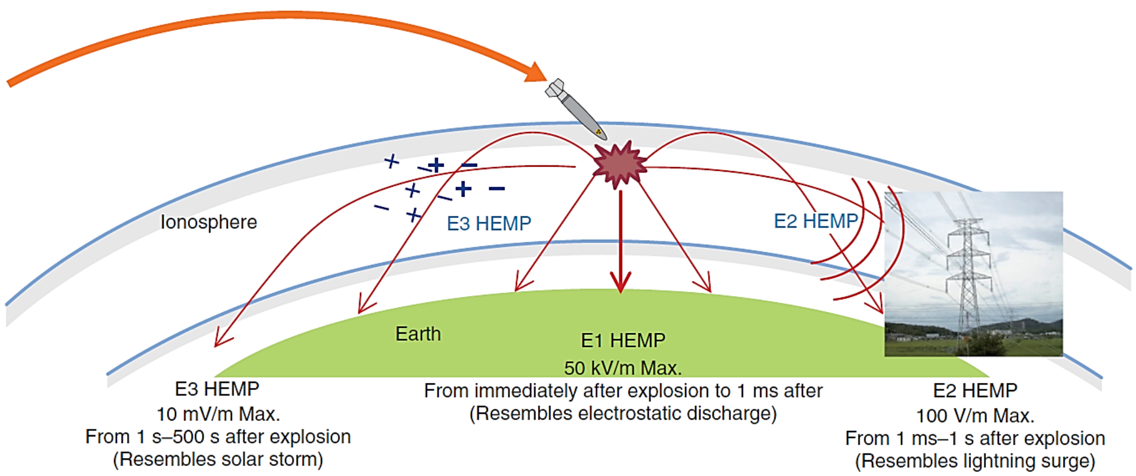

Figure 1.3: HEMP phenomenon [5].

The E1 is an early time wave with a short duration of 1 milliseconds and magnitude in the range of 10^4V/m. The E1 is followed by E2, an intermediate-time wave, that has a time duration of about 1 second. The E2 is followed by the longest portion of HEMP referred as magnetohydrodynamic E3 (MHD-E3) that lasts for about 500 seconds and closely resembles a solar storm. The three regions of a HEMP are shown in Figure 1.4.

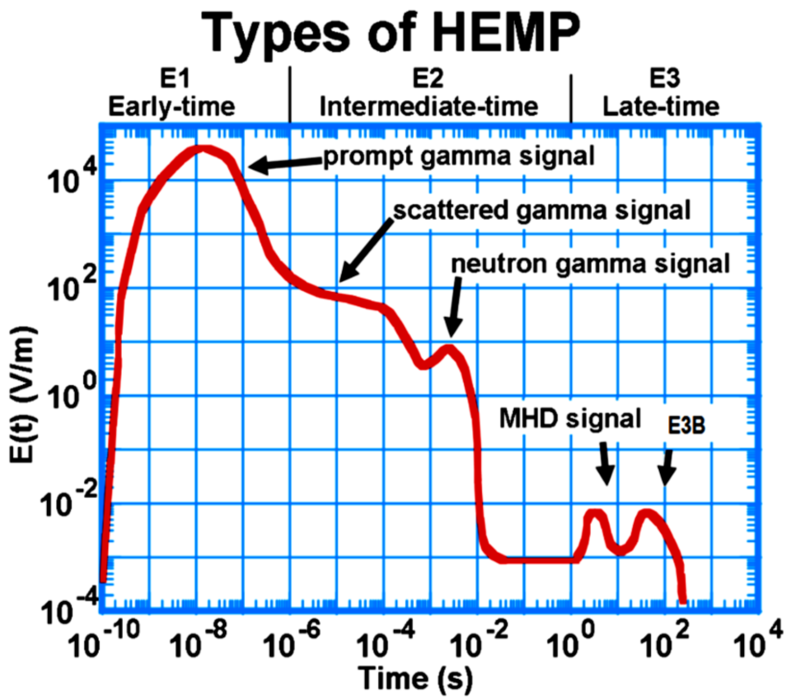

Figure 1.4: Various phases of a HEMP [6].

The high-voltage transmission lines usually spread over long distances and bear lower impedance resulting from bundled conductor configuration for higher ampacity. This increases the GIC magnitude to critical level that is substantial to saturate transformers core that could further lead to transformers internal heating, massive draw of reactive power, increased transformers noise level by more than 20dB(A), heating of generators rotors, damage to shunt capacitors, damage to static VAR compensators (SVCs), damage to harmonic filters and could possibly lead to maloperation of protection equipment [7]. The ultimate result could be a wide area system blackout that will have severe consequences for grid reliability and security. The normal and half-cycle saturation operation of a transformer is depicted in Figure 1.5, where it is observed that the core flux is uniform across the horizontal axis during the normal operation. During enough GIC injection, the flux undergoes a DC offset leading to a very large value of the magnetizing current.

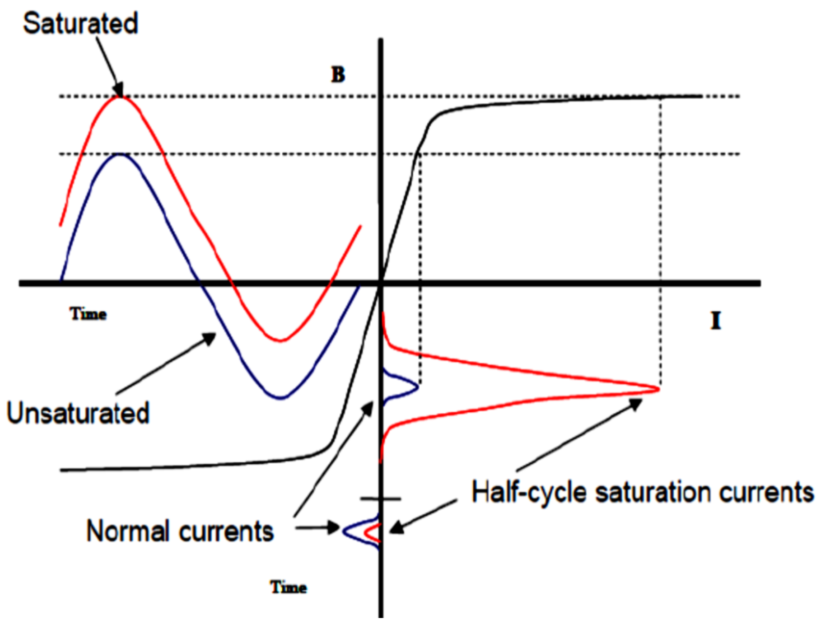

Figure 1.5: Comparison of normal and half-cycle saturation operation of a transformer [8].

The grid reliability across the world has been highly compromised by GMDs due to the augmenting frequency and severity of such events in recent years. A severe solar storm occurred in 1921 that disabled all the telegraphic services from the Atlantic coast up to the Mississippi river [8]. Similarly, in 1989, a severe geo-magnetic storm led to the collapse of the Hydro Quebec system due to tripping of capacitor banks and Static VAR Compensators (SVCs) and dielectric failure of two power transformers. Due to the collapse, 6 million people were without power for a minimum of 9 hours [9]. The associated equipment damage cost was reported as $13.2 million [10]. The GICs of about 80A/phase were recorded at the Public Service Electric & Gas Company (PSE&G), New Jersey, United States [2]. In 2003, the Halloween storm in Sweden led to 330A of neutral current in 3 phase, 5 limb, 400kV power transformers [11]. The instability caused by the 3rd order harmonics led to 20 minutes of blackout. Minor heating and low-level gassing in the transformers were also reported due to the GMD event. In July 2012, the world was scarcely saved from an extreme solar storm that if happened one week earlier, would have severely damaged power networks in many parts of the world with an estimated damage of $2 trillion [12].

In addition to CME and HEMP MHD-E3 GIC, the inverter-based resources (IBRs) also inject small DC currents to the power networks due to non-ideal switching devices [13]-[15]. The increasing interconnections of these devices could increase the DC levels in power networks to critical values. Some of the inverters are equipped with control strategies as proposed in [16], [17] that helps to avoid DC injection, however, there are a myriad of cases where the inverters may not be equipped with such controls, thus, enhancing the need for the DC mitigation devices.

The high-voltage DC (HVDC) transmission is gaining wider popularity due to availability of higher voltages and larger capacity semiconductor devices leading to efficient power converters. The monopolar or ground return mode (GRM) operation of HVDC transmission involves the flow of DC through transmission lines and back through the ground. Due to ground resistivity, that is a function of soil moisture and temperature, the flow of DC leads to a potential difference between the grounded neutrals of adjacent transformers [18], [19]. The ultimate result is the flow of DC in the loop created by transmission lines and ground.

The grid reliability stays compromised without installation of reliable protection strategies against the above discussed threats to grid operation from DC flow. The control and protection approach across strategic locations of the electric grid could provide the most desirable solution and power transformers are the appropriate candidate for this purpose. This dissertation proposes transformation of traditional transformers into hybrid smart transformers (HSTs) to mitigate DC flow in grid. The proposed HST is also capable of performing a variety of advanced grid-support functions in addition to DC mitigation. These include voltage regulation, voltage and impedance balancing, harmonics isolation and power flow control. The overall capabilities introduced by the proposed device in traditional transformers corroborates its wider adoption by electric utilities.

The rest of the thesis is organized as follows:

Chapter two reviews the current work related to the effect of DC flow in AC power networks on critical grid assets. It provides a detailed overview of the existing DC mitigation and elimination strategies with their respective limitations. It also reviews a variety of flexible AC transmission systems (FACTS) devices that are typically utilized by electric utilities to counter one or more of the challenges addressed by the proposed HST scheme. In addition, it discusses and compares the existing HST and solid-state transformer (SST) strategies with the HST strategy proposed in this dissertation work.

Chapter three proposes a novel power electronics-based DC mitigation and grid-support approach that involves a transformerless series active filter (SAF) integrated between the neutral of power transformers and substation ground. This approach effectively transforms conventional transformers into HSTs. This chapter discusses the detailed concept and control architecture of the proposed device. This chapter also presents the implementation strategy of the proposed device on an IEEE benchmark transmission system. A laboratory scale hardware prototype developed to evaluate the proposed approach is introduced in this chapter.

Chapter four presents and discusses the results from the controller hardware-in-the-loop (C-HIL) and power hardware-in-the-loop (P-HIL) strategies utilized to evaluate the proposed approach.

Chapter five proposes a hybrid bypass protection scheme for the proposed module that is critical to avoid damage to the module and the associate transformer. It also evaluates the effectiveness of the proposed scheme in a typical substation protection environment developed in the laboratory.

Chapter six concludes the thesis document with possible future directions. It also provides initial set of guidelines for field implementation and deployment of proposed HST scheme in a real substation environment.

CHAPTER TWO

LITERATURE REVIEW

A variety of studies have been performed to analyze the effect of DC flow in AC power networks on critical grid assets; transformers, synchronous generators, wind farms, protection equipment, Static VAR Compensators (SVCs) etc. [20]-[22].

The operational performance of a grid tied-synchronous hydro-generator under DC scenario is presented in [23]. It performs the vulnerability assessment based on the resultant electrical, mechanical, and thermal stresses. The ultimate result of DC flow in grid is the half-cycle saturation of wye-grounded transformers, particularly the generator step-up transformers (GSUs) that operate close to their rated capacity. The increased reactive demand of the transformers during half-cycle saturation is compensated partially by the generators through automatic adjustment of their respective field excitations and partially by the reactive power supply devices, such as, shunt capacitors, SVCs etc. However, there is a limit up to which this demand could be met and once the threshold is crossed, the system voltage falls. In case it falls below the pickup value of undervoltage (UV) relays, they trip leading towards unintended power system outages. The cylindrical and salient-pole synchronous generators have the largest share in the bulk power grid where they are utilized for thermal generation; fossil-fueled, nuclear steam, gas turbine and in the hydel power plants. The generators are connected to the grid utilizing a delta to wye-grounded transformer, referred as GSU transformer. The half-cycle saturation of the GSU transformer due to DC flow in the power networks leads to generation of harmonics. The delta winding of GSU transformer blocks the flow of resultant zero-sequence currents towards the generator. However, the positive and negative-sequence currents still flow in the stator winding. These currents are responsible for the creation of flux waves that rotate relative to the rotor motion. The positive-sequence waves rotate in the same direction as rotor and with fixed relative speed, whereas the negative-sequence waves rotate opposite to the rotor's rotation. Therefore, the negative-sequence currents rotate at twice synchronous speed relative to the rotor reference frame leading to the flow of eddy currents on the rotor surface, rotor bar slot wedges and field winding [24]. This leads to rotor heating, loss of mechanical strength of rotor wedges, degradation of field winding insulation and arcing. The negative-sequence currents also lead to oscillatory torque and vibration of the generator. All these effects could ultimately lead to generator failure. The generators are typically protected against the excessive stresses caused by the normally encountered negative-sequence odd-order harmonics, particularly fifth harmonic, by utilizing a negative-sequence relay. However, they remain vulnerable to damage caused by even-order negative-sequence currents in the stator winding that result from GSU transformer half-cycle saturation. The previously discussed stresses would be significantly higher for the hydro-power plant facilities where the generator is also utilized in the motoring mode as in the pumped-hydro storage. The harmonic enriched stator current would lead to significant mechanical stresses resulting from torque and speed variations that could be damaging to the various generator components. Similar threats prevail for other facilities that employ rotating machines, whether induction or synchronous, for large scale generation or as motors for industrial applications.

The DC flow in AC networks could also impact the normal operation of the inverter-based generation as discussed in [25]. The transformers connected to generation plants are typically operated close to their full rating, therefore, they are more prone to enter half-cycle saturation under DC flow. The voltage and current signals on both sides of transformers experiencing half-cycle saturation, during the flow of DC in associated transmission network, become harmonic rich. These harmonics present severe challenges to the reliable operation of solar farms. The inverter-based resources are typically equipped with harmonic protection functions that prevent the plants from exceeding the current distortion limits. These protection functions are non-directional and may trip the plant during high levels of current distortion resulting from the flow of DC in the transmission networks. The other issue is the overloading of the DC-bus and resonance resulting from severe harmonic distortion. Due to the distortion in voltage wavefarm of the main transformer on the solar farm side, it is plausible that double zero crossings could occur and as the inverter is grid following, this might lead to mismatched grid alignment or voltage magnitude [26]. It is noteworthy to mention that advanced phase locked loop (PLL) algorithms, such as, second-order generalized integrator-quadrature signals generator (SOGI-QSG), are able to track the grid voltage amplitude and phase accurately even when it is polluted by DC components, unbalance and higher-order harmonics. Although modern inverter designs are capable of avoiding DC injection into the grid from the converter side [16], but the other causes discussed above would still allow the flow of DC on the transmission side that could adversely effect the solar farms operation leading to cascaded failures and ultimate grid collapse during such events. The increased reactive power demand by the main transformer during half-cycle saturation is mainly supplied by the electric grid. The PV plants are equipped with reactive power support capability that gets activated during voltage sag or reactive power deficiency on the main grid. The acute reactive power demand during the flow of DC may lead to activation of this support function, thus, curtailing or reducing the active power supplied by the plant. This could in turn lead to drop in system frequency that could ultimately trip the under-frequency protection once the respective threshold is achieved. The presence of harmonics in the solar farm current during to the flow of DC leads to enhanced winding resistance of GSU transformer and ultimately increased power losses. To avoid exceeding the emergency allowed transformer winding temperature of 180˚C during the flow of DC, the PV farm output must be reduced. This would lead to a modified solar farm capability curve with the controls adjusted accordingly for enhanced grid reliability.

The DC flow in AC networks could also have a significant influence on the power system protection devices. The Current Transformers (CTs) are susceptible to saturation in the same manner as transformers [27]. Also, they are unable to measure primary DC currents on their secondary side. The response of relays to DC is highly dependent upon their design. The electromechanical relays usually respond to rms values whereas the microprocessor-based relays either attenuate or eliminate harmonics by employing digital filters for extracting only the fundamental component [28]. As the flow of DC in AC networks adds a DC component to the primary line current, there are chances that the CTs enter their saturation region. Once a CT saturates, the current fed to the relay doesn't depict the exact profile of the primary current and there are chances of a relay mis-operation if the saturation levels are higher than what can be tolerated by a relay. The distance relays are commonly utilized in the transmission system, where they estimate the positive sequence impedance to the fault using voltage signals from voltage transformers (VTs) and current signals from CTs. Due to CT saturation from DC flow, the amplitude of CT secondary current is severely damped in the initial stages of the fault due to which a delayed response of the breaker is plausible. The delay time of breaker operation increases with an increase in the level of DC in the power system. The increase in the breaker operation time after a fault is undesirable as it could result in additional equipment damage or degradation.

The primary protection usually employed for the transformer protection is the differential relay. The differential relay operation is dependent upon the difference in the per-unit current values on both sides of a transformer with some margin for CT errors, ratio errors, Online Tap Changing transformers (OLTC) and some safety margin. Due to substantial DC flow in AC networks, the differential relay misoperates even during the normal operation without any fault, when the differential between the fundamental components of primary and secondary currents approaches the pickup value with increasing magnitude of DC. During the internal fault of transformer, the chances of misoperation are low as the relay gets enough differential current to operate. The harmonics in the primary current doesn’t play a significant role in this case. However, there might still be situations in which the differential relay doesn’t operate even for internal faults in presence of GICs. This is because the differential relays normally employ the second-harmonic restraint to avoid false tripping during the inrush current. This could be problematic in case the GICs, having a significant second harmonic content, flowing in a power system are of considerable magnitude. Due to the restraint, the relay may not trip even if there is an internal fault during high magnitudes of GICs as the relay might confuse it with the inrush current. Although the differential relays are backed up with instantaneous relays that do not possess the second harmonic restraint, however, the delay in operation during a high-magnitude internal fault might lead to extra damage to the power transformers that is undesirable.

The inverse time overcurrent (ITOC) relays have inverse time-current relationship and operate with different time delays for multiples of the pickup current. Similar to distance relays, the flow of DC in a power network may delay the operation of the ITOC relays due to lesser current magnitude provided by the CTs due to saturation. However, the main and backup ITOC relays coordinate normally due to enough safety margin and both sensing similar magnitudes of the DC in a transmission network. This ensures that the backup relay always operates once the main protection fails even when DC is flowing in a power system.

The undervoltage (UV) relays operate when the voltage at their monitoring point falls below a specific threshold. In case of DC flow in AC networks, the reactive power absorbed by the transformers increases. The increased demand is met by the generators through automatic adjustment of their respective field excitations. However, there is a certain limit up to which the generators could supply the reactive power. Once this limit is reached and other reactive power supply devices in the network, such as, SVCs exhaust, the system voltage falls. In case, it falls below the pickup value of the UV relays, they would operate leading to partial or complete system blackout. The above situations are discussed to provide the relay engineers an idea about the possibilities of relay misoperations or false tripping due to the flow of DC in a power network so that necessary adjustments could be made in the protection designs for automatic reconfiguration of relays when the system experiences DC or GICs flow.

There are a few recommendations that could be helpful to ameliorate the power system reliability by correct operation of the protection equipment under the influence of DC.

1. With advanced GIC modeling tools, their expected levels at various points on the earth can be predicted with decent accuracy [9], [29]-[31]. The protection engineers should consider these models while designing their protection system for the most affected and critical apparatus, such as, transformers, generators, and capacitors.

2. The DC should be continuously monitored by either observing the transformer neutral current or the line current using the microprocessor-based relays. In case, there is a significant DC magnitude, the relays with and without harmonic filtering should be automatically adjusted to avoid the pickup during the normal load operation as the values might seem close to the pickup due to lower settings that are not adjusted accordingly.

3. The second-harmonic restraint should be disabled if there is a higher second-harmonic content for longer period than typical inrush current lengths. A pre-set timing threshold should be in place that would be helpful in avoiding the misoperations due to the DC.

4. A variety of DC mitigation and elimination schemes have been proposed [10], [32]-[37]. These devices should be installed at the most critical points in the transmission systems.

Depending upon their associated efficacy in blocking the DC, the protection engineers could leave their settings unchanged or do minor modifications.

5. Most of the power system protection issues associated with the DC could be avoided by replacing the traditional CTs with the Optical Current Transformers (OCTs). As OCTs do not employ any ferromagnetic core the saturation issue would be automatically resolved. Also, they can accurately measure DC values dependent upon their design.

6. A variety of CT saturation detection and compensation algorithms have been proposed [38], [39]. These techniques could be adopted to avoid CT saturation, thus, resulting in increased power system reliability.

The severe consequencies associated with the flow of DC in AC power networks on critical grid assets have been discussed in detail above. To avoid these repurcussions, various DC mitigation strategies have been proposed in past [40]-[42]. These strategies can be categroized into five classes; elimination of neutral connections, series compensation along the transmission lines, DC diverters, DC compensated transformers, installation of neutral to ground DC blocking and mitigation devices.

The elimination of neutral connections involves either the physical removal of the connection between the neutral and ground of wye-grounded transformers or replacing the wye-grounded transformers with delta transformers [40]. However, the removal of the neutral connections is not recommended from the safety and system protection perspective. The neutral connections to the ground are always desired to avoid overvoltages for the single-phase autotransformers that are highly utilized in power networks. The replacement of wye grounded-wye grounded transformers with delta-wye grounded transformers increases the complexity of interconnections due to the coordination challenges with the associated phase shifts. In addition, this would decrease the number of grounded neutrals in the power networks which will increase the fault current ratings of the remaining grounded neutrals. This approach is shown in Figure 2.1.

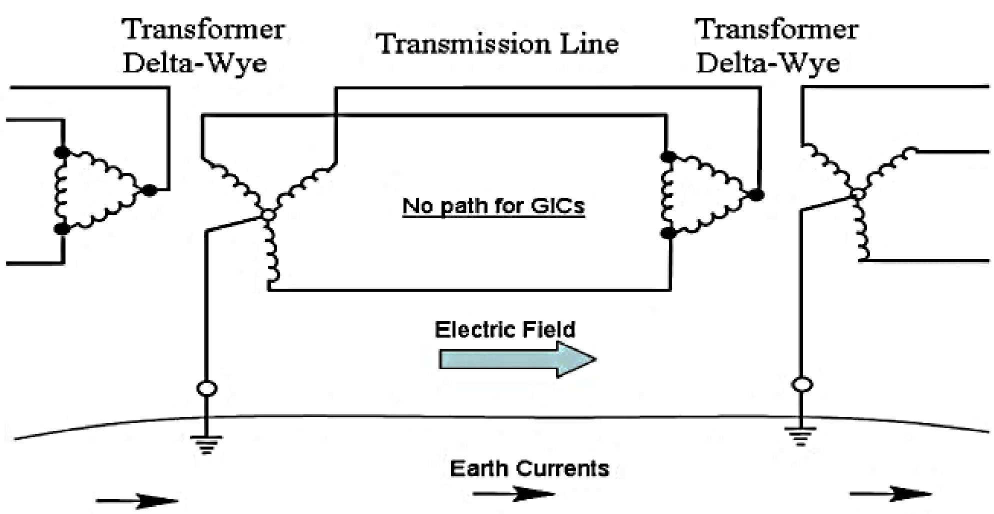

Figure 2.1: Elimination of neutral connections scheme for DC elimination [40].

The second approach could be the utilization of series compensation devices along the length of the transmission lines. The series compensation could be mere capacitors or a series combination of capacitors and variable inductors as in [43]. In [43], the variable inductance is reduced below the capacitive inductance to run the line compensation in the capacitive mode for DC blocking, fault ride through and for boosting the grid voltage during a voltage sag. The inductive mode is enabled where objective is fault current minimization, and mixed mode is used where objective is to regulate the power factor, regulate the grid voltage and to minimize line inductive losses. However, the series compensation may cause series and parallel resonance from line and load impedances [40]. They have also proved to remove DC currents by a very low value of 12-22% [7]. Also, the series compensation devices need to be installed along the length of the transmission lines and are, therefore, not economical. The series compensation strategy is shown in Figure 2.2.

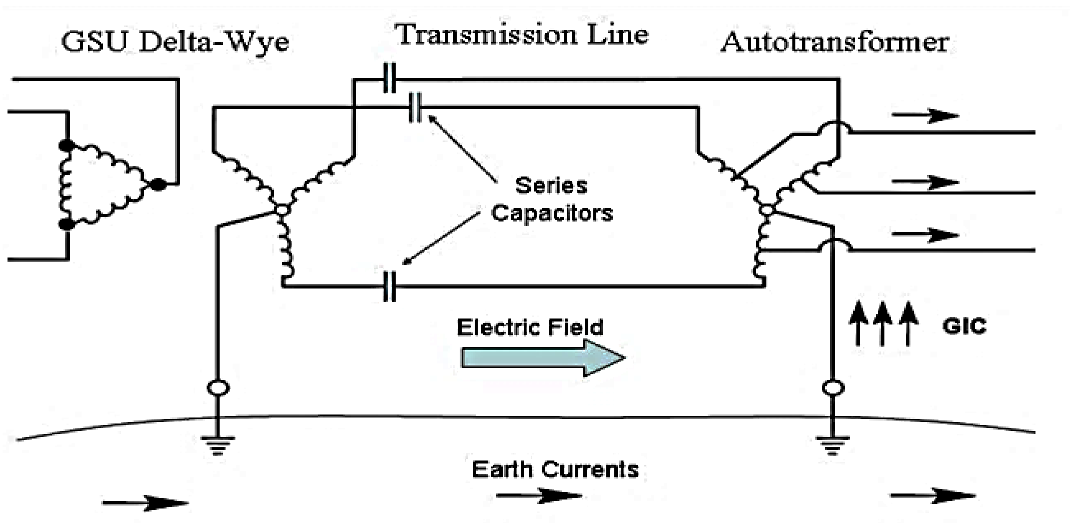

Figure 2.2: Series compensation strategy for DC mitigation [40].

Another approach to mitigate or eliminate DC from the power networks is to utilize DC diverters along the transmission lines [44], [45]. The DC diverters use a special three-legged transformer with compensation windings wound on the same leg as the primary windings but in opposite direction. The DC current is separated from the line current using a filter and then allowed to flow through the compensation windings to cancel out the primary DC currents. However, this technique requires a special three-winding transformer that is highly uneconomical.

A technique based on DC flux cancellation within the transformer core utilizing a separate DC compensation winding has been proposed by Siemens [46]. This strategy utilizes DC flux detection unit to inject a counter flux through a compensation winding wound on the transformer leg as shown in Figure 2.3. This technique requires building special transformers and, therefore, is not applicable to the existing transformers. Also, any damage to the compensation winding requires dis-assembling the transformer followed by rewinding that involves significant expenditure and time.

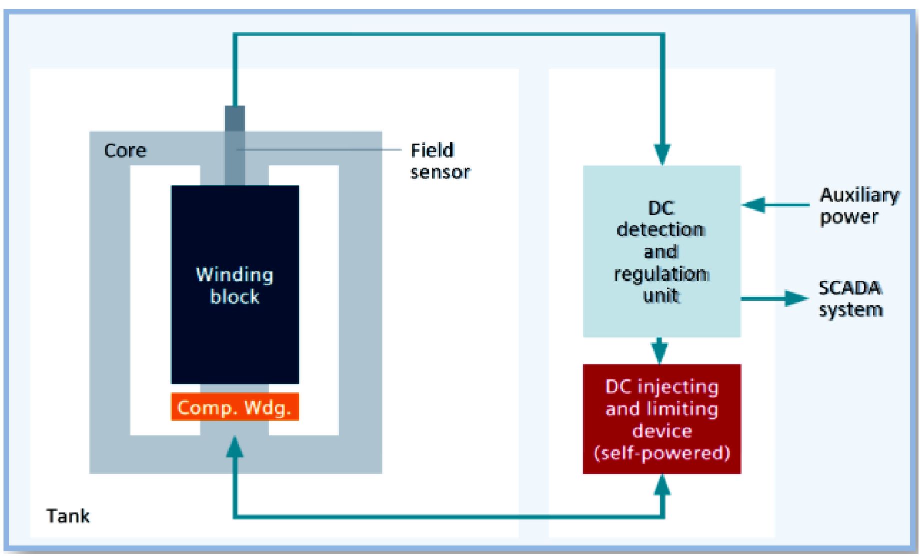

Figure 2.3: DC compensated transformers for GIC mitigation [46].

The most commonly utilized method for the purpose of DC elimination is the installation of DC mitigation or elimination devices between the transformers neutral and ground. One such approach utilizes a DC motor between the two connection points [47]. Whenever DC flows in the power network, the motor turns and the resultant back electromagnetic force (EMF) applies a reverse potential that automatically suppresses these currents. However, this solution is expensive and not reliable due to the involvement of a rotating machinery. A technique utilizing a back-to-back semiconductor switch between the transformer neutral and ground has been proposed in [32]. Under normal operation, the transformer is solidly grounded. In event the DC in network crosses a predetermined threshold, the semiconductor device is switched in and its duty cycle is controlled to effectively reduce the transformer neutral current. Another related strategy utilizes a controlled ground resistance between the two points [48]. The controlled ground resistance is effectively a resistor connected in parallel to an electronic switch where the duty cycle of the switch is controlled to increase the effective ground resistance in event of DC and vice versa. Another technique utilizes a resistive path between the neutral and ground under normal operation and a capacitive path during the flow of DC [49], [50]. There is also a surge arrester or metal-oxide varistor (MOV) connected parallel to the capacitor that ensures its safety from overvoltages during a rare event of a simultaneous DC and a ground fault. A similar technique utilizes a bypass path to the ground instead of a surge arrester [10], where the bypass gets actived only during the inrush or fault currents and returns to capacitive path after 20 cycles. The delay ensures that the inrush current have already damped out or faults already cleared by protection devices before switching back. However, the installation of neutral DC capacitor blockers is accompanied with significant uncertainity and risk owing to transformer impedance changes and ferro-resonance concerns. The large voltage buildups across these blockers during the ground faults or inrush currents require either a large capacitor or fault-current diversion devices that increase the cost and complexity of this solution and augment the reliability concerns. The above discussed scheme for DC mitigation is summarized in Figure 2.4.

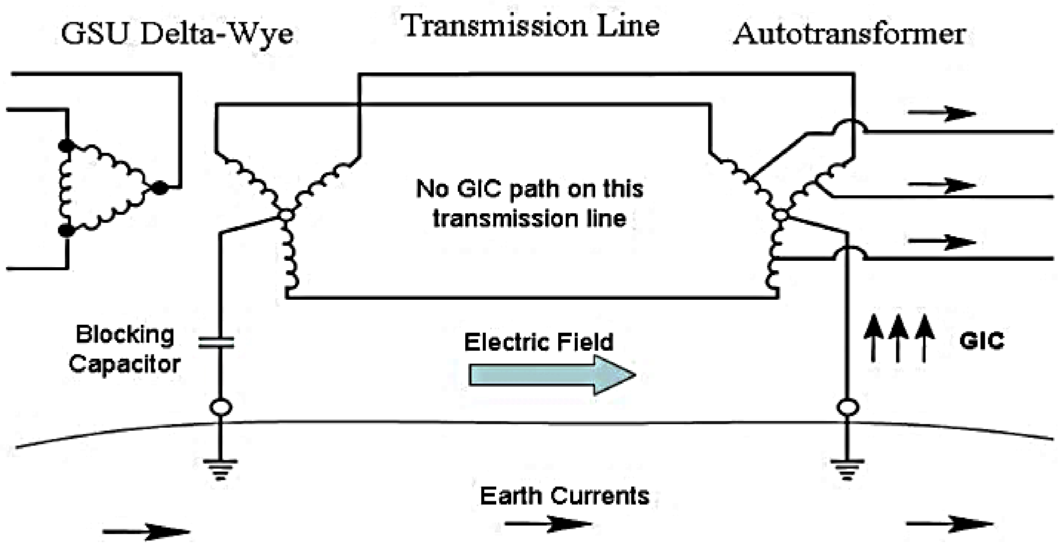

Figure 2.4: Neutral blocking strategy for DC mitigation [40].

Among these approaches, the Neutral Blocking Devices (NBDs) installed between the transformers neutral and substation ground have gained wide popularity.

To counter the majority of the previously discussed issues in modern grids, a myriad of flexible AC transmission systems (FACTS) strategies have been proposed during the preceding few decades; unified power flow controller (UPFC) [51], static VAR compensators (SVCs), thyristor switched series capacitor (TSSC) [52], thyristor controlled series capacitor (TCSC) [53], controllable network transformer (CNT) [54], fractionally rated back to back (FR-BTB) converter and compact dynamic phase angle regulator (CDPAR). Most of the previously discussed power electronics-based devices float at the line voltage that leaves them vulnerable to corona damage and raise serious isolation challenges amid floating and grounded components [55]. This challenge was resolved in the grounded controllable network transformer (G-CNT) scheme proposed in [56], that utilizes a three winding transformer and a fractionally rated converter connected to the tertiary winding that operates close to the ground level. However, the above discussed FACTS devices are in general unable to block the flow of DC in AC electric grids. Accordingly, the grid security stays compromised even with the installation of these dynamic grid control devices.

As discussed in chapter one, the transformers provide the most appropriate point for grid protection against DC. Considering their importance, the concept of smart transformers (STs) arose that bear the capability to address some of the previously discussed reliability concerns. This has led to an increased demand of ST designs that not only provide localized and dynamic control over the grid parameters but also capable of performing their own tuning as the conventional transformers suffer from issues like impedance or power mismatch that happens when one unit is replaced with another either due to failure or for upgradation [57]. The STs can be further divided into two categories; solid-state transformers (SSTs) and hybrid smart transformers (HSTs), where the former involves a fully rated power electronics-based transformer that carries the full load power. The HSTs, on the other hand, involve a fractionally rated converter integrated with conventional transformers that introduce various smart functionalities in addition to traditional operation of power transformers.

Research works related to both above discussed strategies are presented now. A three-stage ST design capable of processing a large amount of reactive power for medium voltage (MV) support as an ancillary service to the electric grid is proposed in [58]. The operational performance of a smart solid-state transformer (SST) for voltage regulation and harmonics isolation utilizing its mathematical model in PLECS has been presented in [59]. The SST is compared with a conventional transformer and is depicted to bear superior performance. A multilevel converter-based three-stage SST topology has been presented in [60], where the SST is demonstrated to be capable of VAR compensation, voltage regulation, voltage-sag compensation and microgrid integration. In [61], an SST is utilized as a real-time power flow regulator to achieve economic dispatch. For this purpose, predictive photovoltaic and load forecasting algorithms are used to optimize charging and discharging of an energy storage followed by optimal routing of energy by the SST to minimize the grid power consumption. An SST has been utilized with online dynamic volt-VAR control (VVC) algorithm in [62] to regulate distribution feeder voltages that are highly volatile due to changes in load and distributed generation. This SST operates in complete isolation from the substation control center and performs well in both radial and meshed distribution networks.

The SSTs are still far from the complete replacement of traditional transformers due to the comparative life span and robustness. Also, there has been a massive investment in the already installed power transformers across the grid and their replacement is accompanied by substantial expenditure and time. In this perspective, approaches that can transform traditional transformers into smart ones emerge as a promising alternative. Moreover, it is concluded from the above discussion that each of the proposed SST designs is equipped with a limited number of features. In this perspective, a smart transformer conversion strategy that introduces all the desired functionalities into traditional transformers ameliorates efficiency and diminishes cost. Correspondingly, a technique utilizing a power electronic converter on the tertiary winding of a three-winding transformer for certain grid-support functions is proposed in [63], [64]. The modified transformer can control the grid voltage, active and reactive power flow and can balance three-phase loads. However, this strategy entails a special three-winding transformer that limits its applicability to the existing networks. This dissertation work is motivated by the traditional transformers conversion concept and proposes a power-electronics based module integrated between the conventional transformers neutral and substation ground leading to their conversion into hybrid-smart transformers. The proposed module enhances power systems protection against DC along with providing a variety of advanced grid-support functions. All the above discussed devices are summarized in table A2 in Appendix A. The proposed HST concept is discussed in detail in Chapter 3.

CHAPTER THREE

HYBRID SMART TRANSFORMER (HST)

From the previous discussion, it can be concluded that the most widely utilized protection against DC in power networks is installation of neutral capacitor blockers between the transformers neutral and substation ground. However, their installation brings significant uncertainty and risk due to transformer impedance changes and ferro-resonance. As the increasing inverter-based generation is also constantly injecting DC into the power networks, any device that constantly eliminates DC without affecting other power system equipment is highly desired. All current technologies utilized for GIC mitigation or elimination remain dormant when there is no flow of these quasi-DC currents in a power system. Therefore, they remain unutilized most of the time due to the low occurrence of such events.

This chapter introduces converter-based solutions as a favorable alternative to the already proposed DC mitigation schemes by presenting two novel strategies. One of the approaches employs a low-cost DC-DC converter between the neutral and ground of a three-phase power transformer for the sole objective of DC mitigation in transmission lines. The other approach employs a transformerless series active filter (SAF) to surpass the effect of DC while performing certain grid-support functions such as harmonics isolation, voltage regulation, voltage and impedance balancing, power flow control [65]-[67]. This strategy effectively transforms a traditional transformer into hybrid smart transformer.

Active Power Filtering (APF) has been widely used for power quality improvement, harmonics isolation [68] and voltage regulation [69]. Transformerless series active filters have been specifically utilized for voltage sag compensation in [65]. A power electronic converter is also utilized for certain grid-support functions on the tertiary low-voltage winding of a three-winding transformer in [63]. The implementation of this approach specifically requires a special tertiary winding transformer and may not be applicable to existing networks. The proposed approach in this chapter can be implemented on existing two winding or auto transformers without the need of a tertiary winding, thus, allowing incorporation to existing power networks.

The evaluation of the two converter-based approaches, against the criteria developed by the North American Electric Reliability Corporation (NERC) GMD Task Force [69], is also performed in this chapter to weigh the effectiveness of these approaches for DC mitigation. In this way, this work opens a new avenue of converter-based solutions as a promising alternative to the subject problem.

Proposed DC Chopper-based Solution

The proposed chopper-based DC mitigation solution utilizes a buck-boost converter integrated between the neutral and ground of a three-phase power transformer as shown in Figure 3.1. The three DC sources between the transformer and power supply mimic the uniform flow of DC within the three-phase transmission lines. When a power system is operating under balanced condition, the neutral current is approximately zero. However, when DC flow occurs in a power system, the primary current of a transformer undergoes DC offset. If the DC injection is of enough magnitude, it could drive the transformer into half-cycle saturation and current starts to flow from the transformer neutral into the ground. In the proposed scheme, the neutral current is continuously monitored using a hall-effect based or an optical current sensor. As the neutral current is desired to be zero as before DC injection, it is regulated using a proportional integral (PI) controller. The output of the PI controller is passed through a PWM generator to generate pulses for the electronic switch within the buck-boost converter. The output DC voltage of the buck-boost converter is adjusted in proportion to the DC flowing in the system. This ensures that the neutral to the ground current of the power transformer is always zero similar to the case without DC injection.

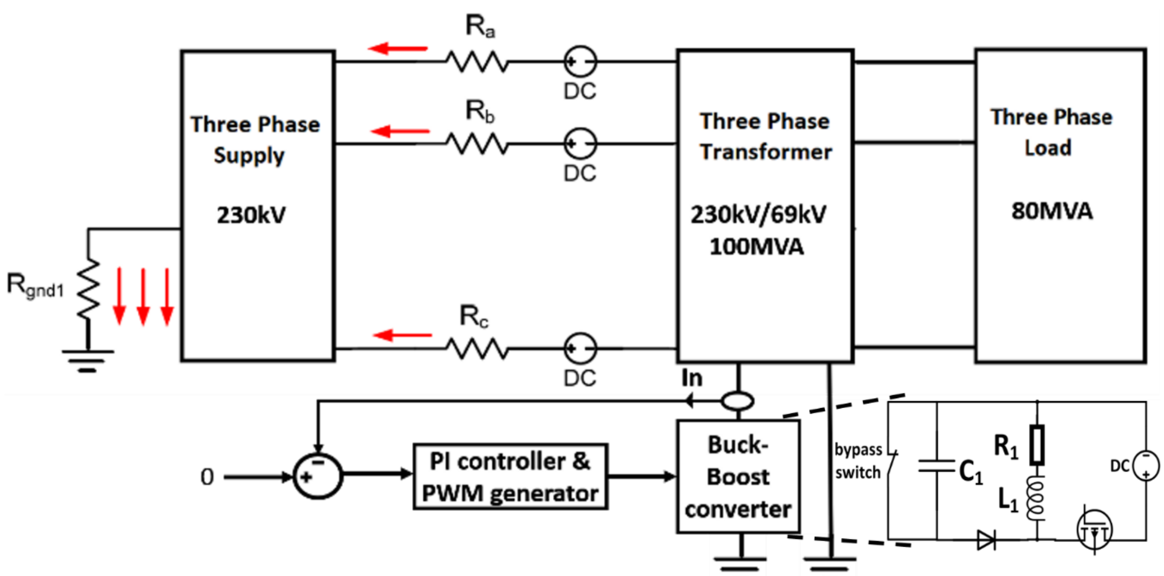

Figure 3.1: Proposed chopper-based circuitry for DC mitigation.

The converter damage is avoided during inrush current or ground faults using a high-speed switch that gets its signals from an overvoltage relay connected at the output of the converter [10]. It is worth mentioning that closing of the bypass switch will curtail the ability of the proposed device to block DC for 20 cycles i.e., 0.33 seconds. However, this time is insufficient to initiate the half-cycle saturation of the transformer due to the large time constant of the *RL* circuit consisting of the unsaturated transformer and source impedance [19].

This device provides a low-cost solution for the sole objective of DC mitigation or elimination. This technique is superior to the neutral capacitor blocking strategies as it doesn't require a large capacitor and complex bypassing strategies that demand a substantial amount of space and are quite expensive. However, this approach does introduce some reliability concerns due to the utilization of a high-speed switching device with no additional benefits. Any device that can perform a variety of grid-support functions in addition to DC elimination would always be a preferable choice for the power utilities. The subsequent section of this paper introduces an all-in-one solution to the routine problems in a power system, such as harmonics, voltage unbalance and voltage sag in addition to DC injection.

Proposed HST Strategy

The single-phase version of the proposed hybrid smart transformer developmental strategy utilizing a traditional transformer and a conversion module is shown in Figure 3.2. It utilizes a transformerless power-electronics based scheme integrated between the transformer neutral and substation ground. The scaled converter utilizes an H-bridge converter with a rating of 25-30% of the line voltage. The DC-link of the proposed module utilizes a capacitor C_2 and an active power storage option, such as, a battery or an ultra-capacitor (UC), for storing the reverse power flow towards the converter and supplying it when needed. The DC-link voltage control is shown in Fig. 1(b). The required energy storage to be integrated to the DC-link is largely dependent upon the application. For instance, if only DC mitigation is the objective, a large DC-link capacitor or UC might be sufficient, but if the objective is power flow control that usually spans over hours, the DC-link might require a continuous power source, such as, a separate converter fed by an independent source. The high-frequency switching harmonics on the AC side are eliminated utilizing a low-pass LC filter that comprises of capacitor C_1 and inductor L_1. The device is proposed to be accompanied with a high-speed hybrid AC/DC solid-state switch, where the solid-state device ensures fast link to ground during ground faults or inrush and the parallel mechanical switch provides a low-loss path to the high-magnitude current. The bypass switch protects the converter and transformer from high voltages that might develop across capacitor C_1 and allows the transformer to perform its traditional functions in the event of converter loss or failure.

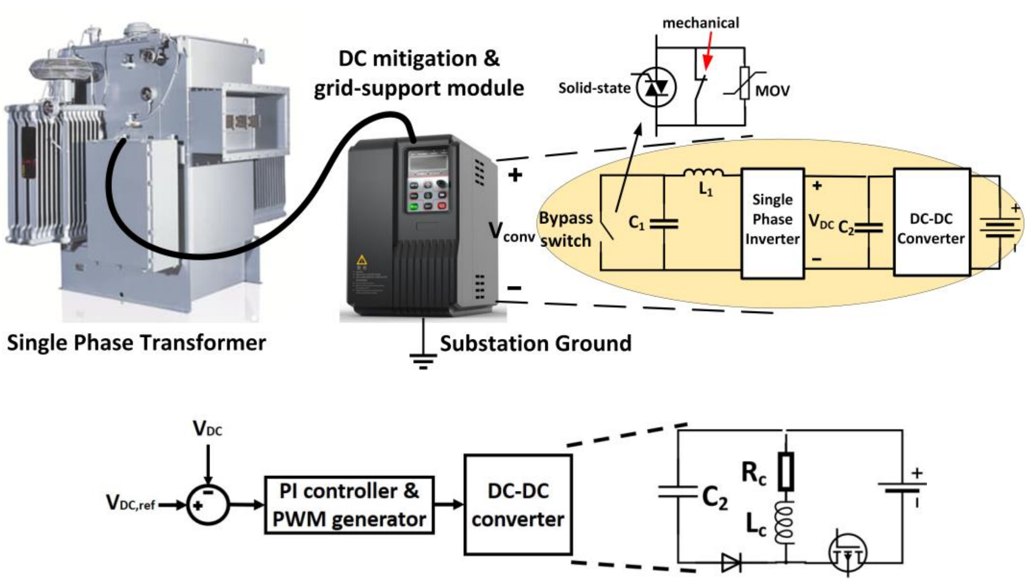

Figure 3.2: (a) Proposed hybrid smart transformer strategy, (b) DC link voltage control of the proposed module.

The converter injects a voltage of varying magnitude and phase angle between its two connection points to operate in different modes; voltage, impedance and power flow control utilizing the concept depicted in Figure 3.3. The proposed approach is equally relevant to both transmission and distribution networks.

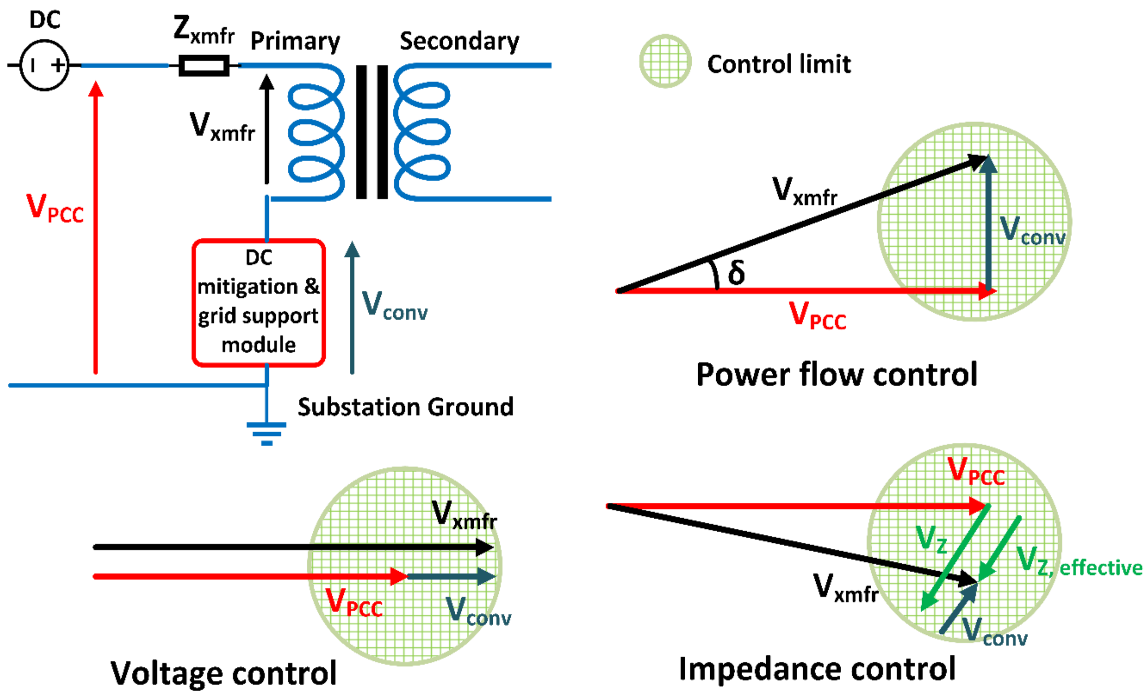

Figure 3.3: Control strategy for the hybrid smart transformer conversion module.

For the purpose of voltage regulation or balancing, the load voltage is maintained constant by injecting the difference between the desired and actual voltage at the point of common coupling (V_{PCC}) between the transformer neutral and substation ground. This effectively retains the transformer primary winding voltage (V_{xmfr}) at its desired value. A similar control loop could be utilized to provide the voltage ride through (VRT) services to the distributed energy resources (DERs), thus enhancing efficiency and diminishing complexity.

The replacement or upgradation of either a single or a three-phase transformer is usually accompanied by concerns like impedance mismatches that adversely effects power flow and grid balance. The proposed device can address this issue through cancellation of the extra voltage across the transformer impedance (Z_{xmfr}) resulting from the mismatch. The impedance control strategy is depicted in Figure 3.3, where the converter injects an opposing voltage (V_{conv}), by adjusting the gain G_1, to nullify the extra voltage (V_z-$V_{z,effective}$) appearing across the transformer inductance, thus restoring its original value ($V_{z,effective}$). This feature of the proposed module is highly attractive to the electric utilities. Large power transformers are the most critical equipment in the grid with their custom development and transportation accompanied with significant lead times and cost. With dynamic impedance control capability, a damaged unit or an upgradation could be easily performed using a spare transformer or by borrowing from the neighboring utility under the programs like spare equipment database (SED) or spare transformer equipment database (STED) initiated by the NERC and Edison Electric Institute (EEI) [70].

The smart conversion module is also capable of controlling the active/reactive power flow across the transformers that could be helpful in removing congestion across certain corridors, utilizing transmission lines and renewable generation at their maximum rated capacity. The active and reactive power flow between PCC and transformer primary shown in Figure 3.3 is given as:

$$P = \frac{3|V_{PCC}||V_{xmfr,eq}|\sin{(\delta_{PCC} - \delta_{xmfr,eq})}}{Z_{xmfr}} \tag{3.1}$$

$$Q = \frac{3(|V_{PCC}|^2 - |V_{PCC}||V_{xmfr,eq}|\cos(\delta_{PCC} - \delta_{xmfr,eq})}{Z_{xmfr}} \tag{3.2}$$

Where, $V_{xmfr,eq}$ is the sum of transformer and converter voltage, δ_{PCC} and $\delta_{xmfr,eq}$ are the angles of V_{PCC} and $V_{xmfr,eq}$ respectively. The proposed strategy provides independent control over the converter voltage and angle, therefore, $V_{xmfr,eq}$ and $\delta_{xmfr,eq}$ could be adjusted individually. This provides decoupled control over both active and reactive power with the quadrature injection of the module voltage to V_{PCC} delivering the highest impact.

Another important feature of the device is its capability to prevent the grid harmonics from travelling further towards the downstream of this smart transformer installation, thus enhancing the power quality. Also, it can mitigate the harmonics generated by non-linear loads from travelling towards the grid. This objective is achieved by measuring the voltage at V_{PCC} and isolating its harmonic content. This unwanted signal is further injected between the transformer neutral and substation ground that ensures the voltage at the transformer terminals is always harmonic free. A similar concept is utilized for suppressing the harmonics generated due to the half-cycle saturation of the transformer resulting from DC flow. Accordingly, the proposed device is an all-in-one solution to multiple grid problems.

The control strategy of the module is implemented in Figure 3.4 where the top branch is dedicated to voltage regulation or balancing. The second branch is for the purpose of impedance matching, where the gain G_1 is adjusted as per the requirement. The third branch is dedicated to harmonic isolation from V_{PCC} utilizing a second order generalized integrator (SOGI) based phase-locked loop (PLL) that are commonly utilized for grid-synchronization of single-phase grid-connected power converters [71]. The bottom branch is utilized for active/reactive power flow control utilizing gain G_2. The different control loops could be activated and adjusted as per the requirement.

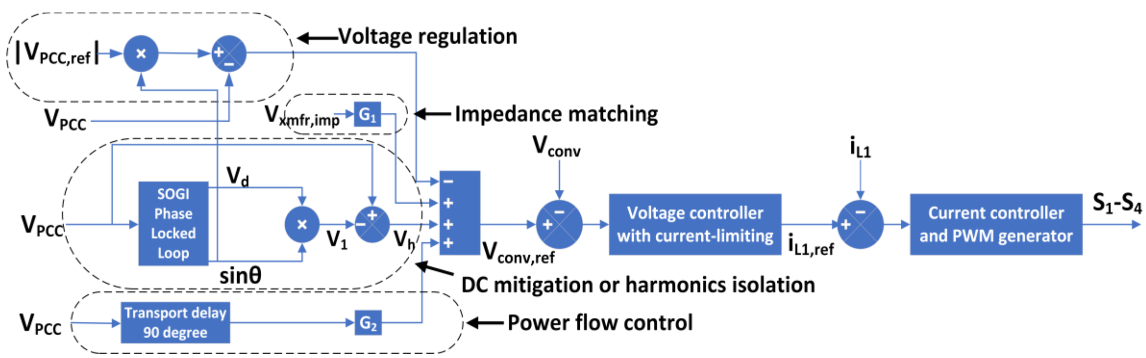

Figure 3.4: PWM generation for the hybrid smart transformer conversion module.

The transformers utilized for transmission purpose are typically three-phase, preferrably built by connecting three single-phase units in appropriate configuration to ease transportation and replacement [72]. The proposed smart transformer configuration for three-phase systems is shown in Figure 3.5 where the previously introduced power-electronics scheme is integrated between the neutral of each transformer and substation ground. The integration configuration of the proposed module allows its applicability to majority of transformer configurations including GSU transformers.

The evaluation of the above discussed converter-based approaches against the criteria developed by the NERC GMD Task Force is presented in table A1 in Appendix A.

This provides insight into the respective features of the two strategies and supports decision making regarding design of specific converter-based solutions depending upon whether DC elimination is the sole objective, or the objective is grid servicing in addition to DC mitigation. A comparison of functionalities of existing FACTS devices and proposed HST scheme is shown in table A2 in Appendix A.

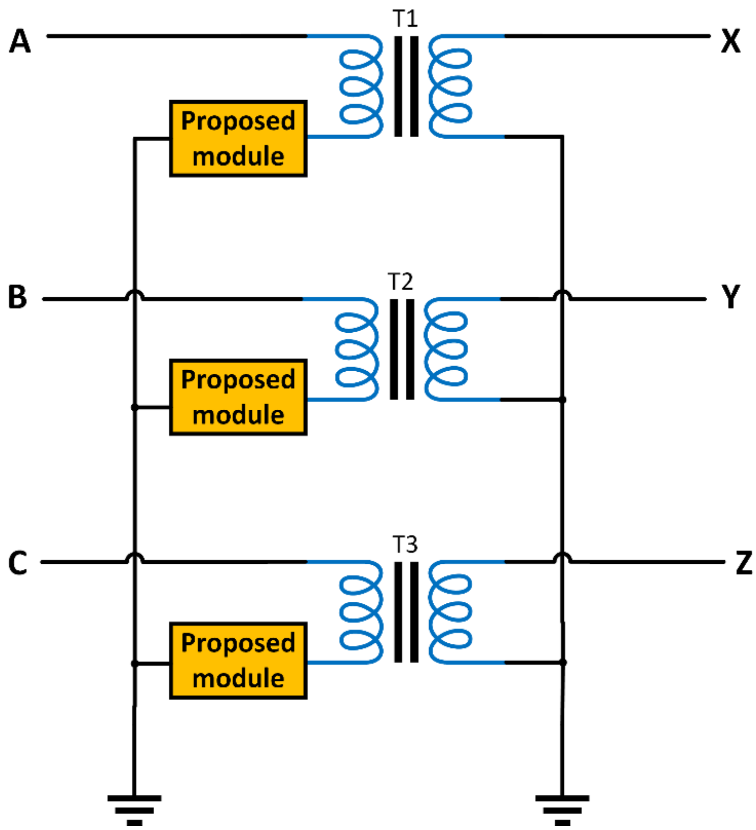

Figure 3.5: Proposed scheme for three single-phase transformers.

Implementation of Proposed HST on a Benchmark Transmission System

The next generation power grid is characterized by two-way flow of electricity and information with advanced smart grid features. The need for smart grids arose due to the desire to have an efficient and reliable supply of electricity for the consumers. Over the decades, the power infrastructure has rapidly transformed from a radial structure into a highly complex meshed power network. There has been a large growth of volatile distributed energy resources (DERs); photovoltaic (PV) and wind farms, that has increased the significance of distributed, autonomous, precise, and reliable control mechanisms. The grid interconnection of DERs is governed by IEEE 1547-2018 [73], that demands them to include a variety of capabilities, where VRT; low voltage ride-through (LVRT) and high voltage ride-through (HVRT) bear prime importance for sub-transmission systems. The LVRT is critical to avoid cascaded failure of generation sources due to increased power demand during low-voltage events. The HVRT is also vital as inverters are programmed to shut down when grid voltage crosses a pre-defined threshold to avoid grid overvoltages [74]. Another important consideration associated to DERs is their volatility that affects the power flows resulting in congestion, inability to fully utilize transmission capacity, thus, leading to curtailment of DERs and inefficient operation. The traditional power flow control utilizing different generator dispatch algorithms is no longer the best solution and is continuously being replaced with distributed control mechanisms [75]. The electric utilities are also relentlessly striving to improve the power quality as it saves cost and enhances efficiency of grid operation [76].

This section focuses on implementation of the proposed hybrid smart transformer strategy on a benchmark transmission system. The IEEE-9 bus benchmark system is utilized with certain modifications to verify the efficacy of the proposed approach. The 90MW, 30MVAR load on bus 6 is connected via a 100MVA, 230kV/69kV smart transformer. A non-linear load is added to bus 4 to inject harmonics into the grid. A

50MVA, 480V photovoltaic (PV) farm is also connected to the grid at bus 5 through a 50MVA, 480V/33kV wye-grounded/delta transformer and later stepped up to 230kV for grid interconnection utilizing a 50MVA, 33kV/230kV wye-grounded/wye-grounded main output smart transformer (MOT). A DC source is utilized on the primary of the smart transformer at bus 6 to mimic the effect of GIC flowing in a transmission network following a GMD event [77]. The overall system under study is shown in Figure 3.6. The simulation results for the scenario depicted in Figure 3.6 are presented in Chapter 4.

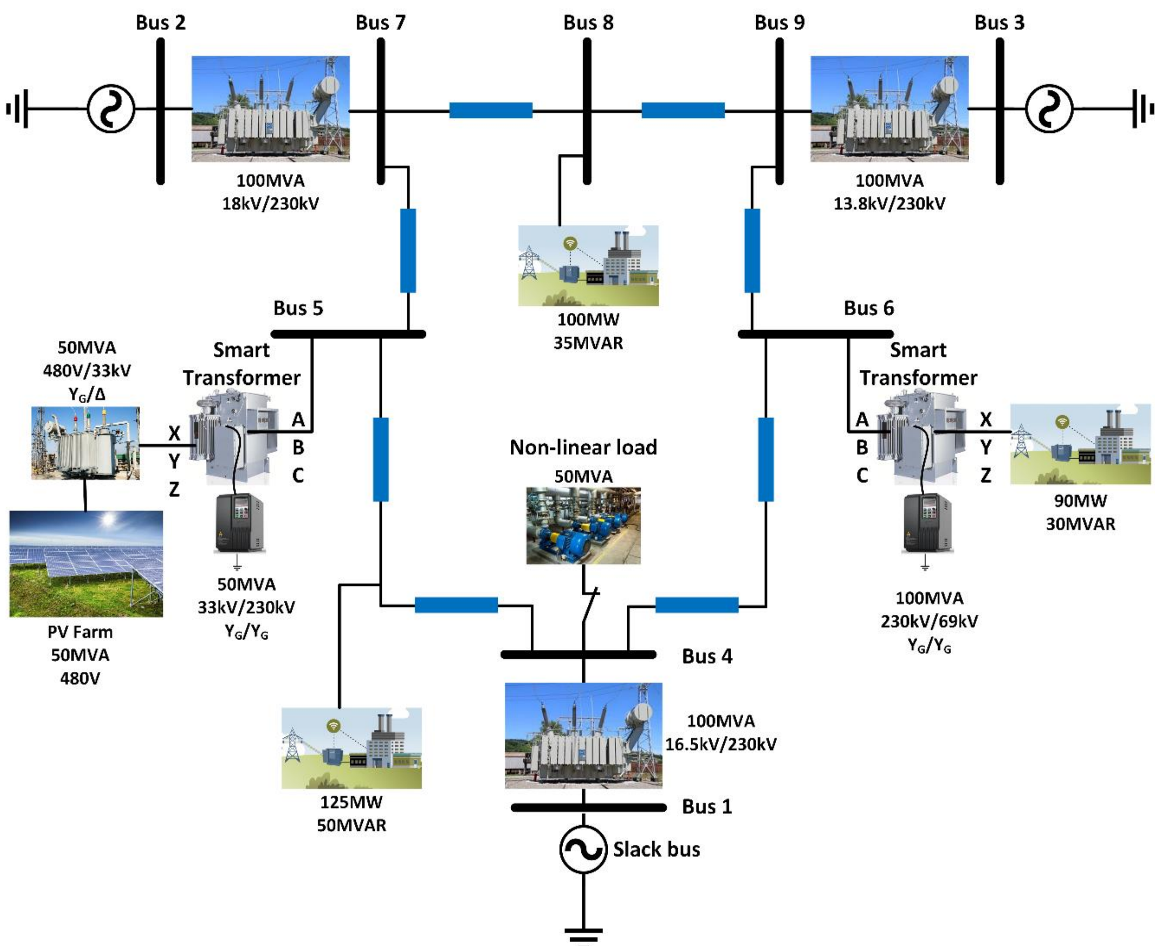

Figure 3.6: Modified IEEE-9 bus system for the current study.

Laboratory Scale Hardware Prototype of Proposed HST

The proposed hybrid transformer strategy is verified on a laboratory scale hardware prototype developed in the power electronics lab as shown in Figure 3.7 with its one-line diagram shown in figure 3.8. It consists of a 1:1 single-phase transformer under test (TUT) supplied from a variac and an isolation transformer to mimic sag/swell on the grid and for personnel safety purposes, respectively. An RL load is attached to the secondary of the TUT loading it to 80% of its rated capacity. To mimic the flow of DC in power lines resulting from the previously discussed natural or man-made events, a DC supply is integrated in the neutral of the isolation transformer. The hybrid transformer conversion module is realized utilizing an IGBT converter/chopper module from Semikron and its operation in a single-phase configuration. The DC link is charged utilizing a variac and an isolation transformer for controlled input and personnel safety, respectively. For experimental DC-link regulation, the DC chopper is activated above a pre-defined threshold followed by the reverse power dissipation across a braking resistor. In the practical scenario, it is desirable to store the reverse active power flow utilizing battery storage with the DC-link and supplying this stored power to the main grid when required. The Typhoon HIL-402 is utilized as a controller for the inverter/chopper module by operating it in a power hardware-in-the-loop (P-HIL) configuration. However, the maximum digital output of Typhoon HIL is 5V that is unable to switch the IGBTs in the module that operate at a 15V pulse signal. To resolve this issue, a Texas Instrument (TI) voltage level shifter IC CD-4504BE is integrated to the digital output of Typhoon.

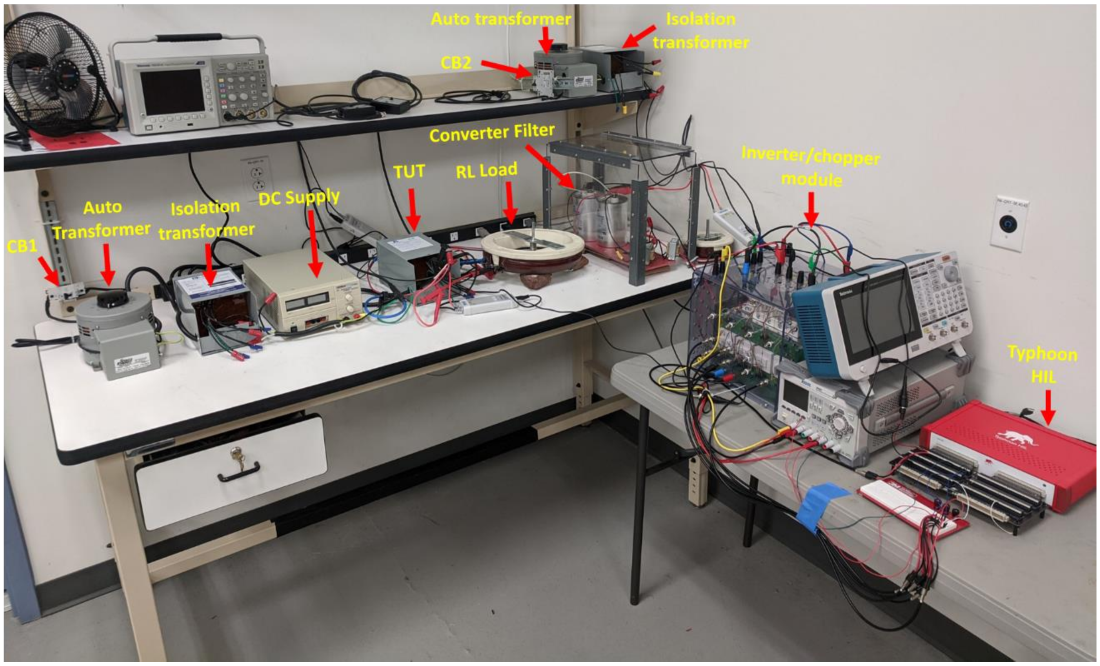

Figure 3.7: Experimental hardware prototype to verify the proposed strategy.

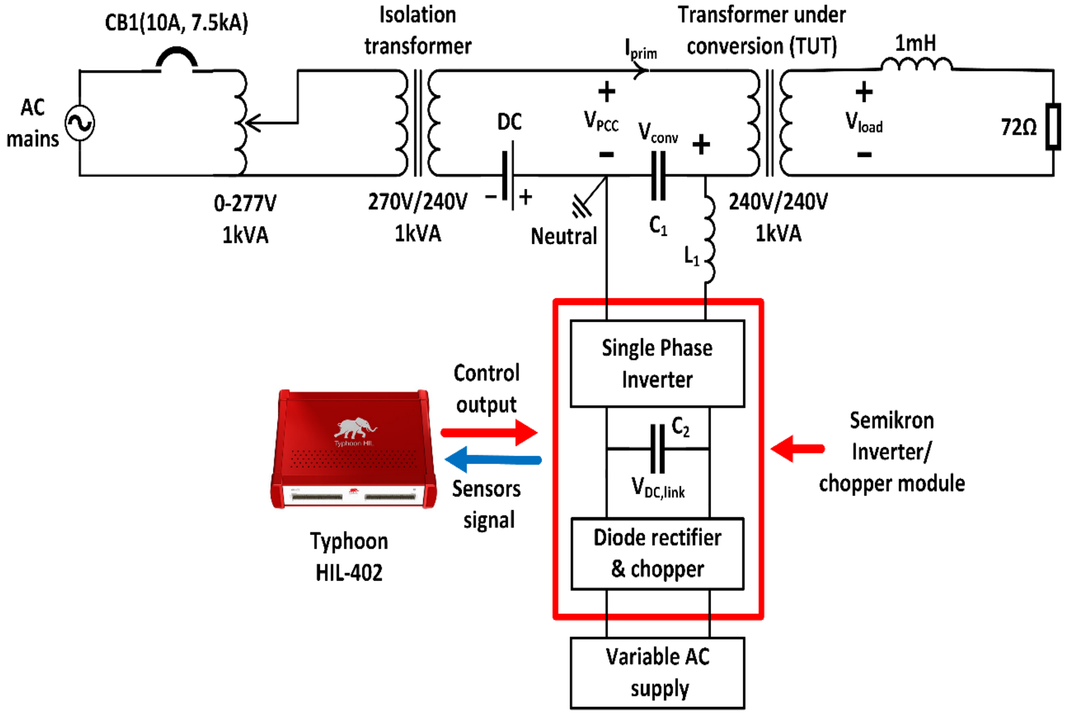

Figure 3.8: One-line diagram of the hardware prototype.

The important equipment and control parameters of the hardware prototype are listed in table 3.1.

TABLE 3.1
PARAMETERS FOR HARDWARE PROTOTYPE

Item	Description
TUT transformer	240V/240V, 1kVA
IGBT/chopper module	Semikron B6U+E1C1F+B6C1
Converter controller	Typhoon HIL-402
Voltage controller	K_p=0.05, K_i=165, Limit=-4 to 4
Current controller	K_p=0.1, K_i=50, Limit=-1 to 1
Switching frequency (f_{sw})	5kHz
Level converter IC	TI CD-4504BE
Filter capacitor (C_1)	50uF
Filter inductor (L_1)	1mH, 10A
Solid state relay	Crydom D2490-10
Mechanical relay	Hiltego 5V, 10A

CHAPTER FOUR

CONTROLLER HARDWARE IN THE LOOP (C-HIL) AND POWER HARDWARE IN THE LOOP (P-HIL) RESULTS

C-HIL Results

After presenting the converter-based schemes for DC mitigation and grid support in the previous chapter, the concept and control approach are evaluated and verified with a Typhoon Hardware-in-the-Loop (HIL) 402 real-time simulator. The HIL-402 unit consists of 4 cores, 16 analog input, 16 analog output, 32 digital input and 32 digital output channels. The HIL control center is utilised to build the power stage that simulates in real time within the HIL unit. The unit provides the interface board for the third party controllers to simulate the control stage. The overall test setup is shown in Figure 4.1. The setup is utilized to test and verify the real time performance of the Texas Instrument (TI) controller TMS320f28335 with the designed power stage in the Typhoon software. The next section presents the C-HIL simulation results and its associated discussion.

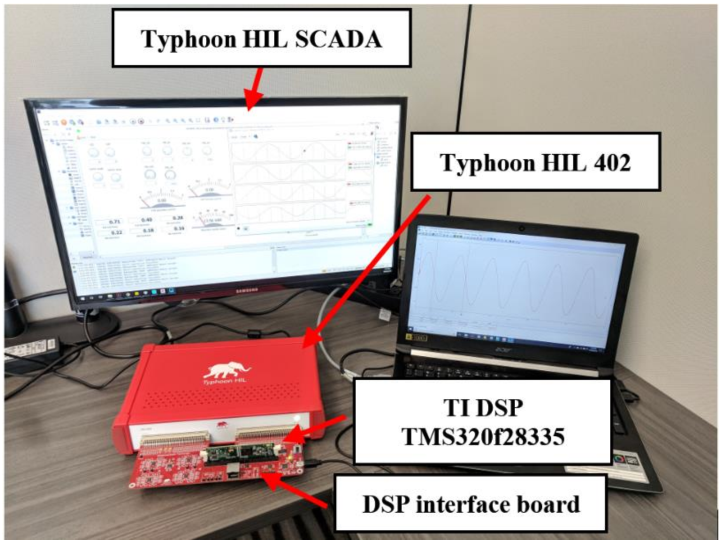

Figure 4.1: C-HIL setup to verify proposed approach

The different circuit elements and the transformer parameters utilised for the proposed chopper-based GIC mitigation approach are presented in Table 4.1.

TABLE 4.1
SYSTEM PARAMETERS FOR DC CHOPPER-BASED SOLUTION

Circuit Component		Component value
C_1		18uF
R_1		1 Ω
L_1		100uF
V_{DC}		100V
Transformer	$V_{primary}$	230kV
	$V_{secondary}$	69kV
	MVA	100

First, the transformer in Figure 3.1 is operated in the half-cycle saturation mode for which DC signals are applied using the series voltage sources between the three-phase transformer and the source. In order to observe the performance of the proposed strategy, variable injected DC voltage signals of equal magnitude are utilized, with the converter deactivated, and the transformer primary and neutral currents are recorded. The results are shown in Figure 4.2. It can be observed in Figure 4.2 (a) that a variable DC voltage signal upto a maximum amplitude of 200V is applied. The resulting primary currents of the transformer can be seen in Figure 4.2 (b), where it is observed that the transformer enters the half-cycle saturation mode when the DC voltage crosses a certain threshold. The neutral current of the transformer is presented in Figure 4.2 (c), where the neutral current magnitude increases in proportion to the half-cycle saturation of the transformer. Now, the

DC chopper is activated and all the previously mentioned signals are again recorded. The results are presented in Figure 4.3.

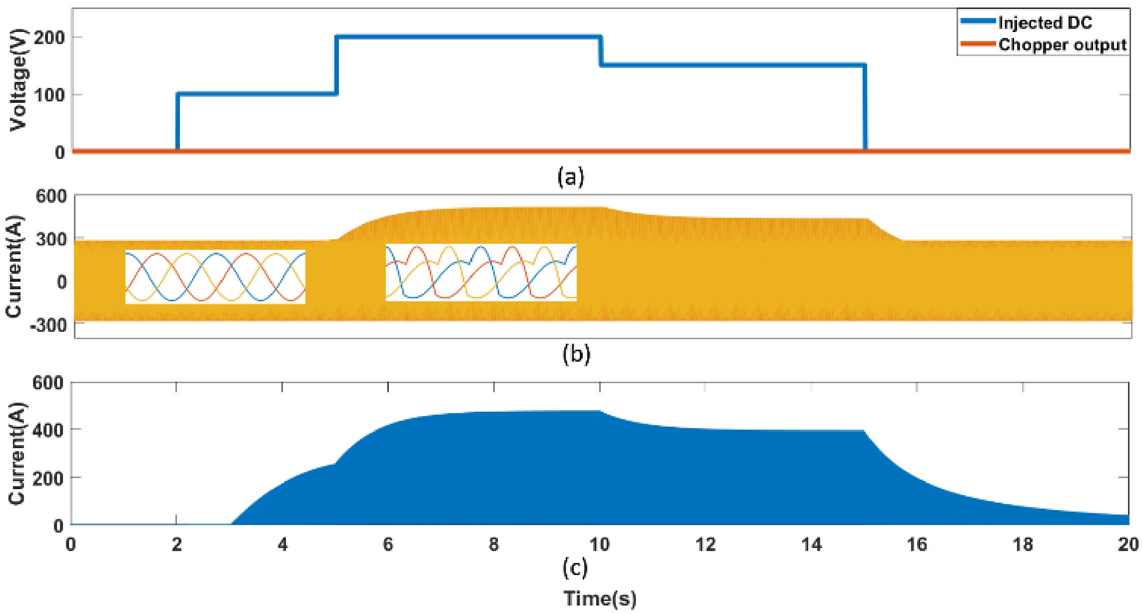

Figure 4.2: Chopper deactivated: (a) Injected DC and chopper output, (b) primary current, (c) neutral current.

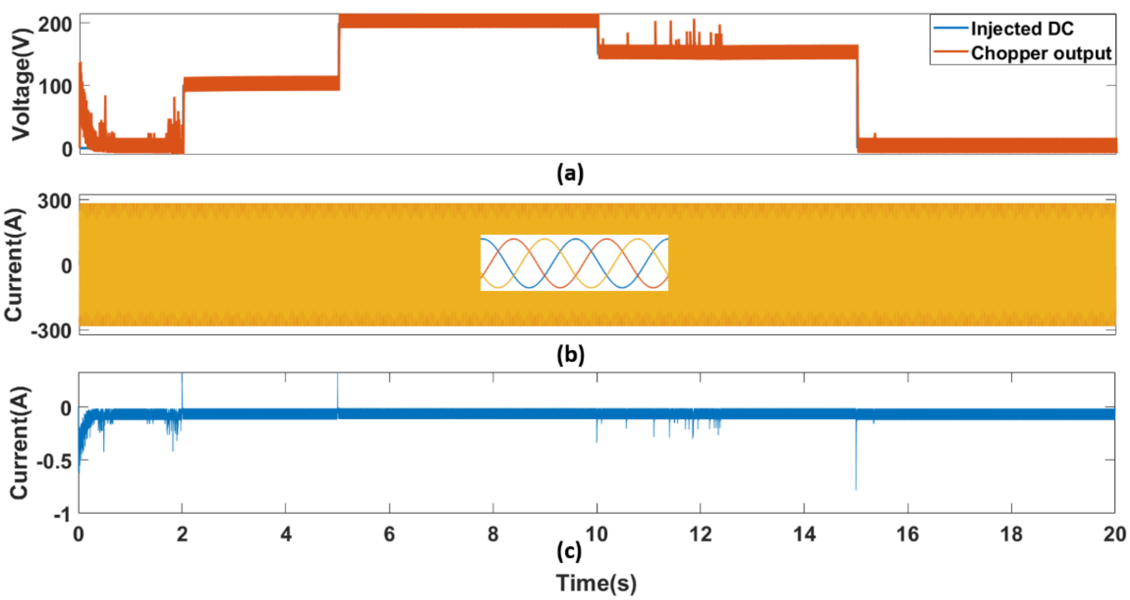

Figure 4.3: Chopper activated: (a) Injected DC and chopper output, (b) primary current, (c) neutral current.

It can be seen in Figure 4.3 (a) that the chopper effectively follows the applied DC voltage, where the chopper output noise in the period 10-15s can be eliminated with further optimization of the associated PI controller. The configuration in Figure 3.1 suggests that the chopper output voltage counters the applied DC voltage, thus nullifying the impact of DC on the power systems. This can be seen in Figure 4.3 (b) that the transformer primary currents have now recovered back to their normal operation. Also, it can be observed in Figure 4.3 (c) that the transformer neutral current has almost died out. The results show that the DC chopper-based solution is an effective DC mitigation strategy.

Now, the performance of the proposed converter-based hybrid smart transformer strategy in Figure 3.2 is analyzed. For this study, the circuit elements and the transformer parameters are presented in Table 4.2.

TABLE 4.2
SYSTEM PARAMETERS FOR CONVERTER-BASED SOLUTION

<table>
<tr><th colspan="2">Circuit Component</th><th>Component value</th></tr>
<tr><td colspan="2">C_1</td><td>100uF</td></tr>
<tr><td colspan="2">C_2</td><td>2.3mF</td></tr>
<tr><td colspan="2">L_1</td><td>3mH</td></tr>
<tr><td colspan="2">L_s</td><td>1mH</td></tr>
<tr><td colspan="2">L_l</td><td>1mH</td></tr>
<tr><td colspan="2">R_l</td><td>3Ω</td></tr>
<tr><td colspan="2">V_{dc}</td><td>60kV</td></tr>
<tr><td rowspan="3">3φ-Transformer</td><td>$V_{primary}$</td><td>765kV</td></tr>
<tr><td>$V_{secondary}$</td><td>345kV</td></tr>
<tr><td>MVA</td><td>900</td></tr>
</table>

First, the filter performance is observed for DC injection into the three-phase transformer. The primary line currents and line-to-neutral load voltages are recorded and presented in Figure 4.4, where the lower plot shows the compensation signal applied by the proposed filter. It is observed that the filter effectively isolates the harmonics from reaching the load. After that, an imbalance is created in the supply voltage, with two of its phases falling below the nominal value. This will resemble a real-world scenario of a high-voltage transformer experiencing voltage sag and unbalance. In the meantime, DC is also injected into the transformer. The performance of the filter for this case is shown in Figure 4.5, where it can be observed that the proposed filter effectively balances the load voltage, recovers its nominal value, and removes harmonics introduced by the flow of DC. The C-HIL results verify the overall capabilities of the proposed series power filter to restore the voltage balance, perform harmonics isolation, perform regulation of the load voltage in addition to DC elimination.

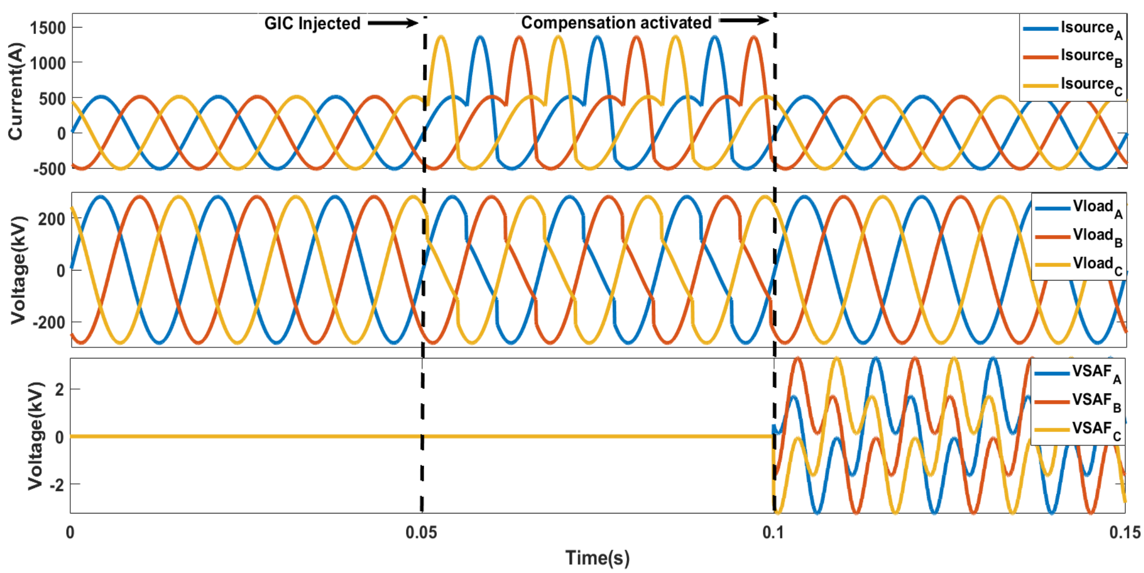

Figure 4.4: Proposed filter performance under DC injection; Top subplot shows line currents on HST primary, middle subplot shows load voltages, bottom subplot shows the generated compensation signals.

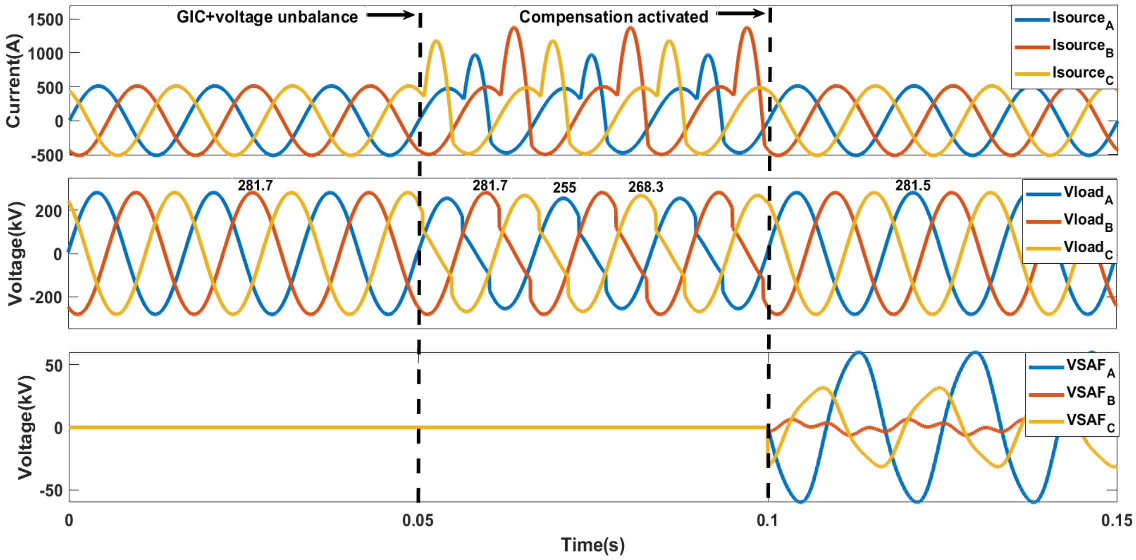

Figure 4.5: Proposed filter performance under DC, voltage sag and unbalance; Top subplot shows line currents on HST primary, middle subplot shows load voltages, bottom subplot shows the generated compensation signals.

The modified IEEE-9 bus system presented in the previous chapter is simulated in Typhoon-HIL environment to verify the working of the proposed strategy. The smart transformer conversion module parameters are shown in Table 4.3.

TABLE 4.3
PARAMETERS FOR PROPOSED MODULE

Circuit Component	Component value
C_1	100uF
C_2	2.3mF
L_1	1mH
V_{dc}	25kV

The individual functionality of the proposed device is depicted under respective scenarios.

Harmonics Injection

Firstly, the ability of the proposed device to perform harmonics rejection is verified. From this perspective, the voltage, and current signals on the load side of the smart transformer on bus 6 are desired to be harmonic free. The source of harmonics on the grid side might be the non-linear load on bus 4 or those generated by the flow of DC in the transmission lines. Both these harmonic sources are individually activated followed by stimulating them together to verify the harmonics elimination capability of the proposed module. The results are shown in Figure 4.6 and Figure 4.7 for the individual scenarios followed by the combined scenario in Figure 4.8, where it is observed that the module effectively isolates the grid-side harmonics from travelling further towards the load side of the smart transformer. The time delay in the middle section is deliberately introduced to depict the transformer behavior without the proposed module. In a real-world scenario, the module initiates the harmonics isolation operation in 1.08 milliseconds.

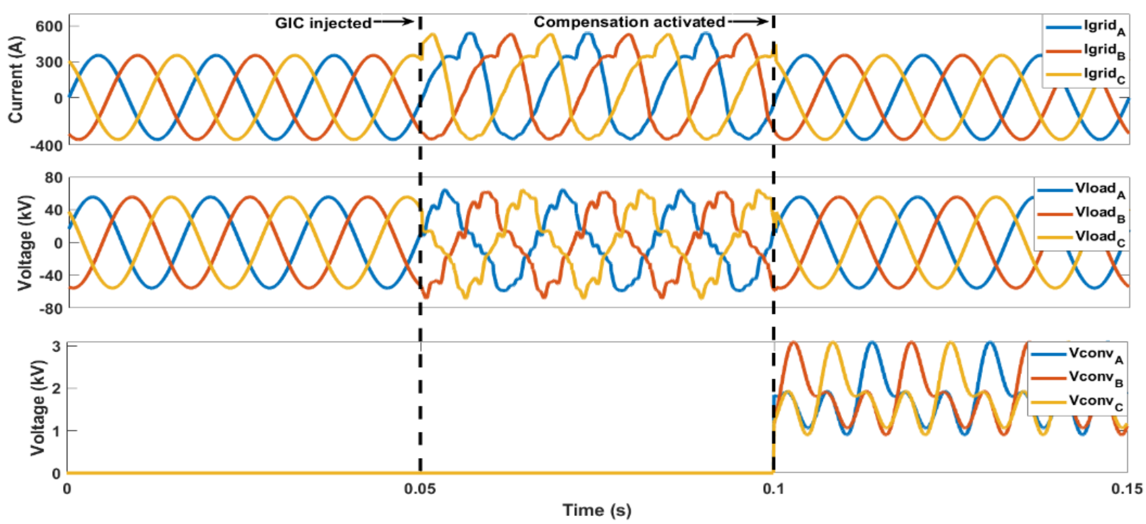

Figure 4.6: Proposed device performance under DC injection; Top subplot shows primary line currents of HST connected to bus 6, middle subplot shows transformer load voltages, bottom subplot shows the compensation signals generated by proposed module.

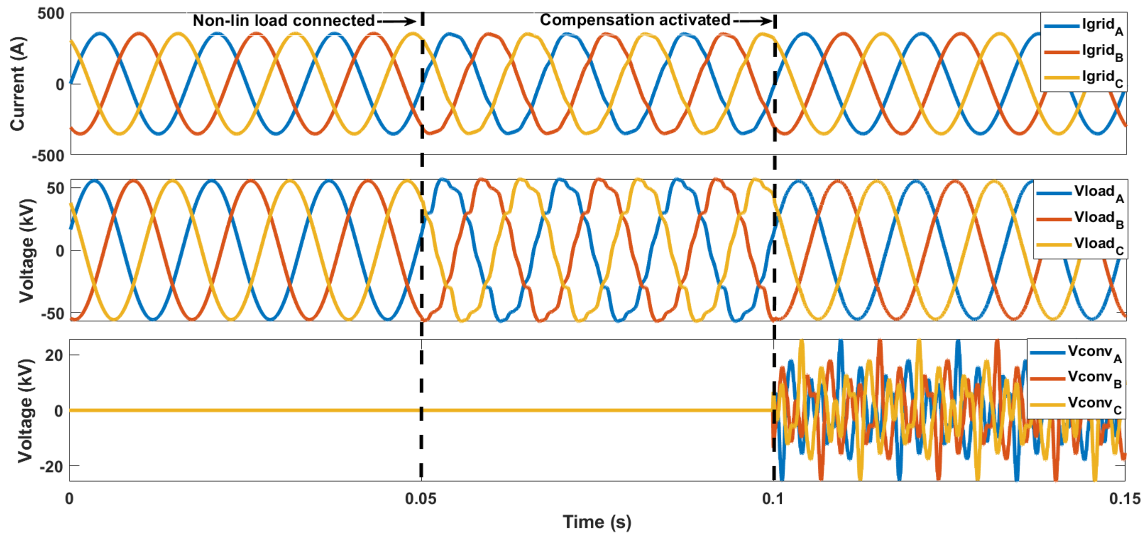

Figure 4.7: Proposed device performance with a non-linear load on bus 4; Top subplot shows primary line currents of HST connected to bus 6, middle subplot shows transformer load voltages, bottom subplot shows the compensation signals generated by proposed module.

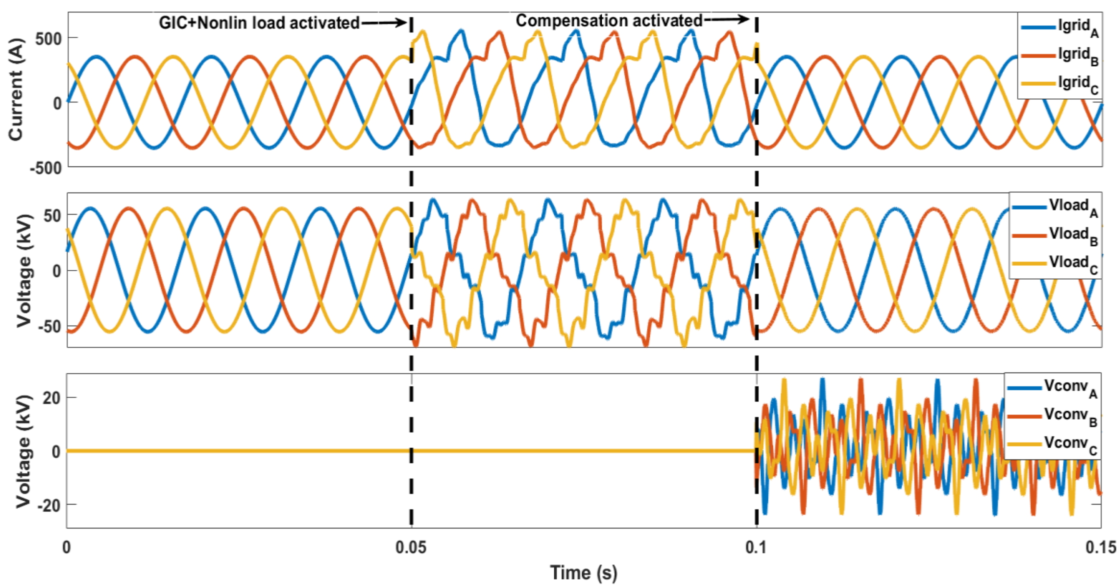

Figure 4.8: Proposed device performance under DC injection and non-linear load; Top subplot shows primary line currents of HST connected to bus 6, middle subplot shows transformer load voltages, bottom subplot shows the compensation signals generated by proposed module.

Now we consider the case in which the non-linear load at bus 4 is connected to the grid through the proposed smart transformer. The objective in this case is to mitigate the load harmonics travelling towards the grid. The module performance for this case is depicted in Figure 4.9, where, the total harmonic distortion (THD) of the grid volage at PCC drops from 5% to 2% leading to substantial drop in the grid harmonics.

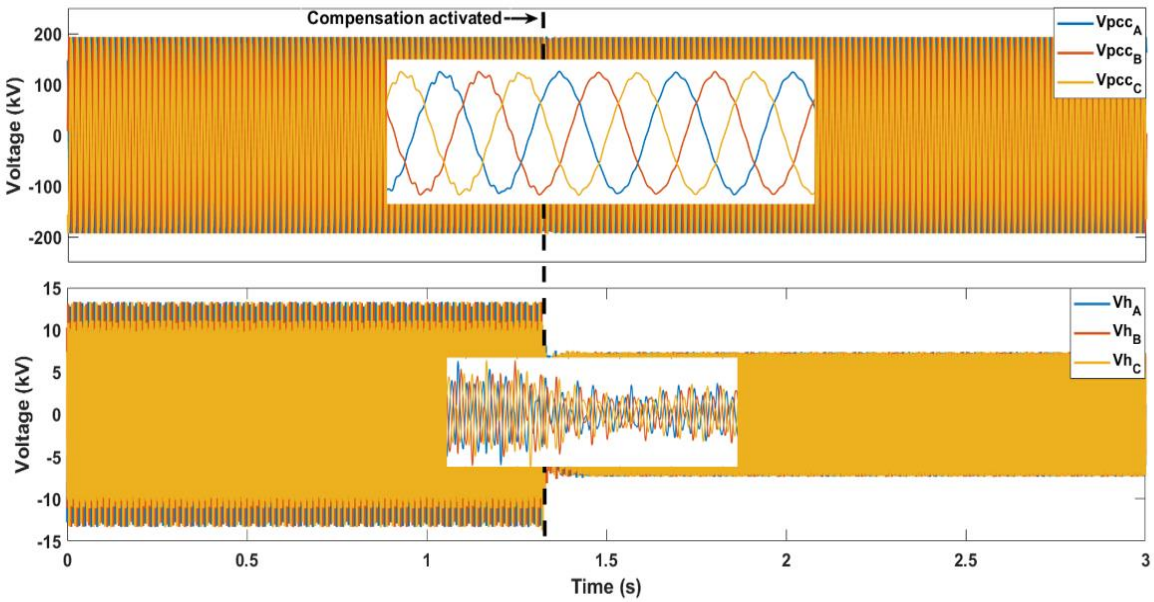

Figure 4.9: Mitigation of non-linear load harmonics by proposed module; Top subplot shows line voltages on HST primary if connected to non-linear load on bus 4, bottom subplot shows the compensation signals generated by proposed module.

Voltage Sag/Swell

In order to initiate a voltage sag on the IEEE-9 bus system, the voltage magnitudes of the three power sources are reduced to 0.85pu. The objective of voltage sag mitigation is to culminate it from disturbing the load voltage on bus 6. The performance of the module is depicted in Figure 4.10, where it is observed that the proposed smart transformer effectively restores the desired load voltage.

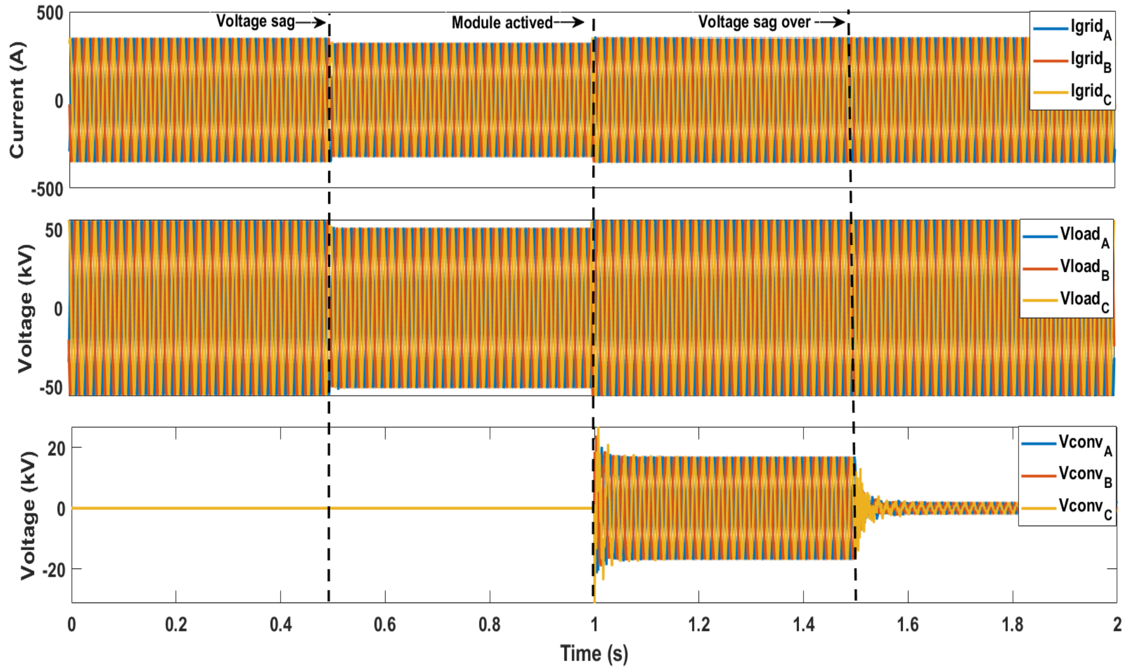

Figure 4.10: Proposed smart transformer operation under grid-voltage sag; Top subplot shows primary line currents of HST connected to bus 6, middle subplot shows transformer load voltages, bottom subplot shows the compensation signals generated by proposed module.

To generate a voltage swell, the respective voltage magnitudes are raised to 1.15pu. The performance of the module for this case is shown in Figure 4.11, where the proposed smart transformer successfully maintains the desired load voltage. The voltage regulation capability of the module has a myriad of applications to the contemporary and future grid due to the addition of volatile renewable energy sources. The traditional autotransformers utilize electro-mechanical taps for varying the turns ratio to achieve desired voltage levels. Due to the rapidly varying power generation from renewables, these taps undergo switching at a high rate that introduces significant wear and tear and is accompanied with substantial delays that are not desirable for grid reliability. To avoid excessive deterioration, deliberate delays are introduced in the tapping operation that further adds to these undesirable control delays. The power electronics enable smart, rapid, and distributed control with much higher resolution and advanced control features. Therefore, the proposed approach could be utilized to enhance the lifetime of the traditional transformers and to provide rapid precise control over the grid voltage levels.

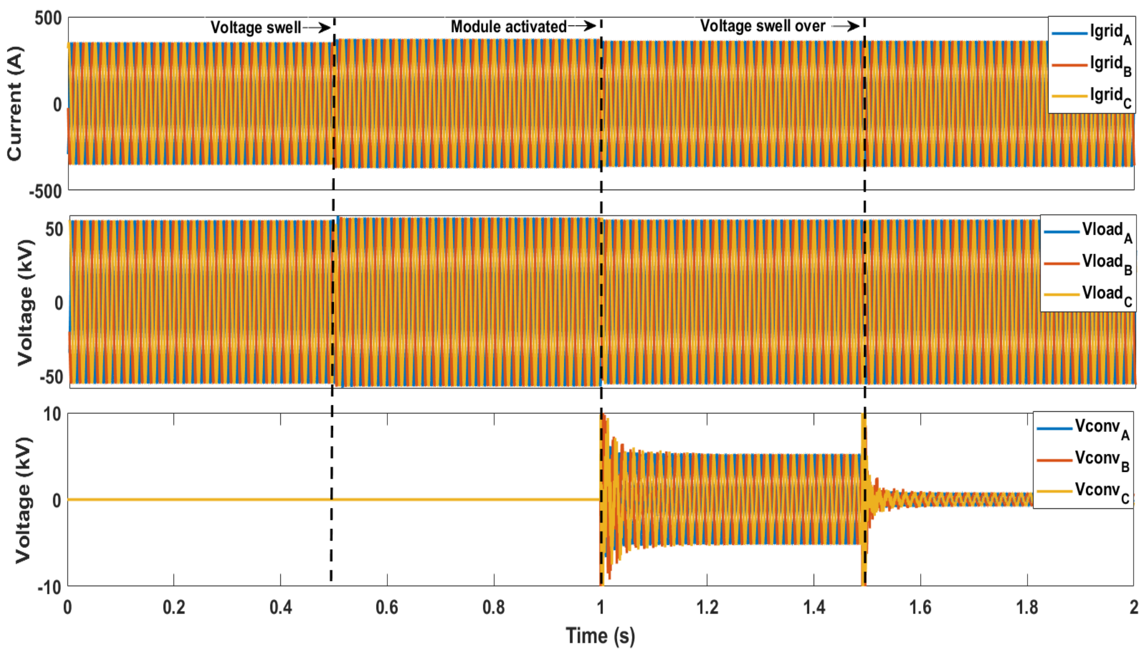

Figure 4.11: Proposed smart transformer operation under grid-voltage swell; Top subplot shows primary line currents of HST connected to bus 6, middle subplot shows HST load voltages, bottom subplot shows the compensation signals generated by proposed module.

The voltage control strategy discussed above could also be utilized to support the VRT requirements for the DERs according to IEEE 1547-2018 or for grid connected IBRs as per IEEE 2800-2022. A 50MVA PV farm is connected on bus 5 of the IEEE-9 bus system through a smart transformer. The modern PV farms are equipped with dynamic grid-support capability that enables them to inject/absorb reactive power in event of grid voltage sag/swell. This capability is limited by the inverter current rating that could be solved by utilizing over- rated converters that is accompanied with an additional expense. The proposed module can share the reactive support capability by working as a STATCOM. To demonstrate this capability, it is assumed that the PV farm is delivering 45MW to the grid. In the meantime, a voltage sag is initiated on the grid by reducing the source voltages to 0.85pu. In a real-world scenario, the momentary voltage sag could be the result of grid faults or generation loss. The reactive support function gets activated that drops the active power to perform the desired grid-support function as shown in Figure 4.12.

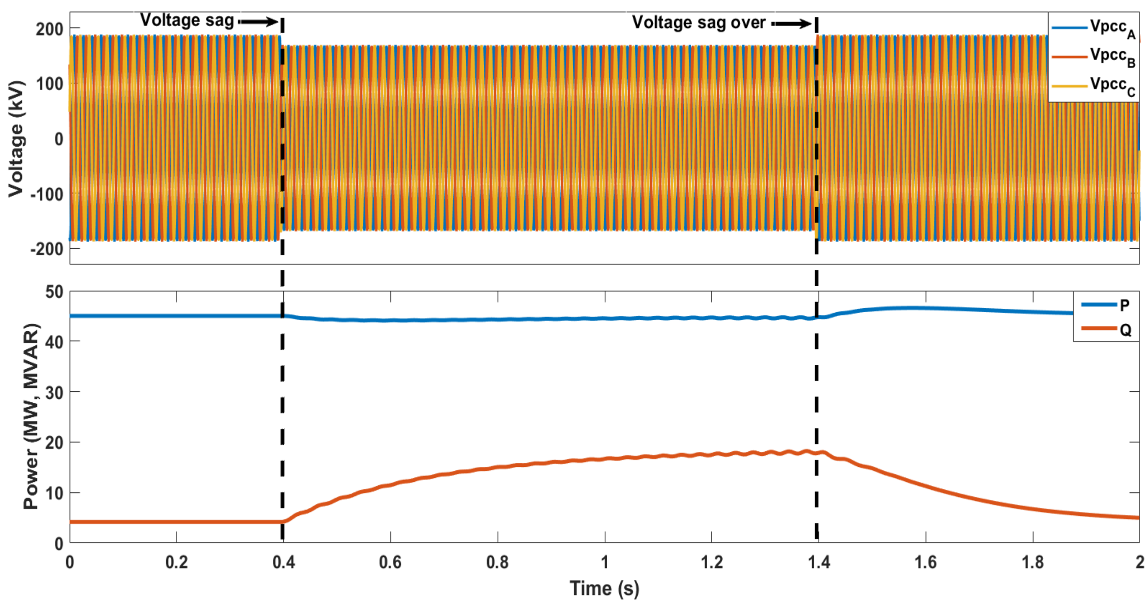

Figure 4.12: PV farm reactive power support under grid-voltage sag; Top subplot shows HST primary voltages, bottom subplot shows the P, Q supplied by PV farm without support from proposed module.

However, the active power is also crucial during voltage sags to avoid grid under frequency operation or collapse. Under this scenario, the reactive power demand could be shared between the PV farm and the proposed module as shown in Figure 4.13. Similarly, for a voltage swell on the grid, the device can share the absorption of reactive power. It is worthy to mention that IEEE 1547-2018 doesn't allow the distributed PV power generation to contribute to the reactive grid support. Correspondingly, the PV inverters are not equipped with the reactive power support capability. The proposed device finds its application at the distribution level by providing momentary VRT services to the distributed PV systems. The inverters are programmed to shut down if the grid voltage falls outside the 0.85-1.05pu limit that could be avoided utilizing the proposed module that helps to maintain the terminal voltage of the distributed PV inverters.

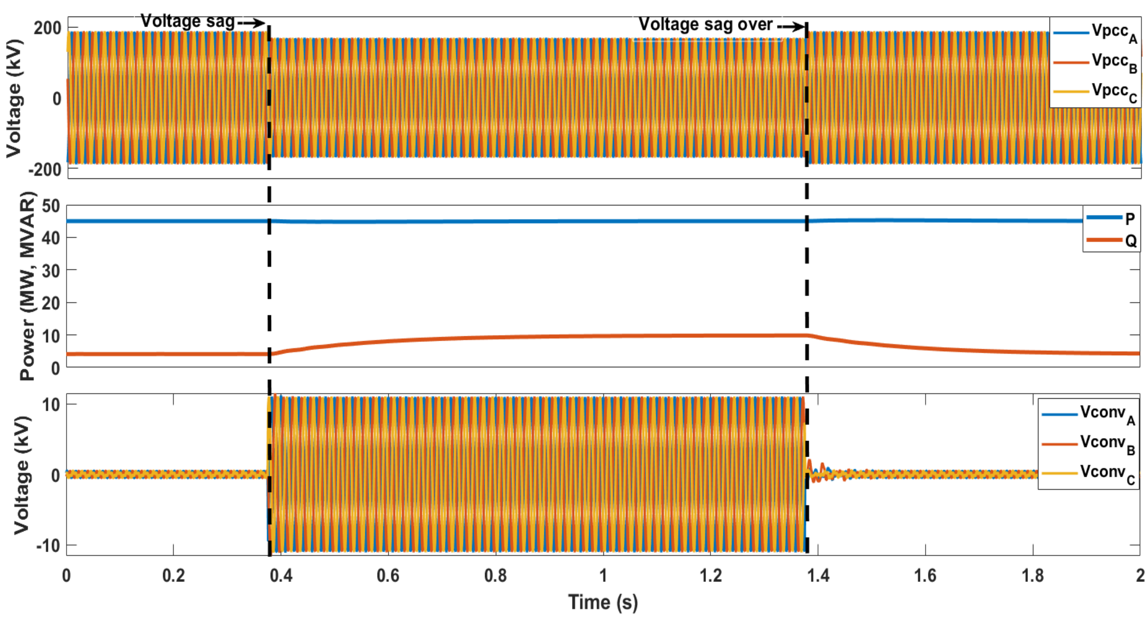

Figure 4.13: PV farm reactive power support under grid-voltage sag; Top subplot shows HST primary voltages, middle subplot shows the P, Q supplied by PV farm with support from proposed module, bottom subplot shows the compensation signals generated by proposed module.

Voltage Unbalance

The transmission systems are typically balanced systems with occasional unbalance not exceeding 10%. The traditional strategies to recover from the grid unbalance are line transposition and static VAR compensators (SVCs) that are accompanied with an additional expense. Apart from the functionalities of the proposed device in the previous sections, it is also capable of restoring the grid balance. For this purpose, an additional load of 50Ω is connected to phase A at bus 4 of the IEEE-9 bus system. The smart transformer operation under this scenario is shown in Figure 4.14, where it effectively restores the voltage unbalance on the downstream side. Although the operation of the module is depicted on a benchmark transmission system, it is also highly relevant for the distribution transformers that typically operate under unbalanced scenarios. The unbalance could be the result of either a load mismatch on the three phases or a generation mismatch under the contemporary scenario of growing grid-connected rooftop PV systems.

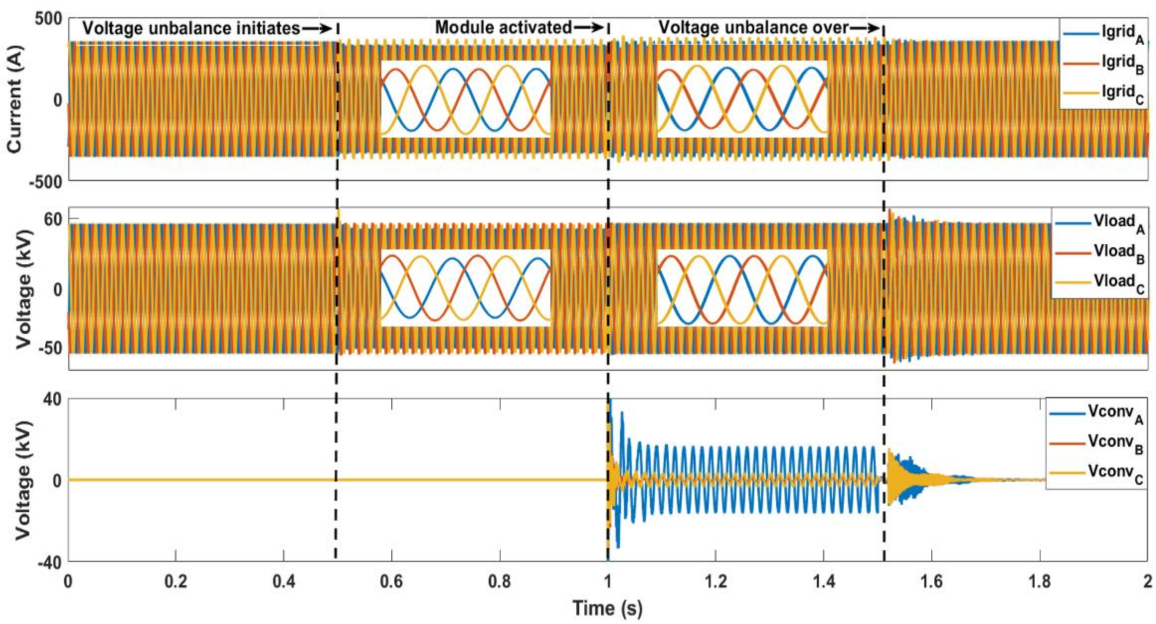

Figure 4.14: Voltage balance restoration by the proposed module; Top subplot shows primary line currents of HST connected to bus 6, middle subplot shows HST load voltages, bottom subplot shows the compensation signals generated by proposed module.

Impedance Mismatch

The electric utilities often encounter situations where single phase or three-phase transformers are replaced either due to upgradation or the result of an irreversible damage. As neither of the two units are exactly identical, there always exists an impedance mismatch. This leads to non-uniform flows over three phases of a single transformer or through parallel transformers. The ultimate result is either congestion or unutilized transmission capacity across certain power corridors. The proposed smart transformer conversion module has the capability to nullify the resultant effects of impedance mismatch as discussed in section 3.3. To verify this case, we add an external impedance to phase A of the transformer connected to bus 6 as shown in Fig. 4.15. This leads to unbalanced power flows across the three phases. The device is activated and the gain G_1 is adjusted to compensate for this mismatch. The result before and after compensation are presented in table 4.4.

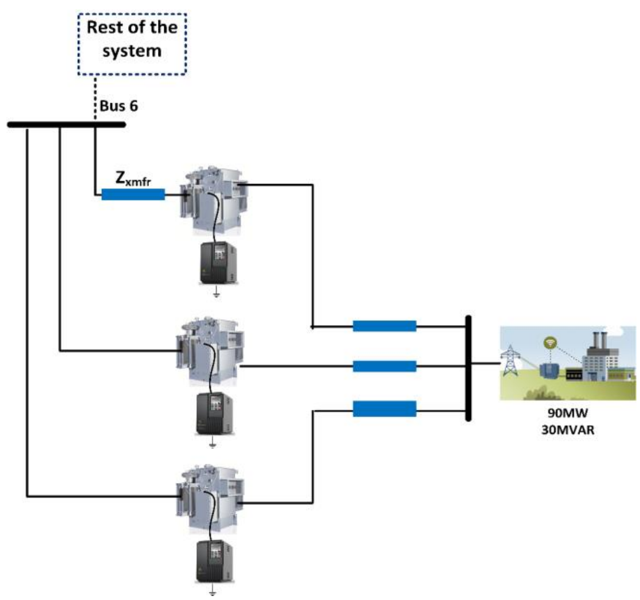

Figure 4.15: Modifications to depict impedance control feature of proposed module.

TABLE 4.4
IMPEDANCE MISMATCH COMPENSATION BY PROPOSED MODULE
(G_{1A}, G_{1B}, G_{1C}: PER-PHASE IMPEDANCE GAIN)

P_1 (MW)			**Q_1 (MVAR)**		
P_a	**P_b**	**P_c**	**Q_a**	**Q_b**	**Q_c**
G_{1A}= 0, G_{1B}= 0, G_{1C}= 0					
30.82	30.91	30.97	12.51	12.38	12.46
G_{1A}= -0.56, G_{1B}= 0, G_{1C}= 0					
30.95	30.95	30.95	12.40	12.40	12.40

Power Flow Control

To analyse the power flow control capability of the proposed device, a parallel wye-grounded/wye-grounded three-phase transformer T_2 is connected to bus 6, as shown in Figure 4.16. Depending upon the parameters of this additional transformer, the active and reactive power divides between the two transformers. We now adjust the gain G_2 of the smart transformer conversion module which effectively alters the power angle between the bus 6 and the transformer T_1. This leads to modified power flow through T_1 and ultimately T_2. This module also has the capability to vary the power flow across individual phases of a transformer. The results for different gain G_2 values and the resultant power flows are shown in table 4.5, where 1-2% of the line voltage injection is sufficient to achieve significant power flow variation across the two transformers.

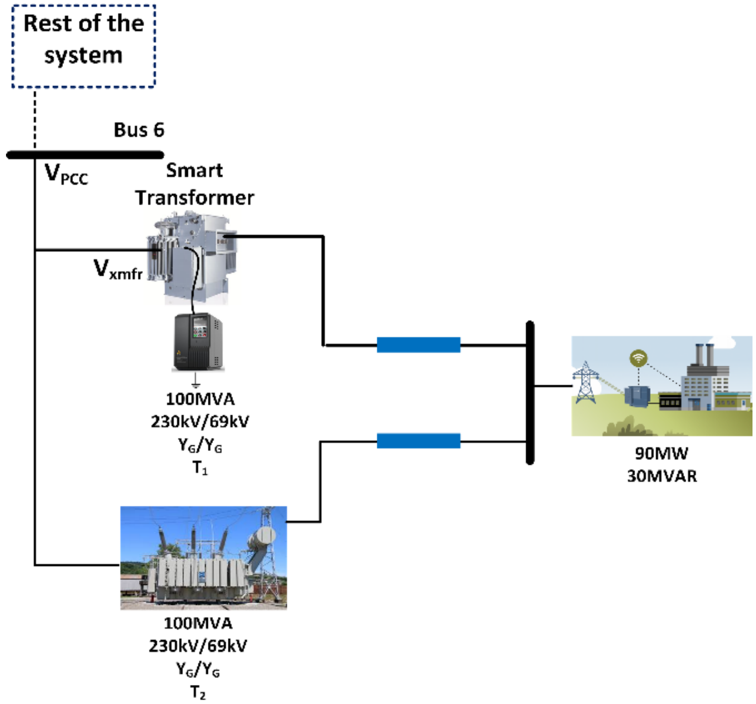

Figure 4.16: Modifications to depict PQ control performance of proposed module.

TABLE 4.5
POWER FLOW CONTROL BY PROPOSED MODULE
(G_{2A}, G_{2B}, G_{2C}: PER-PHASE POWER-FLOW GAIN)

P_1 (MW)			Q_1 (MVAR)			P_2 (MW)			Q_2 (MVAR)		
P_a	**P_b**	**P_c**	**Q_a**	**Q_b**	**Q_c**	**P_a**	**P_b**	**P_c**	**Q_a**	**Q_b**	**Q_c**
G_{2A}= 0, G_{2B}= 0, G_{2C}= 0											
23.82	23.83	23.83	9.75	9.75	9.75	7.83	7.83	7.83	3.17	3.17	3.17
G_{2A}= -0.001, G_{2B}= -0.001, G_{2C}= -0.001											
23.24	23.24	23.24	9.30	9.30	9.30	8.05	8.05	8.05	3.20	3.20	3.20
G_{2A}= -0.01, G_{2B}= -0.01, G_{2C}= -0.01											
20.02	20.02	20.02	9.77	9.77	9.77	11.5	11.5	11.5	3.22	3.22	3.22
G_{2A}= -0.01, G_{2B}= 0, G_{2C}= 0											
20.05	23.76	23.85	9.80	9.75	9.77	11.5	7.81	7.84	3.27	3.18	3.18

This feature of the proposed module is highly desirable under current renewable generation integraton scenario. The volatile nature of DERs introduces congestion in certain parts of the grid accompanied with unutilized transmission capacities across others. The proposed high-speed distributed power-flow control across the transformers could help operate the grid within desired limits through fast redistribution of power thus helping to utilize the DERs at their maximum rated capacities.

Scaled Prototype Simulation Results

A simulation model was created for the laboratory scale hardware prototype whose results will be presented and compared with the actual hardware prototype. First, the DC mitigation performance of the proposed device is evaluated by injecting DC and entering the TUT into half-cycle saturation. Later, module is activated that effectivley counters the injected DC and returns the transformer to its normal operation as shown in Figure 4.17. A simulation of the proposed scheme is also performed for the case of a voltage sag that is generated by reducing the source voltage to 0.85pu. Later, the module is activated to restore the load voltage to its nominal value as shown in Figure 4.18. These two simulation results are discussed here to show the effectivness of the proposed scheme for a scaled prototype. In the next section, P-HIL results from a actual hardware protype are presented and discussed. Finally the simulation and hardware results are compared and discussed in the subsequent section.

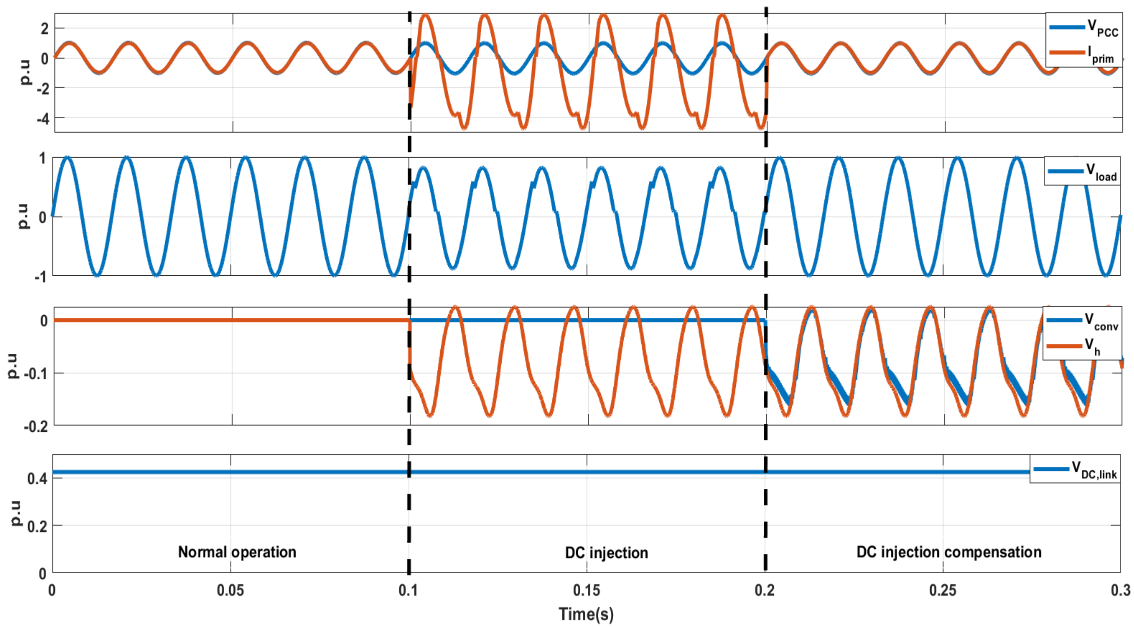

Figure 4.17: Proposed strategy simulation under harmonics injection for scaled prototype; Top subplot shows voltage (V_{PCC}) and current (I_{prim}) on HST primary, second subplot shows HST load voltage (V_{load}), third subplot shows harmonic content in HST primary voltage (V_h) and compensation signal generated by proposed module (V_{conv}), bottom subplot shows DC link voltage ($V_{DC,link}$).

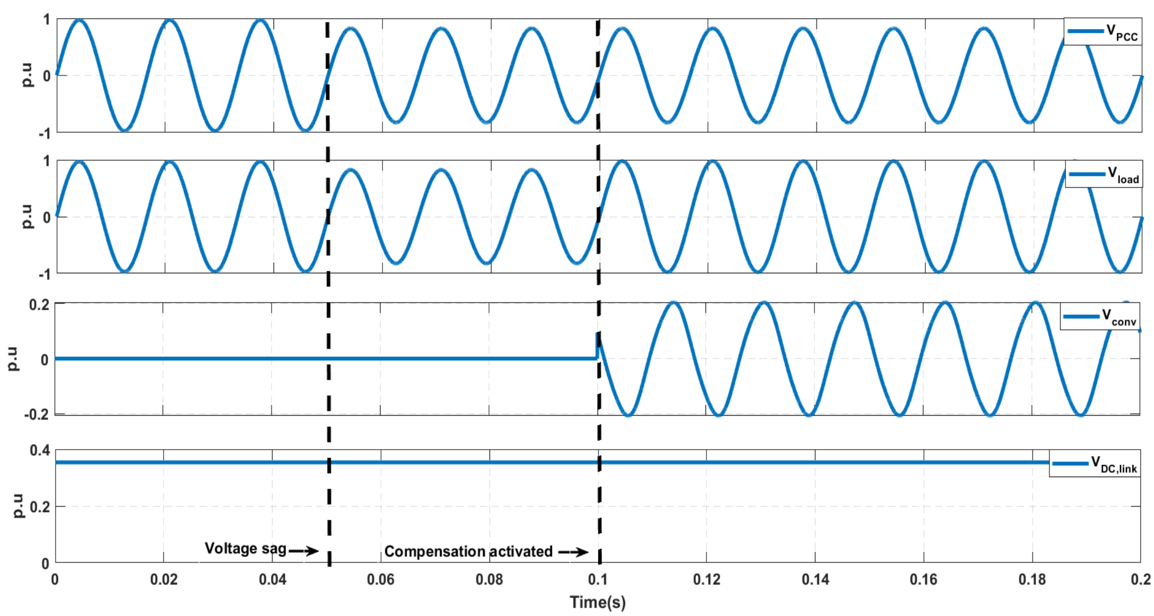

Figure 4.18: Proposed strategy simulation under grid voltage sag for scaled prototype; Top subplot shows voltage on HST primary (V_{PCC}), second subplot shows HST load voltage (V_{load}), third subplot shows compensation signal generated by proposed module (V_{conv}), bottom subplot shows DC link voltage ($V_{DC,link}$).

Scaled Protoype P-HIL Results

The variety of scenarios that could be experienced by a real utility transformer, [13], [19], [78], [79], are generated in the laboratory and the proposed hybrid transformer module is evaluated against addressing these challenges. The experimental results are presented under respective scenarios.

DC Mitigation

First, the capability of the proposed hybrid transformer to isolate DC or harmonics flowing on its primary side to appear on the secondary side is evaluated. The DC supply is activated to enter the TUT under half-cycle saturation by mimicking the previously discussed DC injection scenarios. This leads to enhanced harmonic content in the voltage and current waveforms on each side of the TUT as shown in Figure 4.19. Later, the module is triggered, and it is observed that it effectively follows and resultantly isolates the generated harmonics in the V_{PCC} from travelling towards the load side. This also helps to avoid half-cycle saturation of the transformer during DC or quasi-DC flow and its ultimate damage due to the reasons discussed previously. It is pertinent to mention that this capability of the proposed module is highly desirable under the present scenario of exponential addition of power electronics-based generation resources and loads that lead to unabated injection of harmonics to the grid. The Figure 4.19 when compared with Figure 4.17 shows a slightly different harmonics pattern due to additional line harmonics in electric power supplied by lab's power outlet. A comparison of simulations and experimental P-HIL results is presented in Table 4.7.

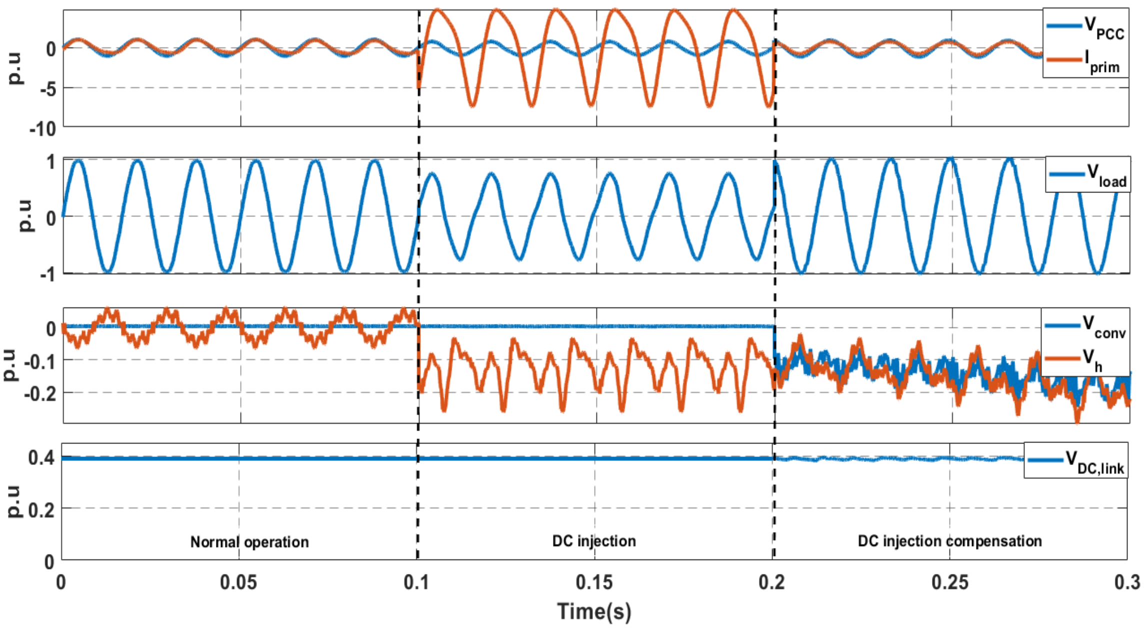

Figure 4.19: Proposed strategy evaluation under harmonics injection; Top subplot shows voltage (V_{PCC}) and current (I_{prim}) on HST primary, second subplot shows HST load voltage (V_{load}), third subplot shows harmonic content in HST primary voltage (V_h) and compensation signal generated by proposed module (V_{conv}), bottom subplot shows DC link voltage ($V_{DC,link}$).

Voltage Regulation

Afterwards, the voltage regulation ability of the proposed device is evaluated. In this case, the objective is to regulate the load voltage irrespective of voltage sags or swells on the grid. To mimic a voltage fall on the grid, the output of the variac connected to the TUT is decreased to 0.85pu. Later, the module is activated, and the result is presented in Figure 4.20. It is seen that the module effectively regulates the secondary voltage to its normal value. Also, a voltage rise is generated in the V_{PCC} by increasing the output of the associated variac followed by compensation from the proposed module. The result is shown in Figure 4.21, where again the hybrid transformer capability to maintain the load voltage is verified.

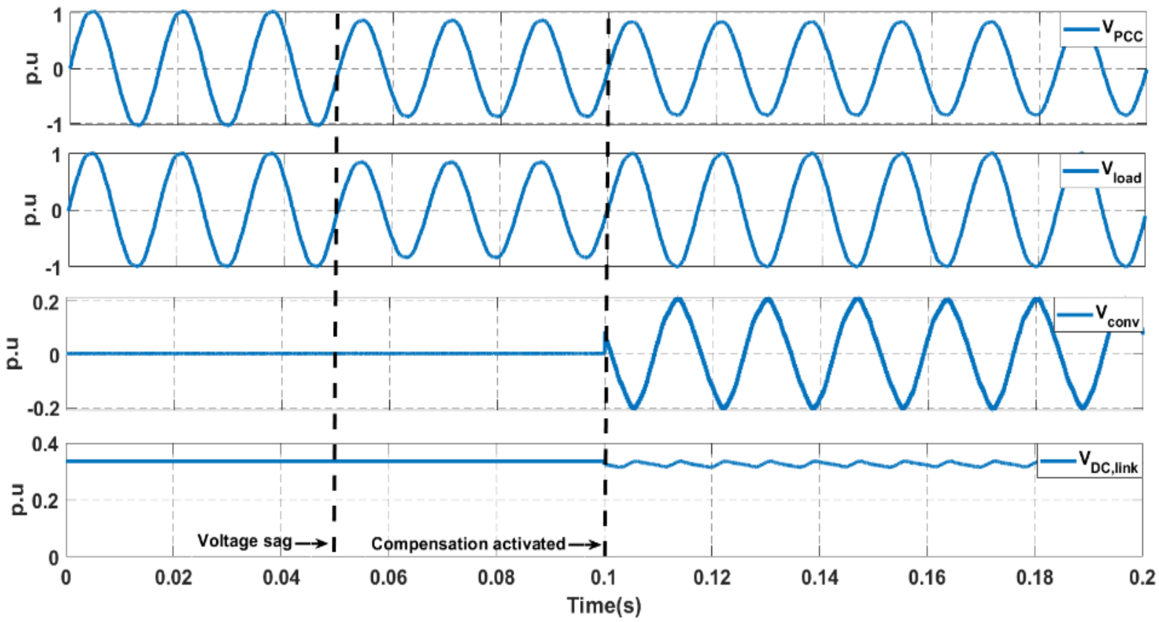

Figure 4.20: Proposed strategy performance under grid voltage sag; Top subplot shows voltage on HST primary (V_{PCC}), second subplot shows HST load voltage (V_{load}), third subplot shows compensation signal generated by proposed module (V_{conv}), bottom subplot shows DC link voltage ($V_{DC,link}$).

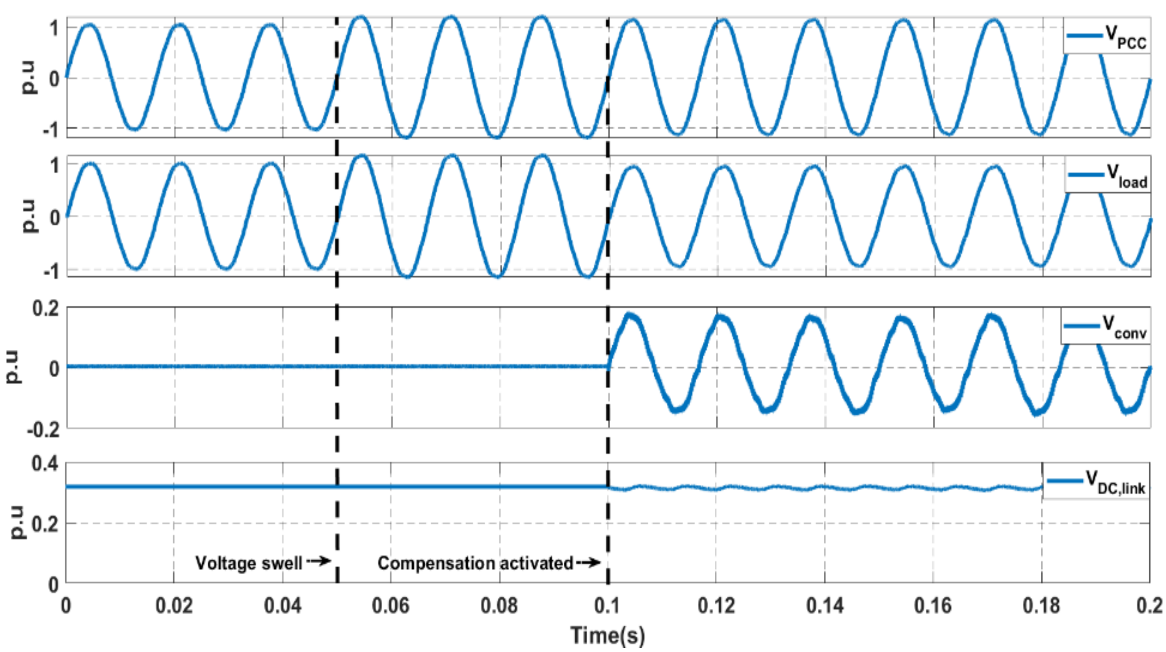

Figure 4.21: Proposed strategy performance under grid voltage swell; Top subplot shows voltage on HST primary (V_{PCC}), second subplot shows HST load voltage (V_{load}), third subplot shows compensation signal generated by proposed module (V_{conv}), bottom subplot shows DC link voltage ($V_{DC,link}$).

A comparison of Figure 4.18 and Figure 4.20 shows the simulation and experimental hardware prototype results to be in complete harmony. Further comparison of these results is shown in Table 4.7. It is pertinent to mention that implementation of the proposed device on a per-phase basis also enables its application for grid unbalance mitigation [80]. In addition, the voltage regulation feature of the proposed device could also be utilized to satisfy IEEE 1547-2018 or IEEE 2800-2022 by providing voltage ride through (VRT) services to DERs or to grid-connected IBRs [73]. More details regarding this feature of the proposed device can be found in [81].

Power Flow Control

To depict the power flow management capability introduced by the module into the traditional TUT, a quadrature voltage injection from the module with respect to the V_{PCC} is utilized. In the first case, the injected voltage (V_{conv}) lags the V_{PCC} by 90 degrees and the resultant response is demonstrated in Figure 4.22. The rise in the power angle leads to an enhanced power flow through the transformer, where the additional power is provided by the converter. In the second case, the quadrature voltage is injected at a leading angle w.r.t. the V_{PCC} and consequently a decreased power flow is observed across the transformer as depicted in Figure 4.23. In this scenario, the power difference starts flowing towards the converter, where it could be stored for later utilization. The above presented power flow control results are summarized in Table 4.6.

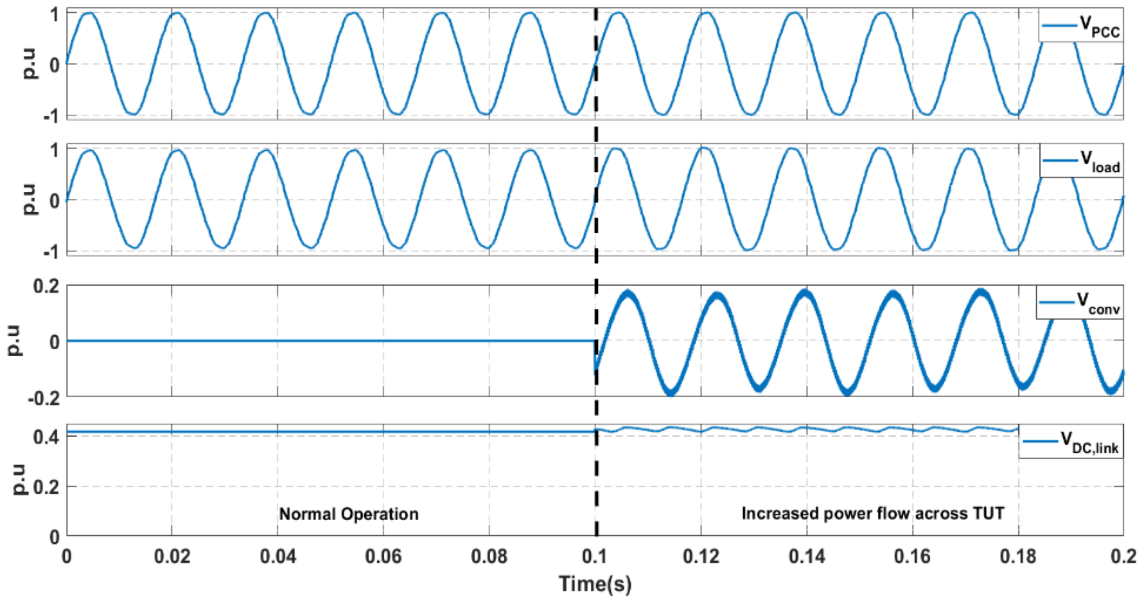

Figure 4.22: Utilization of proposed strategy to increase power flow across TUT; Top subplot shows voltage on HST primary (V_{PCC}), second subplot shows HST load voltage (V_{load}), third subplot shows compensation signal generated by proposed module (V_{conv}), bottom subplot shows DC link voltage ($V_{DC,link}$).

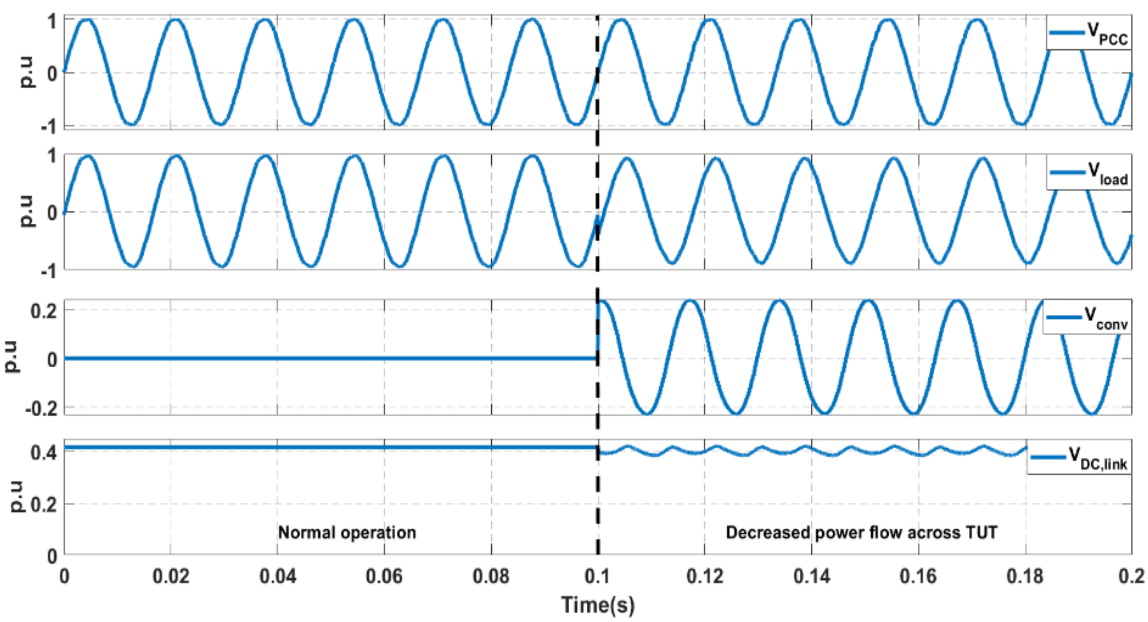

Figure 4.23: Utilization of proposed strategy to decrease power flow across TUT; Top subplot shows voltage on HST primary (V_{PCC}), second subplot shows HST load voltage (V_{load}), third subplot shows compensation signal generated by proposed module (V_{conv}), bottom subplot shows DC link voltage ($V_{DC,link}$).

TABLE 4.6
POWER FLOW CONTROL CAPABILITY OF PROPOSED MODULE

State	P flow across TUT (p.u)	P flow from module (p.u)	Q flow from module (p.u)
Normal operation	0.76	-0.01	0
20% lagging quadrature injection	0.88	0.07	0.05
20% leading quadrature injection	0.6	-0.09	-0.02

The power flow control capability of the hybrid transformer is highly relevant considering the exponential integration of DERs, where there volatile nature leads to congestion or underutilization of transmission capacity under different generation scenarios. The proposed dynamic power flow control ability introduced by the device in conventional transformers can be employed for fast redistribution of power and eventually employing the DERs at their maximum generation capacity. This feature is also highly relevant to the parallel AC/DC transmission that are experiencing a growing trend in China and Europe. The HVDC transmission possesses the inherent feature of performing power flow control whereas the AC-tie lines do not bear this ability that could be introduced utilizing the proposed modules [82].

Impedance Control

To assess the impedance control ability of the proposed device, an impedance mismatch scenario is mimicked by adding an external inductance of 1mH to the primary winding of TUT. This leads to diminished flow across the transformer which is sensed by the proposed module and it injects a voltage by adjusting gain G_1 to nullify the resultant effects of impedance (Z_{xmfr}) addition. The experimental result for this case is presented in Figure 4.24, where it is seen that voltage appearing across the inserted impedance (V_z) is sensed by the controller and it adjusts the gain G_1 to -0.67 for effective cancellation of this additional voltage and restoring the normal operation of the TUT by recovering the load voltage.

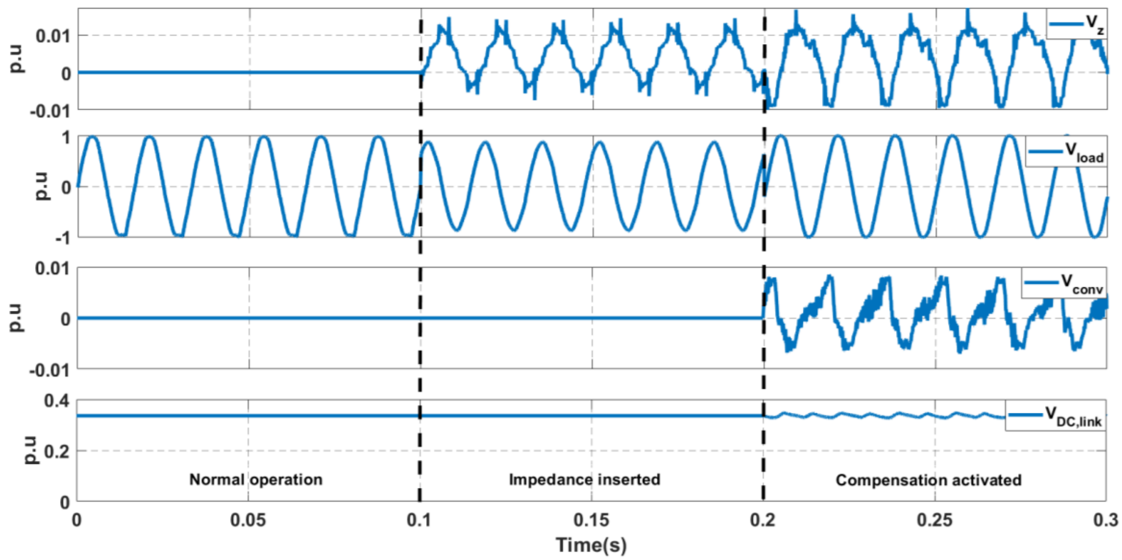

Figure 4.24: Impedance control aspect of the proposed module; Top subplot shows voltage across external impedance added to transformer primary (V_z), second subplot shows HST load voltage (V_{load}), third subplot shows compensation signal generated by proposed module (V_{conv}), bottom subplot shows DC link voltage ($V_{DC,link}$).

The impedance control requires prior knowledge of the voltage drop across the impedance (Z_{xmfr}) of the replaced transformer and the new transformer to automatically adjust the gain G_1. However, once adjusted no continuous tuning of G_1 is required as long as the transformer operates within the linear operating range. The impedance control element of the proposed device could be utilized to balance the power flow across the phases of the three single-phase transformers or two parallel three-phase transformers, where the mismatch could be the result of utilizing of a non-custom built replacement transformer. This approach could also be utilized for rapid transformer replacements or fast power recovery in event of irreversible damage by utilizing a spare unit or borrowing from a neighboring utility.

The maximum converter output voltage as per unit of base voltage and converter output power as a fraction of the power flow across the transformer for the above discussed scenarios are shown in table 4.7. It is pertinent to mention that these values are for the extreme scenarios generated in a laboratory environment to depict different functions of the proposed module. In a real-world scenario, the required power rating of the module will be much lower due to less severe electrical grid disturbances.

TABLE 4.7
CONVERTER RATING AS A FUNCTION OF LINE VOLTAGE AND TRANSFORMED POWER

Function (Refer to Figure 4.17 - Figure 4.24)	**Maximum converter output voltage (AC side), pu of base voltage**		**Maximum converter output power (AC side), pu of transformed power**	
	Simulation	**P-HIL**	**Simulation**	**P-HIL**
DC mitigation	0.19	0.2	0.12	0.14
Voltage regulation (sag of 0.85pu)	0.18	0.2	0.13	0.14
Voltage regulation (swell of 1.15pu)	0.17	0.18	0.11	0.10
Power flow control (decreased power flow)	0.2	0.22	0.26	0.29
Power flow control (increased power flow)	0.2	0.18	0.14	0.15
Impedance control	0.006	0.008	0.017	0.02

The above presented experimental results validate the promising performance of the proposed hybrid transformer strategy thus providing an all-in-one solution to the electric utilities for resolving multiple contemporary grid problems.

CHAPTER FIVE

PROTECTION OF HST FOR ADVANCED GRID SUPPORT

Hybrid Bypass Protection of HST

The proposed power-electronics based module needs to be protected from damaging voltages that might develop at its output terminal during inrush or ground faults. In addition to damage to the module, this might lead to exceeding the protected transformer BIL, that is typically 10 times higher than the nominal rating of a transformer. As already discussed, the power electronics-based SSTs reliability is still significantly lower than the traditional transformers and, therefore, integration of a power electronics-based device without effective protection consideration might compromise the high reliability of conventional transformers. Contemplating the high speed and high current requirement of the bypass switch, an antiparallel solid-state thyristor arrangement with a parallel mechanical switch could provide an ideal protection against the above discussed scenarios, where the solid-state device is utilized for rapid bypass initiation followed by closing of the mechanical switch to carry the fault or inrush current with low loss. A metal oxide varistor (MOV), set at 0.4pu, is also connected parallel to the hybrid switch to avoid momentary voltage transients from damaging the converter. The module output voltage (V_{conv}) is continuously monitored and as soon as it exceeds a pre-defined threshold, a command is passed to close the switch for 25 cycles. The delay of 25 cycles is adequate for the clearance of ground fault by protection devices and for the successful decay of inrush currents [10]. The closing of the bypass switch creates a short circuit across the converter terminals; however, this still prevents the flow of significantly higher currents due to a pre-defined reference current limiting threshold in the module control as shown in Figure 3.4. Utilizing the current-limiting mode instead of blocking the converter aids in rapid servicing by the proposed module as soon as the bypass switch reopens to provide faster response times. The overall bypass switch protection strategy is depicted in Figure 5.1 and the tripping signal generation logic is shown in Figure 5.2.

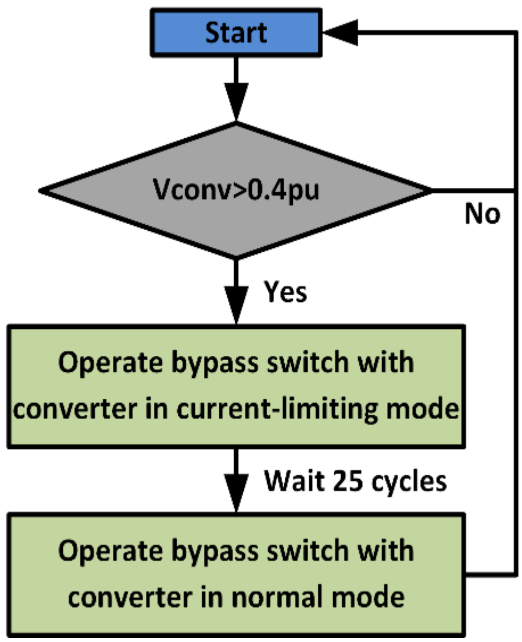

Figure 5.1: Bypass switch protection strategy.

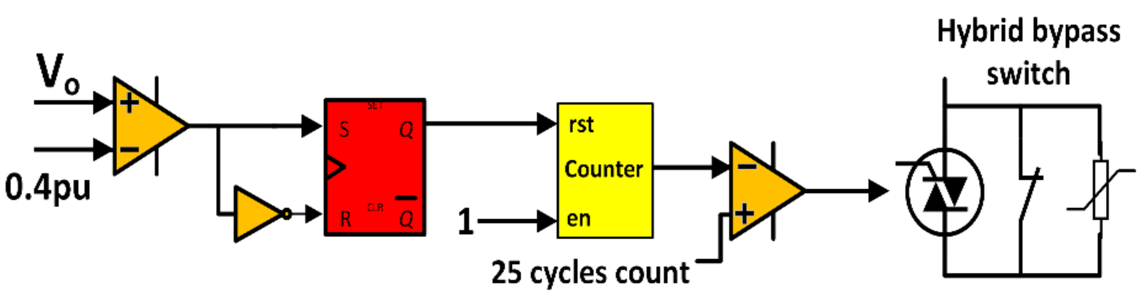

Figure 5.2: Bypass switch trip signal generation.

The evaluation of the module fault protection scheme is performed on the experimental setup to show the working of the proposed strategy. It is observed that the mechanical switch operates almost instantaneously with the application of the trip signal. As this does not replicate the typical tripping behavior of a transmission or distribution breaker, an intentional delay of 3 cycles is introduced between the bypass switch trip initiation due to overvoltage and the mechanical switch operation. From the perspective of field installation of the proposed module, it represents a scenario where the solid-state switch is operated with the embedded controller to avoid the delays introduced by the field relays from damaging the converter, whereas the parallel breaker is tripped by a typical substation relay.

For the experimental evaluation, a fault is created for a few cycles by shorting the primary of TUT at 0.95s while the converter is performing DC mitigation. This scenario mimics a temporary ground fault and the outcome is presented in Figure 5.3, where it is noticed that development of a ground fault raises the module output voltage (V_{conv}). As soon as it crosses the pre-defined threshold of 0.4pu, the controller generates a trip signal for the bypass switch. The solid state switch immediately operates and creates a short circuit across the terminals of the converter, followed by the mechanical switch operation after 3 cycles. This bypass path avoids flow of the significantly higher fault current through the converter, thus, avoiding its overvoltage or overcurrent damage. During this time, the voltage across the converter stays around zero and also the current provided by the module is limited to around 4pu due to the associated current-limiting mode. After a delay of 25 cycles, the converter effectively returns to its normal operation of DC mitigation.

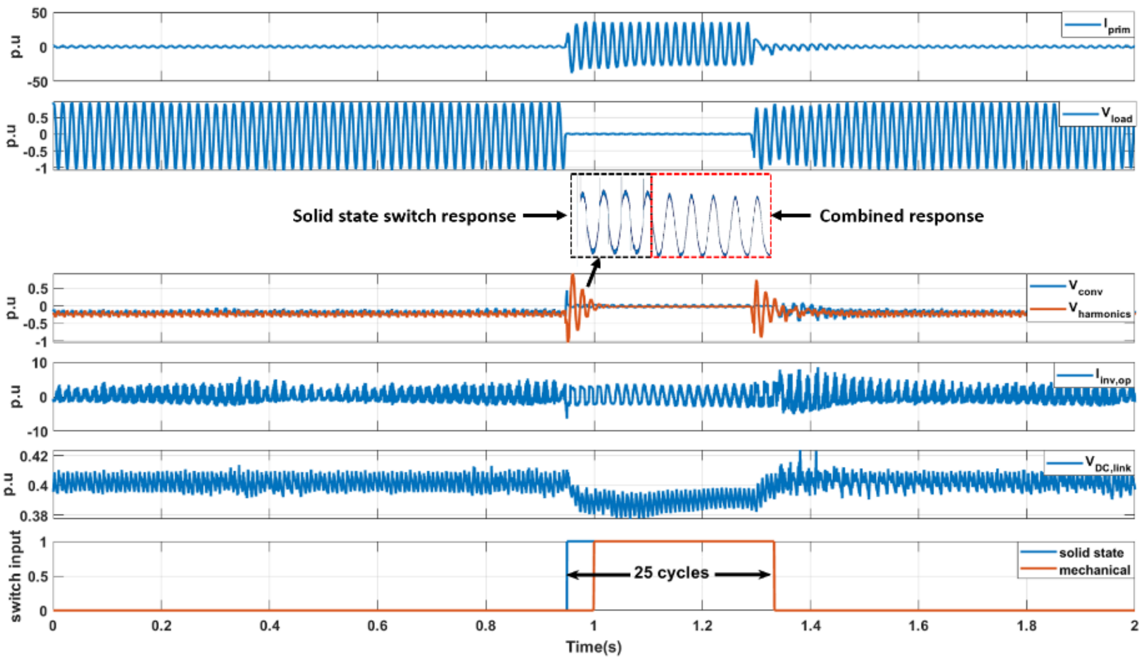

Figure 5.3: Proposed protection scheme performance under a temporary ground fault during DC mitigation; Top subplot shows current on HST primary (I_{prim}), second subplot shows HST load voltage (V_{load}), third subplot shows harmonics in HST primary voltage ($V_{harmonics}$) and compensation signal generated by proposed module (V_{conv}), fourth subplot shows module output current ($I_{inv,op}$), fifth subplot shows DC link voltage ($V_{DC,link}$), bottom subplot shows switching sequence of solid state and mechanical switch.

The protection strategy is also evaluated for the case when the module is performing the grid-support function of voltage regulation under a grid voltage sag. The experimental result for this scenario is presented in Figure 5.4, where it is again noticed that the initiation of a ground fault is successfully detected followed by the bypass switch operation that limits the voltage across the converter and avoids the high fault current to flow through the converter. Also, the module returns to its normal operation of voltage regulation as soon as the bypass switch opens after the delay of 25 cycles. It is pertinent to mention that due to the trip logic shown in Figure 5.2, the bypass switch repeats the same cycle if for some reason the fault stays uncleared or there are consecutive high voltage events across the converter. This ensures the module protection and its effective operation under all scenarios.

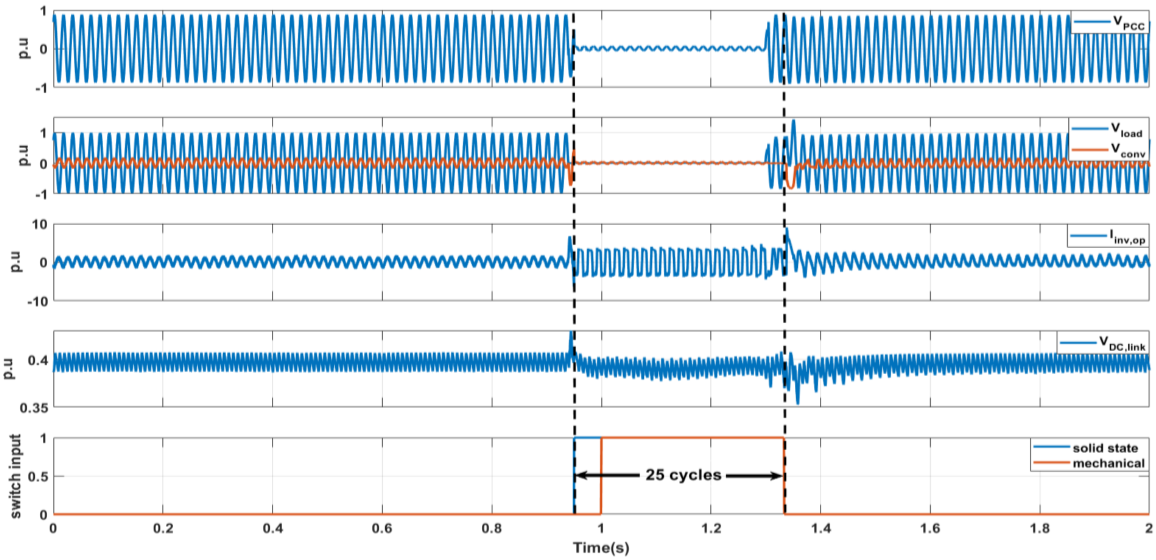

Figure 5.4: Proposed protection scheme performance under a temporary ground fault during voltage regulation; Top subplot shows voltage on HST primary (V_{PCC}), second subplot shows HST load voltage (V_{load}) and compensation signal generated by proposed module (V_{conv}), third subplot shows module output current ($I_{inv,op}$), fourth subplot shows DC link voltage ($V_{DC,link}$), bottom subplot shows switching sequence of solid state and mechanical switch.

The brief closing of the switch still precludes the associated transformer from going into half-cycle saturation due to DC flow owing to substantially longer time constant linked to the RL circuit consisting of magnetizing inductance of the transformer and line impedance [19]. Also, bypassing the module during transformer energization helps to avert any adjustments to the second harmonic blocking ability of differential relays due to this new installation. The bypass switch has an added advantage of enabling the associated transformer to maintain its typical operation in the case of converter failure or damage. The proposed protection topology finds its applications in the majority of modern dynamic grid controllers utilizing converters or similar topologies.

Evaluation of Hybrid Bypass Protection of HST in a Typical Substation Protection Environment

The solid state and mechanical relay utilized for hardware implementation of the proposed bypass protection configuration are shown in Figure 5.5.

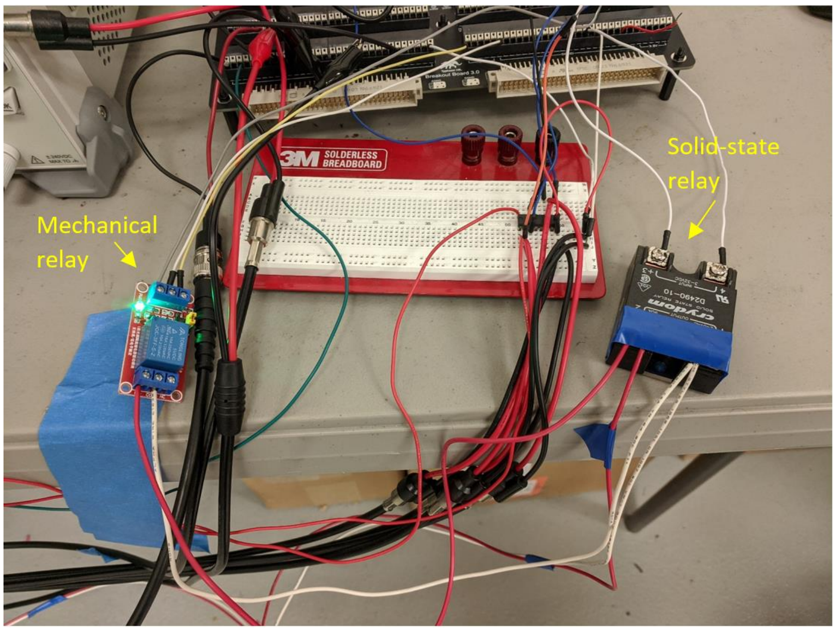

Figure 5.5: Mechanical and solid-state relay utilized for evaluation of bypass switch configuration.

The first step towards transformation of the proposed bypass protection scheme to accommodate within a real substation environment is to integrate it with SEL-751A feeder protection relay. The SEL-751A acts as a backup for the embedded controller to provide the trip/reclose logic to the hybrid switch. It also updates the current switch state to other protection relays in the substation for coordination purposes. The resultant protection scheme is shown in Figure 5.6.

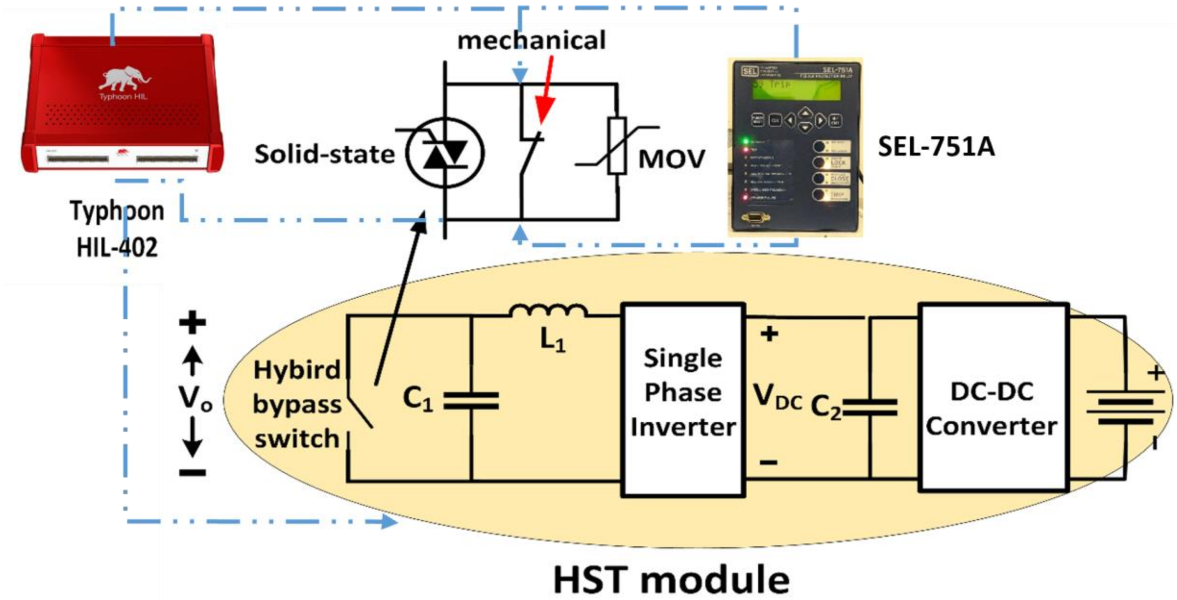

Figure 5.6: Modified operation of the bypass switch configuration to mimic a realistic scenario.

To mimic a real substation environment, two additional protection relays are utilized: differential and feeder protection relays both emulated within Typhoon HIL-402. The SEL-751A is integrated with SEL-3530-4 real time automation controller (RTAC) and Typhoon HIL-402 utilizing IEC-61850 GOOSE protocol. The overall test setup is shown in Figure 5.7.

The emulated differential relay within Typhoon HIL-402 provides trip signal to the breakers on the primary and secondary sides of the transformer. The breakers are mimicked utilizing the same mechanical relay as utilized to represent the breaker parallel to the solid-state protection of the converter shown in Figure 5.5. The differential protection breakers and current transformers (CTs) providing signal to the emulated differential protection are shown in Figure 5.8.

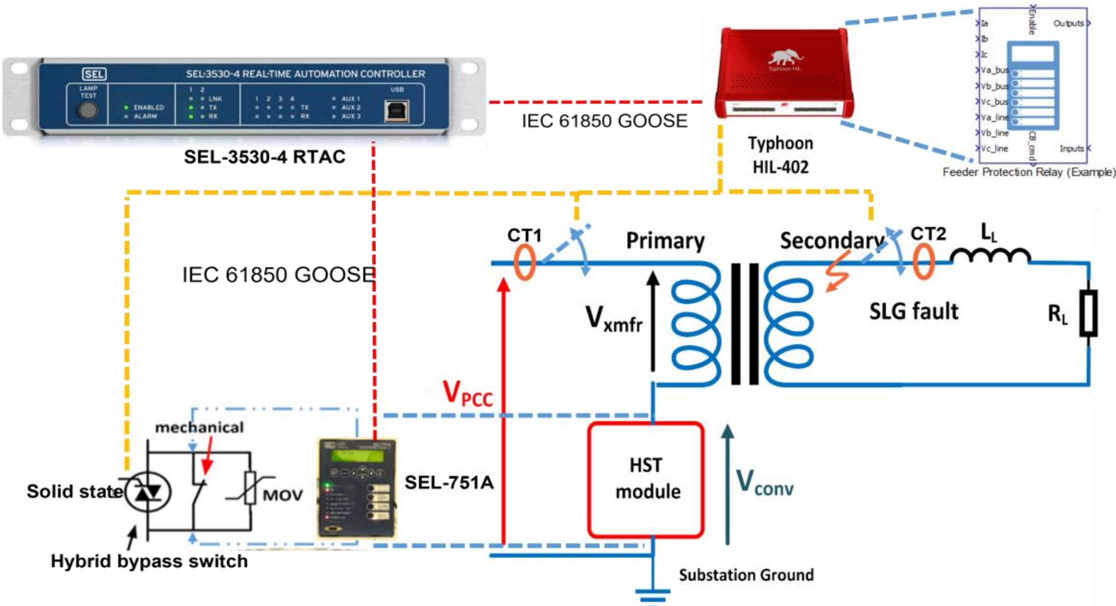

Figure 5.7: Overall lab setup to verify the proposed protection scheme in a real substation environment.

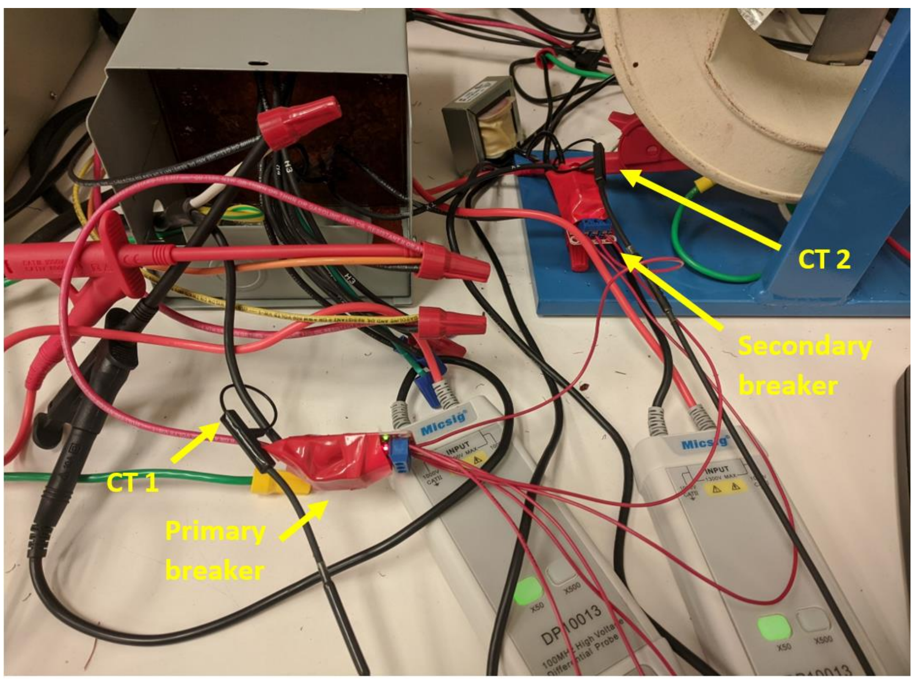

Figure 5.8: Differential protection implemented on the hardware prototype.

Integrating Typhoon HIL with SEL RTAC

The integration of SEL-751A feeder protection relay with SEL-3530-4 RTAC is straightforward due to the same manufacturer. However, the integration of SEL RTAC with Typhoon HIL-402 is challenging due to different manufacturers and non-existent literature regarding their integration.

To integrate Typhoon HIL with SEL RTAC, the following steps are utilized:

- First a SEL Architect project is created where the SEL-2411 programmable automation controller from the IED palette was utilized to mimic Typhoon HIL as shown in Figure 5.9.
- The IP address, subnet mask and gateway of Typhoon HIL are inserted in the IED properties to enable communication between Typhoon HIL and SEL RTAC.
- The appropriate data set to be transmitted by Typhoon HIL is added to the GOOSE transmit tab of Typhoon HIL in SEL Architect.
- Logical devices and logical nodes to be observed in Typhoon HIL are added to GOOSE receive tab of Typhoon HIL in SEL Architect.
- Later this project was uploaded to SEL AcSELerator RTAC and successful communication was established between Typhoon HIL and SEL RTAC.

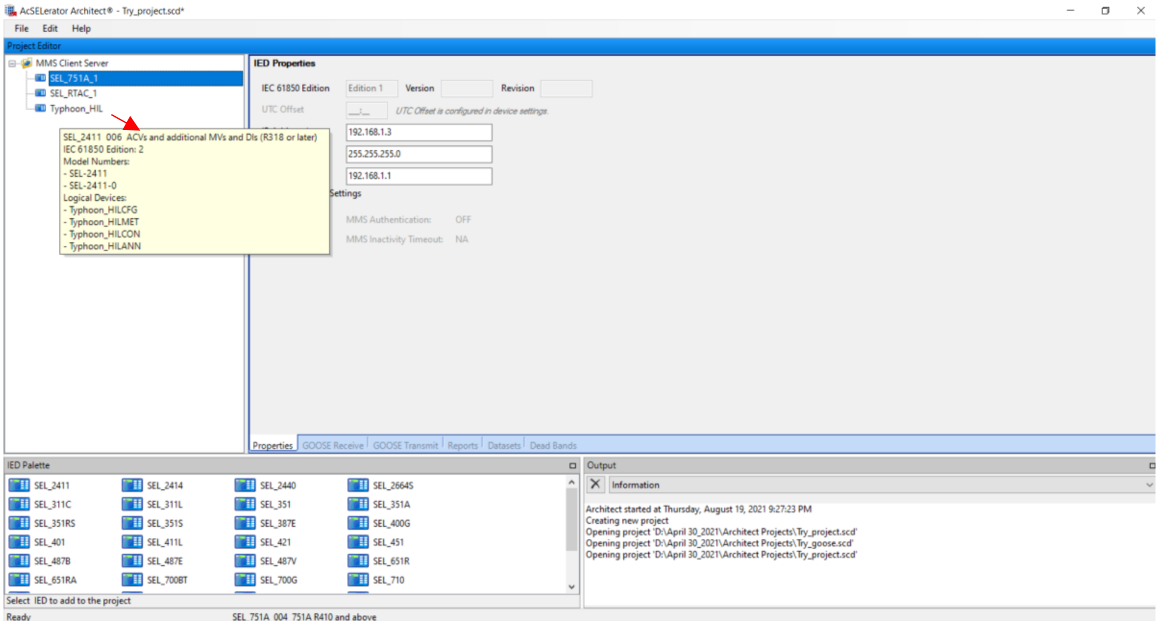

Figure 5.9: Mimicking SEL-2411 as Typhoon HIL in SEL AcSELerator Architect.

Experimental Results

The SEL-751A, SEL RTAC and Typhoon HIL are integrated through network switch for communication via IEC-61850 GOOSE protocol as shown in Figure 5.10. First, the differential relay and SEL-751A are activated to see their response for a single line to ground (SLG) fault right across the secondary winding of the hybrid smart transformer within the differential protection zone, as shown in Figure 5.7. The hardware result for this case is shown in Figure 5.11, where V_{PCC} and I_{prim} are transformer primary voltage and current, respectively. V_{load} and I_{load} are transformer secondary voltage and current, respectively. V_{conv} is the output voltage of the proposed module. $V_{DC,link}$ is the DC-link voltage. It is seen that the SEL-751A operates almost 1.5 cycles after the fault initiation (1.5 cycles is inherent delay of SEL-751A), as it sees a voltage higher than its overvoltage setting. This brings the module output voltage (V_{conv}) around 0 for 20 cycles. The differential protection, abbreviated by Differential relay operates 5 cycles after the fault initiation (2 cycles relay, 3 cycles breaker operating time), as the differential current (I_{diff}) stays higher than the pick-up current (I_{pu}) after the initiation of the ground fault. The operation of the differential protection brings the transformer out of service. The module recovers back to its normal operation after 20 cycles.

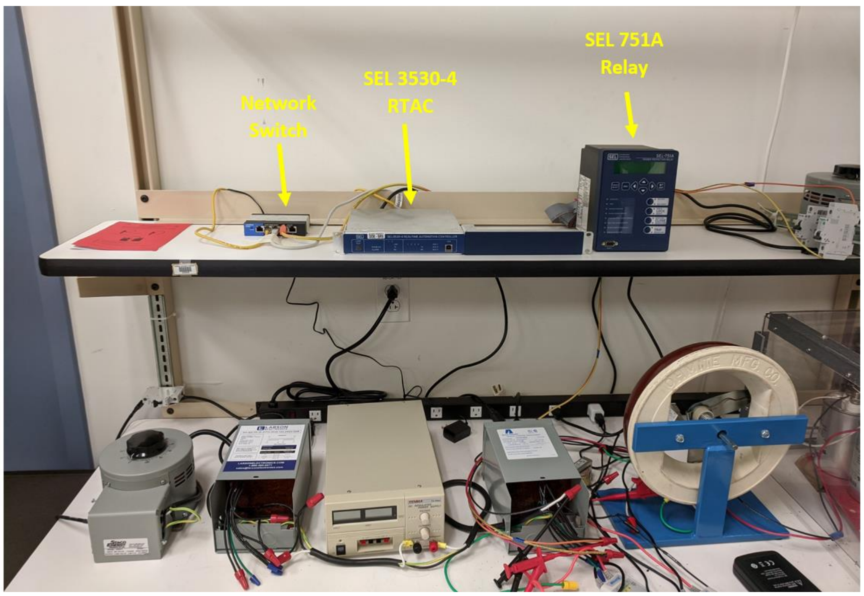

Figure 5.10: Integrating SEL-751A, SEL RTAC and Typhoon HIL through network switch for communication via IEC-61850 GOOSE protocol.

Now all the protection devices are enabled, and the same fault scenario is repeated. It is observed that the hybrid switch, abbreviated as Hybrid switch, in Figure 5.12, operates instantaneously with the initiation of the ground fault at 0s.This keeps the module output voltage (V_{conv}) around 0 for 20 cycles. As the differential current (I_{diff}) is higher than the pick-up current (I_{pu}) after the initiation of the ground fault, the solid-state switch is followed by operation of the differential protection, abbreviated by Differential relay, after 5 cycles

(2 cycles relay, 3 cycles breaker operating time). It is observed that SEL-751A never operates for this case. The discrete fourier trasnformer (DFT) filter within SEL-751A requires a few cycles to stabilize to its final value. However, the solid-state switch instantanously brings the module output voltage (V_{conv}) to 0 with the initiation of the ground fault. Resultantly, SEL-751A never sees V_{conv} to be higher than its tripping threshold and therefore does not trip. This is confirmed by only activating SEL-751A with the previously activated protection relays (differential, solid-state, feedar) disabled. The result for this case is shown in Figure 5.13, where SEL-751A operates as desired.

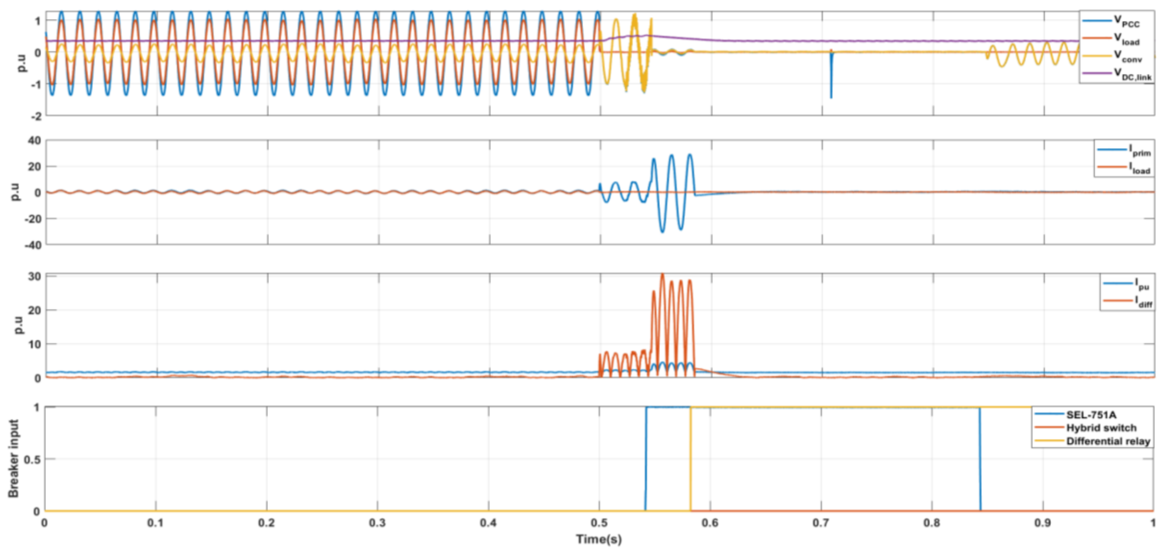

Figure 5.11: With differential and SEL-751A protection enabled; Top subplot shows voltage on HST primary (V_{PCC}) and secondary (V_{load}) along with module output (V_{conv}) and DC link ($V_{DC,link}$) voltage, second subplot shows HST primary (I_{prim}) and secondary current (I_{load}), third subplot shows pickup (I_{pu}) and differential current (I_{diff}) of HST differential protection, bottom subplot shows switching sequence of differential (Differential relay), solid-state (Hybrid switch) and SEL-751A (SEL-751A) protection.

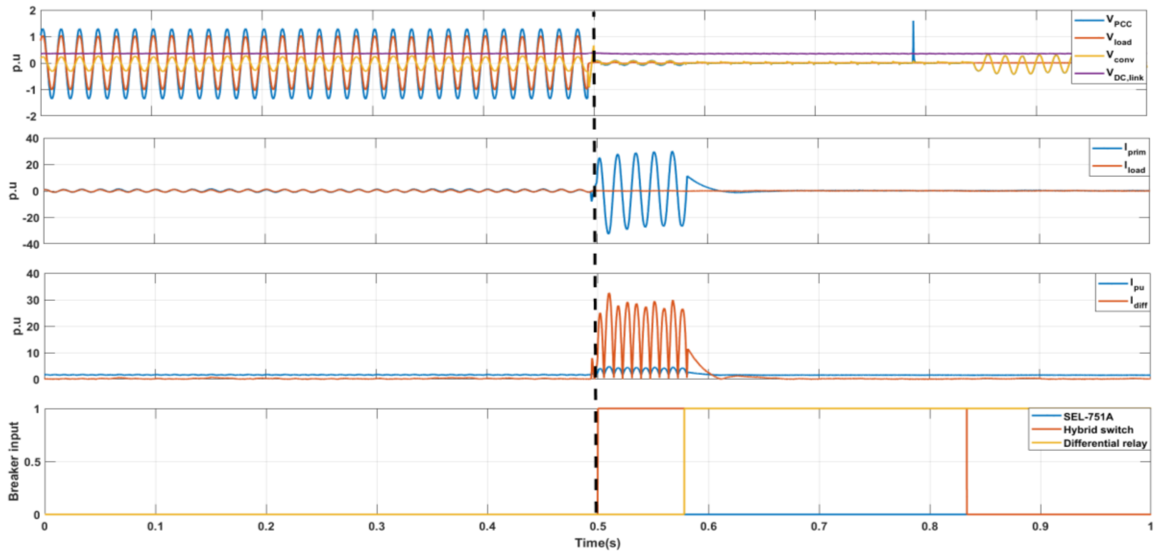

Figure 5.12: With differential, solid-state and SEL-751A protection enabled; Top subplot shows voltage on HST primary (V_{PCC}) and secondary (V_{load}) along with module output (V_{conv}) and DC link ($V_{DC,link}$) voltage, second subplot shows HST primary (I_{prim}) and secondary current (I_{load}), third subplot shows pickup (I_{pu}) and differential current (I_{diff}) of HST differential protection, bottom subplot shows switching sequence of differential (Differential relay), solid-state (Hybrid switch) and SEL-751A (SEL-751A) protection.

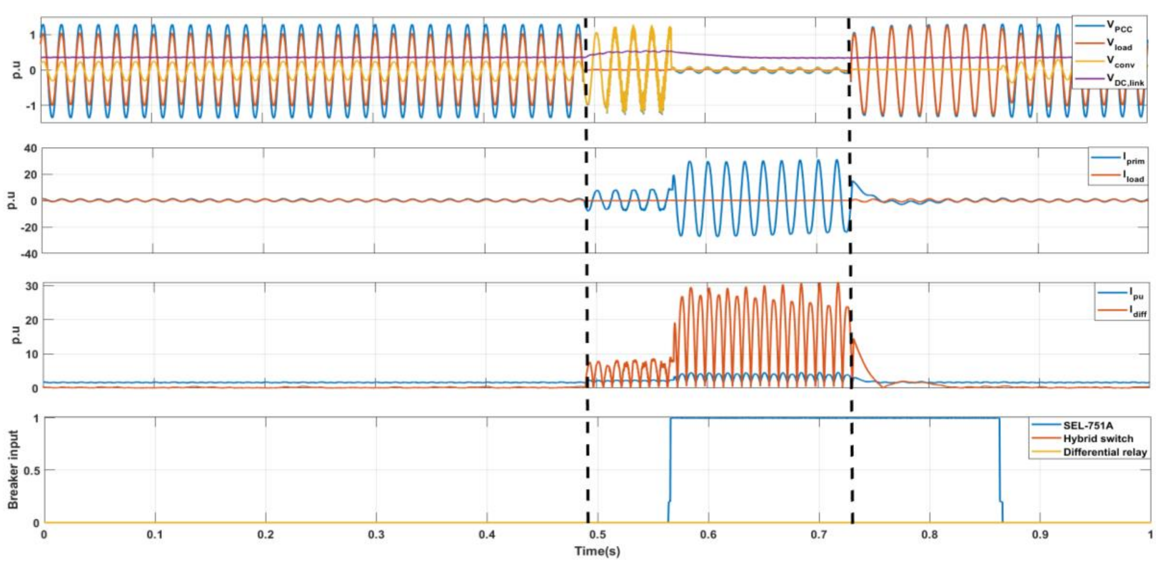

Figure 5.13: Only SEL-751A activated; Top subplot shows voltage on HST primary (V_{PCC}) and secondary (V_{load}) along with module output (V_{conv}) and DC link ($V_{DC,link}$) voltage, second subplot shows HST primary (I_{prim}) and secondary current (I_{load}), third subplot shows pickup (I_{pu}) and differential current (I_{diff}) of HST differential protection, bottom subplot shows switching sequence of differential (Differential relay), solid-state (Hybrid switch) and SEL-751A (SEL-751A) protection.

After a series of simulation and hardware results, the following operation strategy is proposed for the bypass switch configuration:

- The embedded controller utilized to operate the proposed hybrid smart transformer module provides the trip signal to the solid-state switch and the mechanical breaker in event of overvoltage at its output.
- In event of failure of the embedded controller, the feeder protection relay (SEL-751A in our case) provides the backup protection and generates the trip logic for the mechanical breaker. The MOV parallel to the solid-state switch and mechanical breaker should be sufficiently rated to handle the high voltage event for 2-3 cycles prior to operation of mechanical breaker in this case.

The proposed operational strategy discussed above is shown in Figure 5.13.

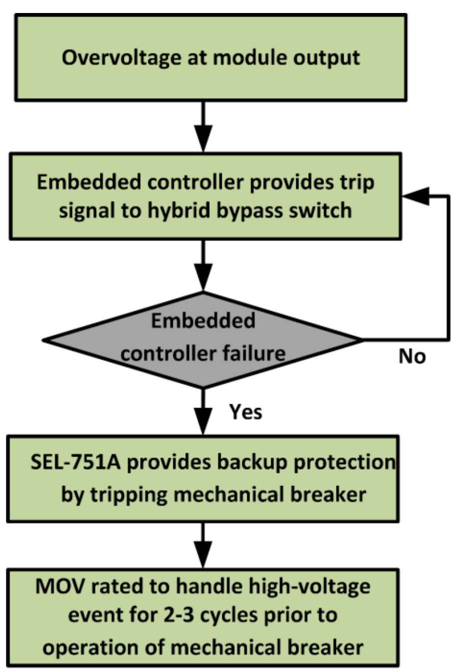

Figure 5.14: Proposed operational strategy of hybrid bypass protection.

CHAPTER SIX

CONCLUSION AND FUTURE DIRECTIONS

In this dissertation work, the repercussions of DC flow in AC electric grid and the current state-of-the-art of the DC blocking devices have been presented. Moreover, an effective DC mitigation and advanced grid support control module, that transforms the traditional transformers into hybrid smart transformers has been proposed and compared with the existing solutions. The hybrid-smart transformer strategy utilizes a power electronics-based module integrated between the neutral of power transformers and substation ground. The proposed strategy has been initially evaluated for its effective operation in a C-HIL environment utilizing Typhoon HIL. The experimental results of a laboratory-scale hardware prototype of the hybrid smart transformer approach are also presented. The results validate the effective working of the proposed strategy in protecting the AC power grids against DC flow and addressing critical challenges encountering electric utilities that involve grid power quality, power flow control, impedance matching and voltage balancing. The dissertation also presents the configuration and operation of a hybrid bypass protection scheme aimed at protecting the proposed module and to circumvent surpassing the transformer BIL rating in event of ground faults or inrush currents. The possible directions for practical implementation of the proposed module are also presented in this dissertation work.

The future directions include evaluation of the proposed hybrid smart transformer scheme utilizing real utility data where the integration of the proposed module with a substation transformer is expected to mitigate instabilities stimulated by the excessive integration of renewable generation. It also involves enhancing reliability of a transmission and distribution network through optimal conversion of power transformers into hybrid smart transformers.

Moreover, the design of a multi-level converter for practical application of the proposed scheme is suggested as a future work. Some guidelines for field implementation and deployment of proposed scheme are discussed in the subsequent section.

Practical Implementation Considerations for Proposed HST

The integration of converter between the transformer neutral and substation ground for the proposed scheme avoids exceeding the basic insulation level (BIL) of transformer neutrals that is a major concern associated to the floating power electronics that are utilized to meet some of the above discussed objectives [83]. Also, the rating of the converter to 25-30% of the nominal voltage reduces its size, cost, and complexity. The development of a single-phase converter for the proposed application requires devices that could provide high-blocking voltage and switching speed. The 15kV wide bandgap (WBG) silicon carbide (SiC) based MOSFETs could be utilized for this purpose [84]. The 15kV SiC MOSFET is best suited for applications requiring higher voltages and lower currents as its R_{on} increases exponentially with temperature that leads to higher conduction loss [84]. Better cooling, such as forced air or water cooling could be utilized to drop thermal resistance significantly. For the proposed device, the thermal management could be efficiently performed utilizing passive cooling where the converter is mounted on plates cooled with the transformer oil. The future transformers to be integrated with this module could be built with increased oil tank capacity and increasing number of radiator plates for effective cooling. The WBG devices have higher peak electric field strength and power devices with blocking voltages in the range of 10kV-24kV have already been demonstrated [85]-[87]. The peak electric field strength of SiC is approximately 10 times higher than silicon, thus, providing an ultra-high voltage blocking device. The SiC MOSFET is preferred over SiC IGBT due to its unipolar characteristic that leads to higher switching speed.

The other approach could be the utilization of low-voltage IGBTs or MOSFETs in series to split the high voltage and in parallel to share the current respectively. However, the resultant converter would be highly intricate requiring numerous gate drivers, power supplies, protection, and control schemes. This would compromise the system's reliability if redundancy is not properly ensured.

The modular multi-level converters (MMC) are a promising technology option for the practical implementation of the proposed module. The MMC provides a modular and scalable solution capable of handling high power and high voltage in electric grid applications. The MMC topology has higher fault tolerance, efficiency, and lower harmonic distortion. In [88], various MMC topologies are compared for the development of energy storage integrated converters suitable for the proposed module. These include single-star bridge cell (SSBC), single-delta bridge cell (SDBC), Double-star chopper cell (DSCC), double-star bridge cell (DSBC) and double-star hybrid cell (DSHC).

For the integration of the battery energy storage system (BESS) in the DC link of the above presented schemes, there are two options; centralized and distributed. The features of both these strategies are summarized in table 3.2.

TABLE 6.1
COMPARISON OF DISTRIBUTED AND CENTRALIZED ENERGY STORAGE

Feature	Distributed Energy Storage (DES)	Centralized Energy Storage (CES)
Battery pack voltage requirement	Utilization of low-voltage battery packs	Batteries must be designed to operate at high voltage
Fault Management	Bypass of faulty battery racks	Operation as conventional STATCOM during battery maintenance
Thermal Management	Thermal management challenging (If batteries installed in converter enclosure)	Thermal management unchallenging leading to increased battery life
Number of DC cables	Massive number of DC cables (If batteries installed in separate enclosures)	Limited number of DC cables

All the above discussed MMC topologies allow for distribution of energy storage among the converter cells. The double-star topologies provide DC-link terminals for the integration of centralized energy storage (CES). A DC/DC converter can be employed between the battery pack and the converter that helps in avoiding degradation of battery life by decoupling cell ripple current. However, this increases the cost and complexity of this converter installation. If no DC/DC converter is employed, more sub-modules are required to account for battery voltage variations and a sophisticated control scheme is required for state of charge (SOC) balancing. The CES and DES option for the DSBC topology is shown in Figure 3.9 and Figure 3.10, respectively.

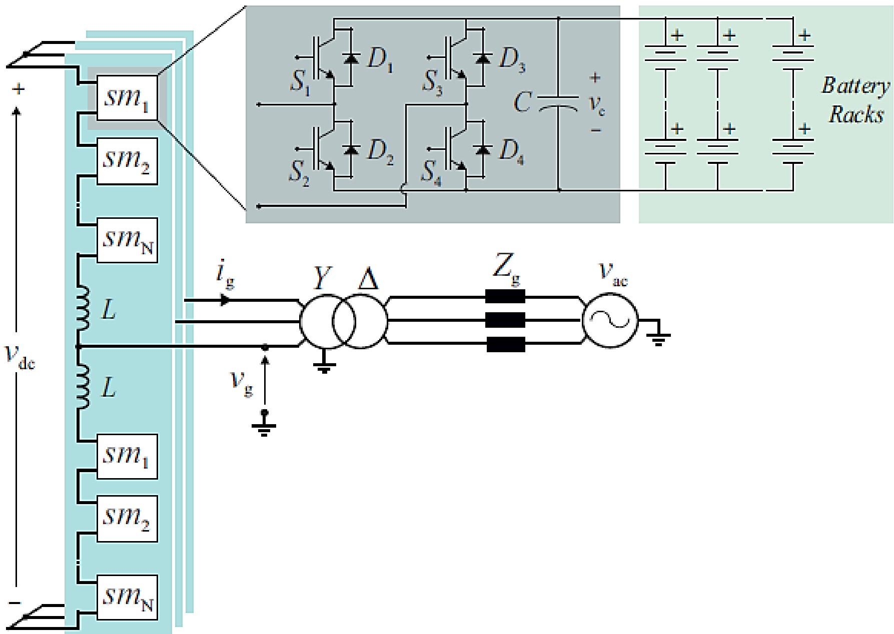

Figure 6.1: Double-star bridge cell MMC with distributed energy storage (DSBC-DES) [88].

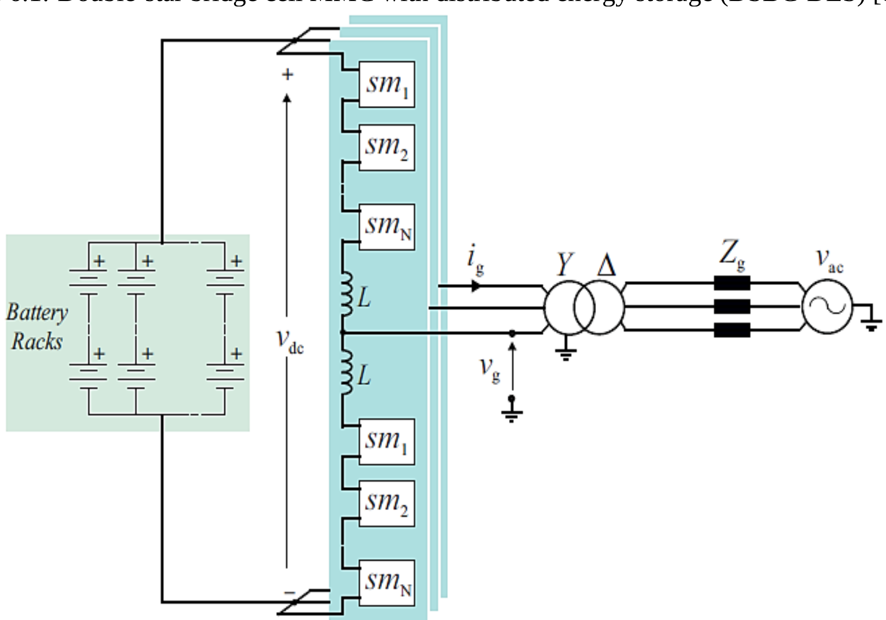

Figure 6.2: Double-star bridge cell MMC with centralized energy storage (DSBC-CES) [88].

In [88], it is concluded that centralized energy storage (CES) is more suitable for such applications due to their design flexibility, smaller volume and low silicon area. As compared to CES, the DES leads to 55% higher silicon area, and 30% higher volume. Although the chopper cells are 30-50% cheaper than the bridge cells, they are not preferred due to better DC short circuit handling capability of the bridge cells. The work in [88] concludes that the DSBC-CES is the most suitable implementation among all the available MMC designs. An illustration of the proposed approach for a three-phase transformer is shown in Figure 3.11.

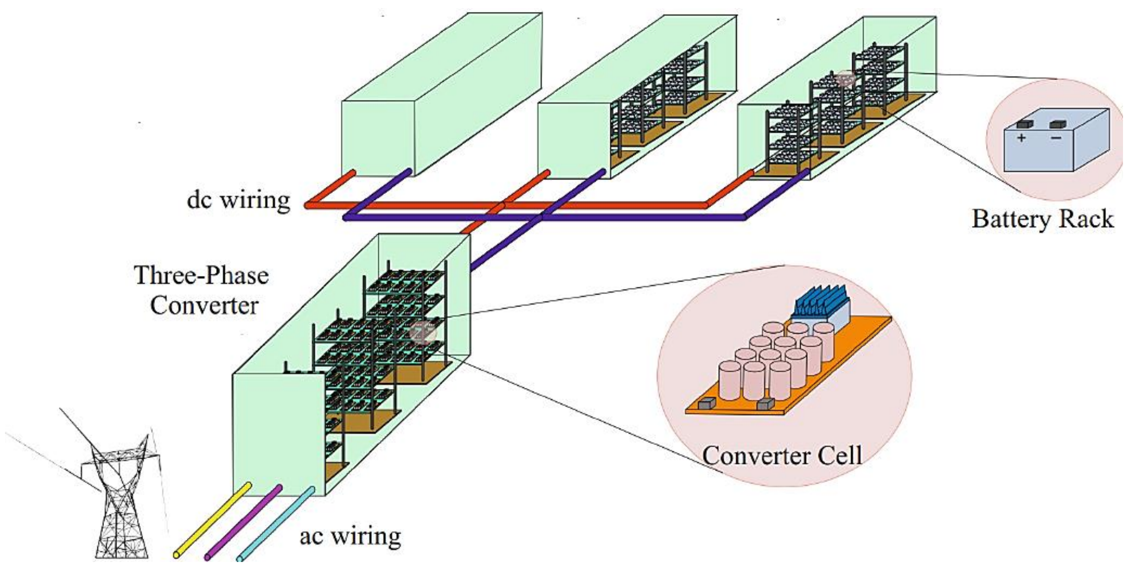

Figure 6.3: Illustration of proposed approach for a three-phase transformer [88].

Appendix A

Evaluation of proposed approach

TABLE A1
EVALUATION OF PROPOSED STRATEGIES AGAINST NERC GMD TASK FORCE CRITERIA

Criteria	DC-chopper-based solution	Converter-based solution
1. Continuous grounded neutral	Yes. Only dangerous situation is if the bypass switch assembly fails to close. High voltage across capacitor during ground fault might blow it or exceed transformer BIL.	Yes. Only dangerous situation is if the bypass switch assembly fails to close. High voltage across capacitor during ground fault might blow it or exceed transformer BIL.
2. Resonance conditions	No, the small value of filter capacitor leads to no or negligible resonance.	No, the small value of capacitor leads to no or negligible resonance.
3. Impact on system characteristics	Yes, capacitive mode increases ground fault impedance.	Yes, capacitive mode increases ground fault impedance.
4. Maintainable without transformer outage	Yes, by closing of bypass breaker followed by closing of maintenance grounding switch.	Yes, by closing of bypass breaker followed by closing of maintenance grounding switch.
5. Capability of handing 200A Unbalance	No, the prime assumption is that the system is balanced.	The device automatically removes the system unbalance .
6. Insertion under GIC conditions	Yes, the bypass switch is closed for device insertion under GIC.	The device is in service at all times, therefore, no action required.
7. Remote controllable with automatic sensing and insertion	Yes, remote controllable. Automatic sensing and mitigation is inherent to the approach.	Yes, remote controllable. Automatic sensing and mitigation is inherent to the approach.

8.	Operational at all time	No, the device is only operational during the GIC flow.	Yes, this device provides grid support functions at all times.
9.	Periodic testing requirement	Yes, remote control capability must be utilized to ensure insertion and removal operations are functional.	Not required as inability to perform regular grid services would immediately indicate problem.
10.	Grid Services (not part of NERC GMDTF)	No, the device is only meant for GIC mitigation.	Yes, provides voltage regulation, harmonic isolation, impedance balancing as added features.

TABLE A2

COMPARISON OF EXISTING SOLUTIONS AND PROPOSED APPROACH

	HVDC Light	UPFC	FR-BTB	G-CDPAR	G-CNT	Proposed scheme
Transformer count & rating	2 fully rated, standard design	2 fractionally rated, custom design	1 fractional rating, standard design	1 fully rated, standard design	1 fully rated, standard design	1 fully rated, standard design
Converter type & rating	VSC B2B, fully rated	VSC B2B, fractional rating	VSC B2B, fractional rating	AC chopper, fractional rating	VSC B2B, fractional rating	AC chopper, fractionally rated
BIL management	Handled by standard transformer	Challenging, relies on series transformer design	Challenging, converter floating at the line voltage	Handled by standard transformer, converter at ground level	Handled by standard transformer, converter at ground level	Handled by standard transformer, converter at ground level
Cooling	Active, deionized water	Active, forced air	Forced air or combined with transformer cooling	Forced air or combined with transformer cooling	Forced air or combined with transformer cooling	Forced air or combined with transformer cooling
System efficiency	~95%	~99%	~99%	~99%	~99%	~99%
DC mitigation/ isolation	No	No	No	No	No	Yes
Voltage scaling	Yes	No	No	Yes	Yes	Yes
Power flow control capability	Complete and independent PQ control	Independent PQ control around base power flow	Independent PQ control around base power flow	Optimized for P or Q control around base power flow	Independent PQ control around base power flow	Independent PQ control around base power flow
Fail normal	No	Yes - large stress on series transformer	Yes	Yes	Yes	Yes
Line unbalance management	Yes	No	No	No	Yes	Yes
Scaling	Yes	BIL management limits scalability	BIL management impairs scalability	BIL management limits scalability	Yes	Yes
Cost	Highest	Higher	Lower	Lowest	Lower	Lower

Appendix B

Relevant publications

The following publications were produced during this PhD dissertation work.

PATENT

[1] M. Nazir, K. W. Burkes, V. J. Ceyssens and J. H. Enslin, "DC Compensation for Power Transformer Through Neutral DC Injection," *U.S. Patent Application*, 17/196, 152, September 16, 2021.

JOURNAL

[1] M. Nazir, K. Burkes and J. Enslin, "Converter-Based Solutions: Opening New Avenues of Power System Protection Against Solar and HEMP MHD-E3 GIC," in *IEEE Transactions on Power Delivery*, doi: 10.1109/TPWRD.2020.3016207.

[2] M. Nazir, K. Burkes and J. H. Enslin, "Electrical Safety Considerations of Neutral Blocker Placements for Mitigating DC," in *IEEE Transactions on Industry Applications*, vol. 57, no. 1, pp. 1113-1121, Jan.-Feb. 2021, doi: 10.1109/TIA.2020.3032081.

[3] M. Nazir, K. Burkes and J. H. R. Enslin, "Converter-Based Power System Protection Against DC in Transmission and Distribution Networks," in *IEEE Transactions on Power Electronics*, vol. 35, no. 7, pp. 6701-6704, July 2020, doi: 10.1109/TPEL.2019.2963313.

[4] M. Nazir, K. Burkes and J. H. R. Enslin, " Hybrid Smart Transformer for Enhanced DC Mitigation in AC Power Networks with Advanced Grid Support," in *Electric Power Systems Research (EPSR)*, Under Review.

CONFERENCE

[1] M. Nazir, J. H. Enslin and K. Burkes, "Hybrid Smart Transformer for Enhanced Power System Protection Against DC with Advanced Grid Support," *2021 IEEE Energy Conversion Congress and Exposition (ECCE)*, 2021, pp. 1295-1300, doi: 10.1109/ECCE47101.2021.9594952.

[2] M. Nazir, J. H. Enslin and K. Burkes, "Hybrid Bypass Protection of Hybrid Smart Transformers for Advanced Grid Support," *2021 IEEE 12th International Symposium on Power Electronics for Distributed Generation Systems (PEDG)*, 2021, pp. 1-5, doi: 10.1109/PEDG51384.2021.9494212.

[3] M. Nazir and J. H. Enslin, "Synchronous Generator Vulnerability Assessment Against Solar and HEMP MHD-E3 GIC," *2020 52nd North American Power Symposium (NAPS)*, 2021, pp. 1-6, doi: 10.1109/NAPS50074.2021.9449744.

[4] M. Nazir and J. H. Enslin, "Hybrid Smart Converter Transformer for HVDC with Advanced Grid Support," *2020 5th IEEE Workshop on the Electronic Grid (eGRID)*, Aachen, Germany, 2020, pp. 1-8, doi: 10.1109/eGRID48559.2020.9330631.

[5] M. Nazir and J. H. Enslin, "Converter-based Intelligent Transformer for Enhanced Grid Monitoring and Control," *2020 5th IEEE Workshop on the Electronic Grid*

(eGRID), Aachen, Germany, 2020, pp. 1-6, doi: 10.1109/eGRID48559.2020.9330675.

[6] M. Nazir and J. H. Enslin, "Hybrid Smart Converter Transformer for Enhanced HVDC Reliability and Reduced Complexity," *2020 4th International Conference on HVDC (HVDC)*, Xi'an, China, 2020, pp. 742-748, doi: 10.1109/HVDC50696.2020.9292697.

[7] M. Nazir, J. H. Enslin and K. Burkes, "Solar Farm Harmonic Analysis and Operation under DC currents," *2020 IEEE 11th International Symposium on Power Electronics for Distributed Generation Systems (PEDG)*, Dubrovnik, Croatia, 2020, pp. 397-402, doi: 10.1109/PEDG48541.2020.9244478.

[8] M. Nazir, K. Burkes, M. Babakmehr, F. Harirchi and J. H. Enslin, "Transformerless Converter-based GMD Protection for Utility Transformers," *2020 IEEE Applied Power Electronics Conference and Exposition (APEC)*, New Orleans, LA, USA, 2020, pp. 568-573, doi: 10.1109/APEC39645.2020.9123997.

[9] M. Nazir, J. H. Enslin and M. Babakmehr, "Power System Protection response under Geomagnetically Induced Currents," *2020 Clemson University Power Systems Conference (PSC)*, Clemson, SC, USA, 2020, pp. 1-6, doi: 10.1109/PSC50246.2020.9131172.

[10] M. Babakmehr, F. Harirchi, M. Nazir, S. Wang, P. Dehghanian and J. Enslin, "Sparse Representation-based Classification of Geomagnetically Induced Currents," *2020 Clemson University Power Systems Conference (PSC)*, Clemson, SC, USA, 2020, pp. 1-7, doi: 10.1109/PSC50246.2020.9131288.

[11] M. Nazir, J. H. Enslin and K. Burkes, "Enhanced Grid Stability through GIC elimination and Grid Support," *2020 IEEE Power & Energy Society Innovative Smart Grid Technologies Conference (ISGT)*, Washington, DC, USA, 2020, pp. 1-5, doi: 10.1109/ISGT45199.2020.9087691.

[12] M. Nazir, J. H. Enslin and K. Burkes, " Performance Evaluation of Hybrid Bypass Protection of Hybrid Smart Transformers in a Substation Environment," *2022 IEEE 13th International Symposium on Power Electronics for Distributed Generation Systems (PEDG)*, Kiel, Germany, Under Review.

Appendix C

Relevant awards

The following awards were granted related to this PhD dissertation work.

[1] Clemson University Harris Award for Outstanding Graduate Researcher 2021

https://blogs.clemson.edu/electrical-and-computer-engineering/2021-harris-award-recipients/#:~:text=Moazzam%20Nazir%20is%20the%20recipient,research%20productivity%20and%20scholarship%20outstanding

[2] Clemson University 3-Minute Thesis (3MT) Award 2020

https://gsg.people.clemson.edu/initiatives/3mt.php

[3] IEEE IAS Electrical Safety Prevention through Design Student Engineering Initiative Award 2020

https://electricalsafetyworkshop.com/students/

[4] NREL Postdoc and Graduate Student Network (PDaGS) single-slide summit First-Place Award 2021

REFERENCES

[1] D. Bressan, “Ice Cores Reveal Massive Geomagnetic Storms Hit Earth About 2,600 And 1300 Years Ago,” Accessed on: March 28, 2020. [Online].Available:https://www.forbes.com/sites/davidbressan/2019/03/12/ice-cores-reveal-massive-geomagnetic-storms-hit-earth-about-2600-and-1300-years-ago.

[2] R. Girgis, “Effects of GIC on Power Transformers and Power Systems,” Presentation @ Meeting with SRNL, ABB Power Transformers, Feb 2019.

[3] J. N. Towle, F. S. Prabhakara and J. Z. Ponder. (1992, Aug). Geomagnetic effects modelling for the PJM interconnection system. I. Earth surface potentials computation. *IEEE Transactions on Power Systems*. vol. 7, no. 3, pp. 949-955.

[4] “Screening criterion for transformer thermal impact assessment,” [Online]. Available: https://www.nerc.com/pa/Stand/TPL0071RD/Screening_criterion_clean_May12.pdf. Accessed: Jun. 15, 2020.

[5] M.Maruyama, “Investigating countermeasures against high-altitude electromagnetic pulse (HEMP),” [Online]. Available: https://www.ntt-review.jp/archive/ntttechnical.php?contents=ntr201806ra2.html. Accessed: Mar. 28, 2020.

[6] A. K. Mattei, “Response of power system protective relays to solar and HEMP MHD-E3 GIC,” in *Proc. Texas A&M Conf. Protective Relay Eng.*, Texas, USA, 2019.

[7] M. Nazir, J. H. Enslin and M. Babakmehr, "Power System Protection response under Geomagnetically Induced Currents," *2020 Clemson University Power*

Systems Conference (PSC), Clemson, SC, USA, 2020, pp. 1-6, doi: 10.1109/PSC50246.2020.9131172.

[8] H. Schrayshuen, "Geomagnetic Disturbances (GMD) of the Power System, NERC Geomagnetic Disturbance Reliability Standards for Utilities," Presentation @ CNY Expo, Nov 2017.

[9] A. Pulkkinen, E. Bernabeu, J. Eichner, C. Beggan and A. W. P. Thomson, "Generation of 100-year geomagnetically induced current scenarios," *Space Weather*, Apr. 2012.

[10] L. Bolduc, M. Granger, G. Pare, J. Saintonge and L. Brophy, "Development of a DC current-blocking device for transformer neutrals," in *IEEE Transactions on Power Delivery*, vol. 20, no. 1, pp. 163-168, Jan. 2005.

[11] R. J. Pirjola and D. H. Boteler, "Geomagnetically Induced Currents in European High-Voltage Power Systems," *Canadian Conference on Electrical and Computer Engineering, 2006. CCECE '06*, pp.1263-1266, May 2006.

[12] T. Phillips, "Near Miss: The Solar Superstorm of July 2012," Accessed on: March 28, 2020. [Online]. Available: https://science. nasa.gov /science-news/science-at-nasa/2014/23jul_superstorm.

[13] V. Salas, E. Olias, M. Alonso, F. Chenlo and A. Barrado, "DC Current Injection Into the Network from PV Grid Inverters," *2006 IEEE 4th World Conference on Photovoltaic Energy Conference*, Waikoloa, HI, 2006, pp. 2371-2374, doi: 10.1109/WCPEC.2006.279668.

[14] A. Medina, J. C. Hernández, M. J. Ortega and F. Jurado, "DC current injection into the network from transformerless and LF transformer photovoltaic inverters," *2014 16th International Conference on Harmonics and Quality of Power (ICHQP)*, Bucharest, 2014, pp. 234-238, doi: 10.1109/ICHQP.2014.6842878.

[15] V. Salas, M. Alonso-Abella, E. Olias, F. Chenlo and A. Barrado. (2007, May) DC current injection into the network from PV inverters of <5 kW for low-voltage small grid-connected PV systems. *Solar Energy Materials and Solar Cells*, vol. 91, no. 9, pp. 801-806.

[16] Active filter for reduction of common mode current, by B. R. Pelly. (2003, October 21). Patent US 6,636,107 B2 [Online]. Available: https://patents.google.com /patent/US6636107?oq=US6636107B2.

[17] G. He, D. Xu and M. Chen, "A Novel Control Strategy of Suppressing DC Current Injection to the Grid for Single-Phase PV Inverter," in *IEEE Transactions on Power Electronics*, vol. 30, no. 3, pp. 1266-1274, March 2015, doi: 10.1109/TPEL.2014.2317288.

[18] D. L. Dickmander, S. Y. Lee, G. L. Desilets and M. Granger, “AC/DC harmonic interactionsb in the presence of GIC for the Quebec-New England Phase II HVDC transmission”, *IEEE Trans. Power Delivery*, vol. 9, no. 4, pp. 68-78, 1994.

[19] M. Yang, D. Deswal and F. de León, "Mitigation of Half-Cycle Saturation of Adjacent Transformers During HVDC Monopolar Operation—Part I: Mitigation Principle and Device Design," in *IEEE Transactions on Power Delivery*, vol. 34, no. 6, pp. 2232-2239, Dec. 2019, doi: 10.1109/TPWRD.2019.2907607.

[20] EPRI, “Assessment Guide: GMD Harmonic Impacts and Asset Withstand Capabilities,” EPRI technical report no. 3002006444, August 2016.

[21] I. Babaeiyazdi, M. Rezaei-Zare and A. Rezaei-Zare, "Wind Farm Operating Conditions Under Geomagnetic Disturbance," in *IEEE Transactions on Power Delivery*, vol. 35, no. 3, pp. 1357-1364, June 2020, doi: 10.1109/TPWRD.2019.2940913.

[22] A. K. Mattei and W. M. Grady, "Response of Power System Protective Relays to Solar and HEMP MHD-E3 GIC," *2019 72nd Conference for Protective Relay Engineers (CPRE)*, College Station, TX, USA, 2019, pp. 1-7, doi: 10.1109/CPRE.2019.8765893.

[23] M. Nazir and J. H. Enslin, "Synchronous Generator Vulnerability Assessment Against Solar and HEMP MHD-E3 GIC," *2020 52nd North American Power Symposium (NAPS)*, 2021, pp. 1-6, doi: 10.1109/NAPS50074.2021.9449744.

[24] EPRI, “Assessment Guide: GMD Harmonic Impacts and Asset Withstand Capabilities,” EPRI technical report no. 3002006444, August 2016.

[25] M. Nazir, J. H. Enslin and K. Burkes, "Solar Farm Harmonic Analysis and Operation under DC currents," *2020 IEEE 11th International Symposium on Power Electronics for Distributed Generation Systems (PEDG)*, 2020, pp. 397-402, doi: 10.1109/PEDG48541.2020.9244478.

[26] J. H. R. Enslin and P. J. M. Heskes, "Harmonic interaction between a large number of distributed power inverters and the distribution network," in *IEEE Transactions*

on Power Electronics, vol. 19, no. 6, pp. 1586-1593, Nov. 2004, doi: 10.1109/TPEL.2004.836615.

[27] A. Hargrave, M. J. Thompson and B. Heilman, "Beyond the knee point: A practical guide to CT saturation," *2018 71st Annual Conference for Protective Relay Engineers (CPRE)*, College Station, TX, 2018, pp. 1- 23.

[28] S. E. Zocholl and G. Benmouyal, "How microprocessor relays respond to harmonics, saturation, and other wave distortions". In *Proceedings of the 24th Annual Western Protective Relay Conference*, Spokane, WA, USA, 1997.

[29] A. Viljanen, R. Pirjola, M. Wik, A. Ádám, E. Prácser, Y. Sakharov and J. Katkalov, "Continental scale modelling of geomagnetically induced currents," *Journal of Space Weather and Space Climate*, 2012.

[30] D. H. Boteler and R. J. Pirjola, "Modeling geomagnetically induced currents," in *Space Weather*, vol. 15, no. 1, pp. 258-276, Jan. 2017.

[31] S. Marsal and J. M. Torta, "Quantifying the performance of geomagnetically induced current models," in *Space Weather*, vol. 17, no. 7, pp. 941-949, Jul. 2019.

[32] Reduction of Geomagnetically Induced Currents, by B. Kovan and F. D. Leon. (2018, May 24). Patent US 2018/0145504 A1 [Online]. Available: https://patents.google.com/patent/ US2018/0145504.

[33] M. Nazir, K. Burkes and J. H. R. Enslin. (2020, July). Converter-Based Power System Protection Against DC in Transmission and Distribution Networks. *IEEE Transactions on Power Electronics*, vol. 35, no. 7, pp. 6701-6704.

[34] M. Nazir, J. H. Enslin and K. Burkes, "Enhanced Grid Stability through GIC elimination and Grid Support," *2020 IEEE Power & Energy Society Innovative Smart Grid Technologies Conference (ISGT)*, Washington, DC, USA, 2020, pp. 1-5, doi: 10.1109/ISGT45199.2020. 9087691.

[35] M. Nazir, K. Burkes, M. Babakmehr, F. Harirchi and J. H. Enslin, "Transformerless Converter-based GMD Protection for Utility Transformers," *2020 IEEE Applied Power Electronics Conference and Exposition (APEC)*, New Orleans, LA, USA, 2020, pp. 568-573, doi: 10.1109/APEC39645.2020.9123997.

[36] H. Zhu and T. J. Overbye, "Blocking Device Placement for Mitigating the Effects of Geomagnetically Induced Currents," in *IEEE Transactions on Power Systems*, vol. 30, no. 4, pp. 2081-2089, July 2015.

[37] J. G. Kappenman et al., "GIC mitigation: a neutral blocking/bypass device to prevent the flow of GIC in power systems," in *IEEE Transactions on Power Delivery*, vol. 6, no. 3, pp. 1271-1281, July 1991.

[38] D. Y. Shi, J. Buse, Q. H. Wu and L. Jiang, "Fast compensation of current transformer saturation," *2010 IEEE PES Innovative Smart Grid Technologies Conference Europe (ISGT Europe)*, Gothenberg, 2010, pp. 1-7.

[39] E. Hajipour, M. Vakilian and M. Sanaye-Pasand, "Current-Transformer Saturation Compensation for Transformer Differential Relays," in *IEEE Transactions on Power Delivery*, vol. 30, no. 5, pp. 2293-2302, Oct. 2015.

[40] EPRI, “Monitoring and Mitigation of Geomagnetically Induced Currents,” EPRI report no. 1015938, December 2008.

[41] J. Kappenman, Storm Analysis Consultants, "Analysis of GIC Reduction Strategies for the Electric Power Grid," PowerPoint presentation, NERC GMD Workshop, Atlanta, April 19-20, 2011.

[42] R. Lordan, "Geomagnetic Disturbance (GMD) Neutral Blocking Device Analysis," EPRI Report, 2014.

[43] A. A. Hussein, "Mitigation of geomagnetically induced currents by variable series reactor," *2017 North American Power Symposium (NAPS)*, Morgantown, WV, 2017, pp. 1-6.

[44] Method and equipment for the protection of power systems against geomagnetically induced currents, by M. A. F. K. Alakula and S. Lindhal. (2009, February 10). Patent US 7,489,485 B2 [Online]. Available: https://patents.google.com/patent/US7489485.

[45] Protective device for protecting a transformer against geomagnetically induced currents, by P. Hamberger. (2017, June 09). Patent CA 2,949,019 A1 [Online]. Available: https:// patents.google .com/patent /CA2949019A1.

[46] "Restoring efficiency, removing sound. Direct-current compensation (DCC) for power transformers," Accessed on: March 28, 2020. [Online]. Available: https://new.siemens.com/global/en/products/energy/high-voltage/transformers/ dc-compensation.html, Accessed March 2020.

[47] Method and means for suppressing geomagnetically induced currents, by B. M. Oliver. (1992, August 04). Patent US 5,136,453 [Online]. Available: https://patents.google.com/patent/US5136453.

[48] A. A. Hussein and M. H. Ali. (2016, Nov). Suppression of geomagnetic induced current using controlled ground resistance of transformer. *Electric Power Systems Research*. vol. 140, pp. 9-19.

[49] Sensing and Control Electronics for A Power Ground Protection System, by F. R. Faxvog et. al. (2013, September 17). Patent US 8,537,508 B2 [Online]. Available: https://patents.google.com/patent/US8537508B2.

[50] A. D. Rajapakse et al., "Power grid stability protection against GIC using a capacitive grounding circuit," *PES T&D 2012*, Orlando, FL, 2012, pp. 1-6.

[51] L. Gyugyi, "Unified power-flow control concept for flexible AC transmission systems," in *IEE Proceedings C - Generation, Transmission and Distribution*, vol. 139, no. 4, pp. 323-331, July 1992, doi: 10.1049/ip-c.1992.0048.

[52] N. Johansson, L. Angquist and H. Nee, "An Adaptive Controller for Power System Stability Improvement and Power Flow Control by Means of a Thyristor Switched Series Capacitor (TSSC)," in *IEEE Transactions on Power Systems*, vol. 25, no. 1, pp. 381-391, Feb. 2010, doi: 10.1109/TPWRS.2009.2036484.

[53] L. F. W. de Souza, E. H. Watanabe and J. E. da Rocha Alves, "Thyristor and Gate-Controlled Series Capacitors: A Comparison of Components Rating," in *IEEE Transactions on Power Delivery*, vol. 23, no. 2, pp. 899-906, April 2008, doi: 10.1109/TPWRD.2008.917941.

[54] D. Das, D. M. Divan and R. G. Harley, "Power flow control in networks using controllable network transformers," in *IEEE Transactions on Power Electronics*, vol. 25, no. 7, pp. 1753-1760, July 2010, doi: 10.1109/TPEL.2010.2042076.

[55] R. P. Kandula et al., "Field test results for a 3-phase 12.47 kV 1 MVA power router," *2016 IEEE Energy Conversion Congress and Exposition (ECCE)*, Milwaukee, WI, 2016, pp. 1-8, doi: 10.1109/ECCE.2016. 7855115.

[56] M. J. Mauger, P. Kandula, F. Lambert and D. Divan, "Grounded Controllable Network Transformer for Cost-Effective Grid Control," *2018 IEEE Energy Conversion Congress and Exposition (ECCE)*, Portland, OR, 2018, pp. 3732-3739, doi: 10.1109/ECCE.2018.8557956.

[57] R. Jinsiwale, M. J. Mauger, R. P. Kandula, D. Divan, M. Jaroszewski and J. Schatz, "Cost-Effective Dynamic Control for Transmission Systems," *2018 IEEE Electronic Power Grid (eGrid)*, Charleston, SC, 2018, pp. 1-6, doi: 10.1109/eGRID.2018.8598680.

[58] L. Ferreira Costa, G. De Carne, G. Buticchi and M. Liserre, "The Smart Transformer: A solid-state transformer tailored to provide ancillary services to the distribution grid," in *IEEE Power Electronics Magazine*, vol. 4, no. 2, pp. 56-67, June 2017, doi: 10.1109/MPEL.2017.2692381.

[59] F. Vaca-Urbano and M. S. Alvarez-Alvarado, "Power quality with solid state transformer integrated smart-grids," *2017 IEEE PES Innovative Smart Grid Technologies Conference - Latin America (ISGT Latin America)*, Quito, 2017, pp. 1-6, doi: 10.1109/ISGT-LA.2017.8126684.

[60] X. She, X. Yu, F. Wang and A. Q. Huang, "Design and Demonstration of a 3.6-kV–120-V/10-kVA Solid-State Transformer for Smart Grid Application," in *IEEE*

Transactions on Power Electronics, vol. 29, no. 8, pp. 3982-3996, Aug. 2014, doi: 10.1109/TPEL.2013.2293471.

[61] S. Hambridge, A. Q. Huang and R. Yu, "Solid State Transformer (SST) as an energy router: Economic dispatch based energy routing strategy," *2015 IEEE Energy Conversion Congress and Exposition (ECCE)*, Montreal, QC, 2015, pp. 2355-2360, doi: 10.1109/ECCE.2015.7309991.

[62] D. Shah and M. L. Crow, "Online Volt-Var Control for Distribution Systems With Solid-State Transformers," in *IEEE Transactions on Power Delivery*, vol. 31, no. 1, pp. 343-350, Feb. 2016, doi: 10.1109/TPWRD.2015.2457442.

[63] R. P. Kandula, D. Divan , R. Jinsiwale, and M. Mauger, "Modular Controllable Transformers (MCT)," United States. doi:10.2172/1488762. https://www.osti.gov/servlets/purl/1488762.

[64] "The Hybrid Transformer - Towards a Smarter Grid," Accessed on: May 05, 2022. [Online]. Available: https://esc.ethz.ch/news/archive/2016/11/the-hybrid-transformer---towards-a-smarter-grid.html.

[65] A. J. Visser, J. H. Enslin, and H. de T Mouton. "Transformerless series sag compensation with a cascaded multilevel inverter," *IEEE Transactions on Industrial Electronics*, 49.4 (2002): pp. 824-831.

[66] A. Horn, L. A. Pittorino, and J. H. R. Enslin, "Evaluation of active power filter control algorithms under non-sinusoidal and unbalanced conditions," in *Proc. 7th Int. Conf. Harmonics Qual. Power*, 1996, pp. 217–224.

[67] Z. Salam, P. C. Tan and A. Jusoh, “Harmonics mitigation using active power filter: A technological review,” *Elektrika Journal of Electrical Engineering*, 8(2), 17-26, 2006.

[68] P. Salmeron and S. P. Litran, “Improvement of the electric power quality using series active and shunt passive filters,” *IEEE transactions on power delivery* 25.2 (2009): pp. 1058-1067.

[69] "Geomagnetic Induced Current (GIC) Mitigation System Summary for the White paper," [Online]. Available:https://www.nerc.com/pa/Stand/Geomagnetic%20Disturbance%20Task%20Force%20DL/NERC%20Mitigation%20System%20Summary%20for%20White%20Paper%20-%20Final.pdf. Accessed: March 20, 2020.

[70] “Benefits of Using Mobile Transformers and Mobile Substations for Rapidly Restoring Electrical Service,” a report to the United States Congress pursuant to Section 1816 of the Energy Policy Act of 2005, U.S. Department of Energy, August 2006. [Online].

[71] F. Xiao, L. Dong, L. Li and X. Liao, "A Frequency-Fixed SOGI-Based PLL for Single-Phase Grid-Connected Converters," in *IEEE Transactions on Power Electronics*, vol. 32, no. 3, pp. 1713-1719, March 2017, doi: 10.1109/TPEL.2016.2606623.

[72] “Assessment of Large Power Transformer Risk Mitigation Strategies,” A report prepared for the Office of Energy Policy and System Analysis, U.S. Department of Energy. Accessed on: May 27, 2022. [Online]. Available:

https://www.energy.gov/sites/prod/files/2017/01/f34/Assessment%20of%20Large%20Power%20Transformer%20Risk%20Mitigation%20Strategies.pdf.

[73] IEEE Standard for Interconnection and Interoperability of Distributed Energy Resources with Associated Electric Power Systems Interfaces," in IEEE Std 1547-2018 (Revision of IEEE Std 1547-2003) , pp.1-138, 6 April 2018, doi: 10.1109/IEEESTD.2018.8332112.

[74] N. Bilakanti, F. Lambert and D. Divan, "Integration of Distributed Energy Resources and Microgrids - Utility Challenges," *2018 IEEE Electronic Power Grid (eGrid)*, Charleston, SC, 2018, pp. 1-6, doi: 10.1109/eGRID.2018.8598678.

[75] K. P. Schneider et al., "A Distributed Power System Control Architecture for Improved Distribution System Resiliency," in *IEEE Access*, vol. 7, pp. 9957-9970, 2019, doi:10.1109/ACCESS .2019.2891368.

[76] K. Deng, J. Cao, P. Guo and X. Xu, "Energy Saving Analysis of Harmonic Suppression in a Distribution Network," *2013 Fourth International Conference on Networking and Distributed Computing*, Los Angeles, CA, 2013, pp. 121-125, doi: 10.1109/ICNDC.2013.13.

[77] U. Bui, “Geomagnetically induced current sensitivity to assumed substation grounding resistances in the power system,” M.S. thesis, University of Illinois at Urbana-Champaign, 2016. Accessed on: Jul 18, 2019. [Online]. Available: https://www.ideals.illinois.edu/bitstream/handle/2142/95508/BUI-THESIS-2016.pdf.

[78] Hearing of the U.S. Senate Homeland Security and Governmental Affairs Committee February 2019, "Perspectives on Protecting the Electric Grid from an Electromagnetic Pulse or Geomagnetic Disturbance," Accessed on: December 03, 2020. [Online]. Available: https://www.hsgac.senate.gov/imo/media/doc/Testimony-Horton-2019-02-27.pdf.

[79] J. Kappenman, "Geomagnetic Storms and their Impacts on the U.S. Power Grid," Metatech Corporation, Meta-R-319, prepared for Oak Ridge National Laboratory for the Federal Energy Regulatory Commission (FERC), the U.S. Department of Energy (DOE), and the U.S. Department of Homeland Security (DHS), January 2010.

[80] M. Nazir, K. Burkes and J. Enslin, "Converter-Based Solutions: Opening New Avenues of Power System Protection Against Solar and HEMP MHD-E3 GIC," in *IEEE Transactions on Power Delivery*, doi: 10.1109/TPWRD.2020.3016207.

[81] M. Nazir and J. H. Enslin, "Converter-based Intelligent Transformer for Enhanced Grid Monitoring and Control," *2020 5th IEEE Workshop on the Electronic Grid (eGRID)*, Aachen, Germany, 2020, pp. 1-6, doi: 10.1109/eGRID48559.2020.9330675.

[82] M. Nazir and J. H. Enslin, "Hybrid Smart Converter Transformer for HVDC with Advanced Grid Support," *2020 5th IEEE Workshop on the Electronic Grid (eGRID)*, 2020, pp. 1-8, doi: 10.1109/eGRID48559.2020.9330631.

[83] A. Prasai, R. P. Kandula, R. Moghe, T. Heidel, C. Schauder, and D. Divan, “Compact dynamic phase angle regulator for power flow control,” in *2015 IEEE Energy Conversion Congress and Exposition (ECCE)*, pp. 4985–4992, Sep. 2015.

[84] A. Q. Huang, Q. Zhu, L. Wang and L. Zhang, "15 kV SiC MOSFET: An enabling technology for medium voltage solid state transformers," in *CPSS Transactions on Power Electronics and Applications*, vol. 2, no. 2, pp. 118-130, 2017, doi: 10.24295/CPSSTPEA.2017.00012.

[85] L. Cheng, et al., “15 kV, large area (1 cm2), 4H-SiC p-type gate turnoffthyristors,” Mater. Sci. Forum, vol. 740–742, pp. 978-981, Jan. 2013.

[86] L. Cheng, et al., “20 kV, 2 cm2, 4H-SiC gate turn-off thyristors for advanced pulsed power applications,” in *Proc. 19th IEEE Pulsed Power Conf. (PPC)*, San Francisco, CA, USA, Jun. 2013, pp. 1-4.

[87] E. V. Brunt, et al., “22 kV, 1 cm2, 4H-SiC n-IGBTs with improved conductivity modulation,” in *Proc. IEEE 26th Int. Symp. Power Semicond. Devices IC’s (ISPSD)*, Waikoloa, HI, USA, Jun. 2014, pp. 358-361.

[88] S.K. Chaudhary, A.F. Cupertino, R. Teodorescu, and J.R. Svensson, “Benchmarking of modular multilevel converter topologies for ES-STATCOM realization,” in *Energies*, 2020, 13(13), p.3384.